UNCLASSIFIED

AD-A251 073

REPORT DOCUMENTATION

Form Approved
OMB No. 0704-0188

1a. REPORT SECURITY CLASSIFICATION
Unclassified

2a. SECURITY CLASSIFICATION AUTHORITY

DTIC
ELECTE
JUN 01 1992
S A D

2b. DECLASSIFICATION / DOWNGRADING SCHEDULE

3. DISTRIBUTION / AVAILABILITY OF REPORT
Approved for public release;
distribution is unlimited

4. PERFORMING ORGANIZATION REPORT NUMBER(S)

5. MONITORING ORGANIZATION REPORT NUMBER(S)
AFOSR-TR· 2 0453

6a. NAME OF PERFORMING ORGANIZATION
Illinois Institute of Technology

6b. OFFICE SYMBOL (If applicable)

7a. NAME OF MONITORING ORGANIZATION
AFOSR/NA

6c. ADDRESS (City, State, and ZIP Code)
Department of Civil Engineering
Illinois Institute of Technology
Chicago, Illinois 60616

7b. ADDRESS (City, State, and ZIP Code)
Bolling AFB
Washington, DC 20332-6448

8a. NAME OF FUNDING / SPONSORING ORGANIZATION
AFOSR

8b. OFFICE SYMBOL (If applicable)
NA

9. PROCUREMENT INSTRUMENT IDENTIFICATION NUMBER
AFOSR-91-0136

8c. ADDRESS (City, State, and ZIP Code)
Bolling Air Force Base
Washington, DC 20332-6448

NA

10. SOURCE OF FUNDING NUMBERS

PROGRAM ELEMENT NO.	PROJECT NO.	TASK NO.	WORK UNIT ACCESSION NO.
61102F	2302	C2	

11. TITLE (Include Security Classification)
FATIGUE, HYSTERESIS AND ACOUSTIC EMISSION

12. PERSONAL AUTHOR(S)
Guralnick, S.A. and Erber, T.

13a. TYPE OF REPORT
FINAL

13b. TIME COVERED
FROM 1/1/ TO /_/

14. DATE OF REPORT (Year, Month, Day)
1922, May, 15

15. PAGE COUNT
176

16. SUPPLEMENTARY NOTATION

--

17. COSATI CODES

FIELD	GROUP	SUB-GROUP

18. SUBJECT TERMS (Continue on reverse if necessary and identify by block number)
HYSTERESIS, ACOUSTIC EMISSION FATIGUE FAILURE,
FATIGUE DAMAGE,

19. ABSTRACT (Continue on reverse if necessary and identify by block number)

The basic objective of this research program is to characterize the development of material fatigue by means of stress-strain hysteresis and acoustic emission measurements. We have conjectured that the accumulation and organization of damage in material fatigue is similar to the progressive failure of structures under cyclic loading. And, specifically, that the endurance limit of a material in fatigue is the analogue of the incremental collapse load of a structure. Since the principal features of the service life and failure of structures can be completely described by hysteresis methods, it is plausible that similar means can be used to characterize the inception and organization of microplastic processes in materials. All of the experimental results obtained during the current research program confirm these conjectures.

20. DISTRIBUTION / AVAILABILITY OF ABSTRACT
☒ UNCLASSIFIED/UNLIMITED   ☐ SAME AS RPT.   ☐ DTIC USERS

21. ABSTRACT SECURITY CLASSIFICATION
Unclassified

22a. NAME OF RESPONSIBLE INDIVIDUAL
Spencer T Wu

22b. TELEPHONE (Include Area Code)
(202) 767-6962

22c. OFFICE SYMBOL
AFOSR/NA

DD Form 1473, JUN 86   *Previous editions are obsolete.*   SECURITY CLASSIFICATION OF THIS PAGE

UNCLASSIFIED

FATIGUE, HYSTERESIS AND
ACOUSTIC EMISSION

FINAL REPORT - PARTS I and II

Submitted to

THE AIR FORCE OFFICE OF SCIENTIFIC RESEARCH

by

The Department of Civil Engineering

of

Illinois Institute of Technology

Chicago

Air Force Grant Number: AFOSR-91013 DEF,
ORA NO. A0103-1-29110

Principal Investigator: Dr. S.A. Guralnick

Co-Principal Investigator: Dr. T. Erber

Graduate Research Assistant: S.S. Michels

Date of Submission: May 15, 1992

_____
S.A. Guralnick
Principal Investigator

92-14176

FATIGUE, HYSTERESIS AND ACOUSTIC EMISSION

FINAL REPORT - PART I

Submitted to

THE AIR FORCE OFFICE OF SCIENTIFIC RESEARCH

by

The Department of Civil Engineering

of

Illinois Institute of Technology

Chicago

Air Force Grant Number: AFOSR-91013 DEF, ORA NO. A0103-1-29110

Principal Investigator: Dr. S.A. Guralnick

Co-Principal Investigator: Dr. T. Erber

Graduate Research Assistant: S.S. Michels

Date of Submission: February 1, 1992

S.A. Guralnick
Principal Investigator

TECHNICAL ABSTRACT

The existence of mechanical hysteresis is generally recognized to be a necessary but not sufficient condition for failure of a metal in fatigue. On the other hand, it has been noted by others that if the total irrecoverable mechanical work done on a metal specimen during 500,000 cycles of loading were converted to the thermal energy equivalent, then this thermal energy is more than nine times the energy required to melt the metal. Yet, it is entirely possible for a metal specimen to exhibit some mechanical hysteresis and still sustain millions of cycles of loading before rupturing. Hence, since the early 1960's, it has been assumed that total hysteresis energy cannot be directly equated with fatigue damage. On the other hand, at stress or strain levels in the neighborhood of the endurance (or fatigue) limit, hysteresis manifests itself from the first cycle onward — long before the first microcracks occur. This means that hysteresis must somehow be connected to the processes occurring within a material subjected to cyclic loading which are leading to the origination or inception of microcracking which, in turn, must lead to the development of crack networks, the growth of the cracks within these networks and the ultimate penetration of these cracks throughout the critical cross-section thus causing complete separation or rupture.

From their prior research on the incremental collapse behavior of structural frameworks, the writers became convinced that the question of the connection between mechanical hysteresis and the origin and inception of fatigue damage in metals should be reopened. In particular, the writers arrived at the notion, recently confirmed by others, that the total mechanical hysteresis exhibited by a metal subjected to cyclic loading could be split into two parts. One part, which is rather large, is converted into thermal energy and is harmlessly dissipated to the environment during the loading history of the material. The other part, which is rather small compared to the total hysteresis energy, leads to the accumulation of fatigue damage in the material which, if indefinitely prolonged, will result in complete rupture.

To test this hypothesis, experiments were conducted upon nearly 100 specimens made of Rimmed AISI 1018 Unannealed Steel. This material was selected because extensive data on its performance exists in the engineering literature and because its stress - strain curve is of the gradual yielding type thus mirroring at least the monotonic stress - strain behavior of many of the kinds of metals of used in the aircraft industry.

One important result of the experiments reported herein, also confirmed by others, is that the total hysteresis energy associated with one cycle is essentially a constant. This means that the accumulated total hysteresis energy is a linear function of the number of cycles of load application for nearly the entire loading history to final rupture. Hence, if the total hysteresis energy may be split into two parts, one part being harmlessly dissipated as heat and the other part causing the accumulation of damage, then the latter part is a constant for each cycle and total damaging energy also accumulates as a linear function of the number of cycles of load application. This result indicates that combining acoustic emission measurements, hysteresis measurements and post-mortem examinations of ruptured specimens may lead to new insights concerning the origin and inception of the fatigue process in metals.

TABLE OF CONTENTS

LIST OF TABLES

LIST OF FIGURES

LIST OF NOTATION AND SYMBOLS

Notation	Description
σ	Unit Stress (ksi)
ϵ	Unit Strain (ksi)
$\Delta\sigma$	Stress Range (ksi)
$\Delta\sigma/2$	Stress Amplitude (ksi)
N_f	Number of Cycles to Failure
σ_{el}	Stress Amplitude Representing the Endurance Limit of the Material (ksi)
$\bar{\sigma}$	Mean Stress (ksi)
σ_{max}	Maximum Applied Tensile Stress During Cyclic Experiment (ksi)
σ_{min}	*Maximum Applied Compressive Stress During Cyclic Experiment* (ksi)
σ_o	Endurance Limit for Non-Alternating Stress Between σ_{max} and 0 (ksi)
r	Range Ratio, $\sigma_{min}/\sigma_{max}$
S_u	Ultimate Strength in Tension (ksi)
σ_{-1}	Endurance Limit for Alternating Stress between $\pm\ \sigma$ (ksi)
$\Delta\epsilon_p$	Plastic Strain Range (in/in)
$\Delta\epsilon_e$	Elastic Strain Range (in/in)
$\Delta\epsilon_t$	Summation of Plastic and Elastic Strain Ranges (in/in)
ϵ_t	Unit Total Strain (in/in)
ϵ_p	Unit Plastic Strain (in/in)

ϵ_e	Unit Elastic Strain (in/in)
n	Strain Hardening Exponent
K	Strength Coefficient, Stress Intercept at $\epsilon_p = 1$
σ_f	True Fracture Strength, True Stress at Failure (ksi)
ϵ_f	True Fracture Ductility, True Strain at Failure (in/in)
n'	Cyclic Strain Hardening Exponent
K'	Cyclic Strength Coefficient (ksi)
σ_f'	Fatigue Strength Coefficient (ksi)
ϵ_f'	Fatigue Ductility Coefficient (in/in)
ΔW	Plastic Strain Energy Associated with One Load Cycle (kip-in)/(in^3)
W_p	Cumulative Plastic Strain Energy (kip-in)/(in^3)
n_i	Number of Cycles at the ith Stress Level
N_i	The Number of Cycles to Cause Failure at the ith Stress Level
N_c	Number of Plastic Hinges Required to Create a Mechanism
S	Degree of Statical Indeterminacy
$U_T(W_{max}, n)$	Total Amount of Energy Absorbed by a Structure When Cycled to Failure (kip-in)
$U_i(W_{max})$	Amount of Energy Absorbed by a Structure in One Load Cycle (kip-in)
$\Delta U_{ijk}(W_{max})$	Amount of Energy Absorbed by the kth Plastic Hinge of the jth Program Step of the ith Load Cycle Applied to a Structure
$\Delta U_i(\epsilon)$	Hysteresis Loss of Cycle i (kip-in)/(in^3)
$U_f(N_f, \epsilon)$	Cumulative Hysteresis Loss at Failure (kip-in)/(in^3)

N_o	Cycle Number in which Energy and Organization Rates are Coincident
U_m	Amount of Energy Associated with a Monotonic Tension Test to Failure (kip-in)/(in^3)
U_d	Amount of Damaging Energy Associated with a One Stroke Failure (kip-in)/(in^3)
$U_d(\epsilon)$	Function Describing Damage Accumulation
$<\Delta U_i(\epsilon)>$	Average Hysteresis Loss per Cycle (kip-in)/(in^3)
$<\Delta U_d(\epsilon)>$	Average Damaging Energy per Cycle (kip-in)/(in^3)
$\epsilon_{th}^{(1)}$	Strain Amplitude at which One-Sided Hysteresis Becomes Zero (in/in)
$\epsilon_{th}^{(2)}$	Strain Amplitude at which Two-Sided Hysteresis Becomes Zero (in/in)

CHAPTER I

INTRODUCTION

General

The research reported herein was undertaken to investigate the validity of a structural model for fatigue originally proposed by Guralnick (1975). This model utilizes the incremental collapse behavior of structural frameworks subjected to cyclically repeated loading to phenomenologically describe the mechanisms that occur in a metal while the metal itself is subjected to cyclically repeated loading. It has been shown (Guralnick, 1973; Guralnick, 1975; Guralnick et al., 1984; and Guralnick et al., 1986) that a structure's response to cyclic loading can be fully described by using an energy approach. One of the goals of this research is to determine whether a similar type of energy approach is applicable to investigate the behavior of metals subjected to cyclically repeated loading.

Overview

Chapter II presents a historical survey of pertinent research in the area of fatigue from the earliest to the most current studies. Chapter III presents a detailed examination of the proposed model and its applicability to the study of metal fatigue. Chapter IV describes the material, equipment and experimental procedures used to investigate the proposed model. Chapter V is a presentation of experimental results and their respective interpretation. Included are the results pertaining to a classical fatigue analysis as well as those stemming from the model itself. Chapter VI contains conclusions drawn from the results presented in Chapter V, suggestions for future research, and a brief summary of the most salient points of this research.

CHAPTER II

HISTORICAL SURVEY

The phenomenon known as fatigue has been studied by many researchers since the earliest recorded work done by Albert in 1829 (published 1896). Fatigue is the fracture or failure of a material due to repeated stressing or straining. A more descriptive term suggested by Moore and Kommers (1927) is "progressive failure." The remainder of this chapter describes related research performed by some of the pioneers in the field.

Traditional Approach

As the terms fatigue or progressive failure imply, failure occurs in a step-wise manner. In other words, every stress or strain cycle brings the material one step closer to failure no matter how infinitesimal that step may be. This was most notably studied by Wöhler (1860-71). He is referred to as the "outstanding pioneer in the experimental study of the strength of materials under repeated stress" by Moore and Kommers (1927), and was the first to employ stress-cycle diagrams to determine a material's response to repeated cycles of stress. Wöhler performed experiments on railroad axle steel in the first rotating beam testing machines ever used; and similar machines are still being used today, virtually unchanged. When specimens were cycled to failure at varying levels of stress, and the stress amplitude, σ_a, plotted versus the logarithm of the number of cycles to failure, N_f, a "knee" developed in an otherwise linear diagram. Beyond this knee, the diagram became essentially linear once again but at a near zero slope. This knee in the diagram is what Wöhler termed the "fatigue limit," or in more modern terms, the "endurance limit," and will be denoted as σ_{el}. The endurance limit of a material, σ_{el}, is the stress below which failure will not occur, even after an indefinitely large number of cycles of stress have been applied to the material. The American Society of Metals

(I -1986) currently defines the endurance limit for most steels to be the stress at which the material can withstand approximately 10 million cycles of loading.

In addition to the work of Wöhler, there have been many theories concerning what mechanisms are acting and what changes the material is undergoing while it is being repeatedly stressed or strained. One such theory documented by Ewing and Rosenhain (1899), was based on the observation of what they called "slip bands" forming on fatigue specimens after stress cycling. They postulated that slipping had the effect of breaking up the polished surface of a grain boundary into elevations and depressions. Further work by Ewing and Humfrey (1903) reported that slip bands appeared in materials at stress levels below the yield stress after a few stress reversals. After further cycling, more bands appeared and the original bands broadened. They reported that "experiments indicated that some crystals reach their limit of elasticity sooner than others due to their favorable orientation to slip." French (1933) reported that these slip bands were, ultimately, the place where cracks first form and the paths along which they later propagate. French also states that "visible slip does not necessarily connote impending fatigue failure." This theory is fundamental, and even today, plays an important role in the area of fracture mechanics.

Early research typically concentrated on completely reversed, or alternating stress cycles. However, much was to be learned from studying the effect of mean stress and stress range as was notably performed by Gerber (1874), Launhardt (1873) Weyrauch (1880-81), Goodman (1899), and Johnson (1922). The notion of mean stress and stress range can be thought of as the superposition of a constant stress, $\bar{\sigma}$, and a fluctuating stress, or stress amplitude. An example of this is shown in Figure 1. Mean stress, as the name implies, is the average stress during one full cycle, and is computed based upon the maximum and minimum stresses for a given experiment, and is represented by $\bar{\sigma} = \dfrac{(\sigma_{max} + \sigma_{min})}{2}$, while the stress range is represented by $\Delta\sigma = (\sigma_{max} - \sigma_{min})$, and
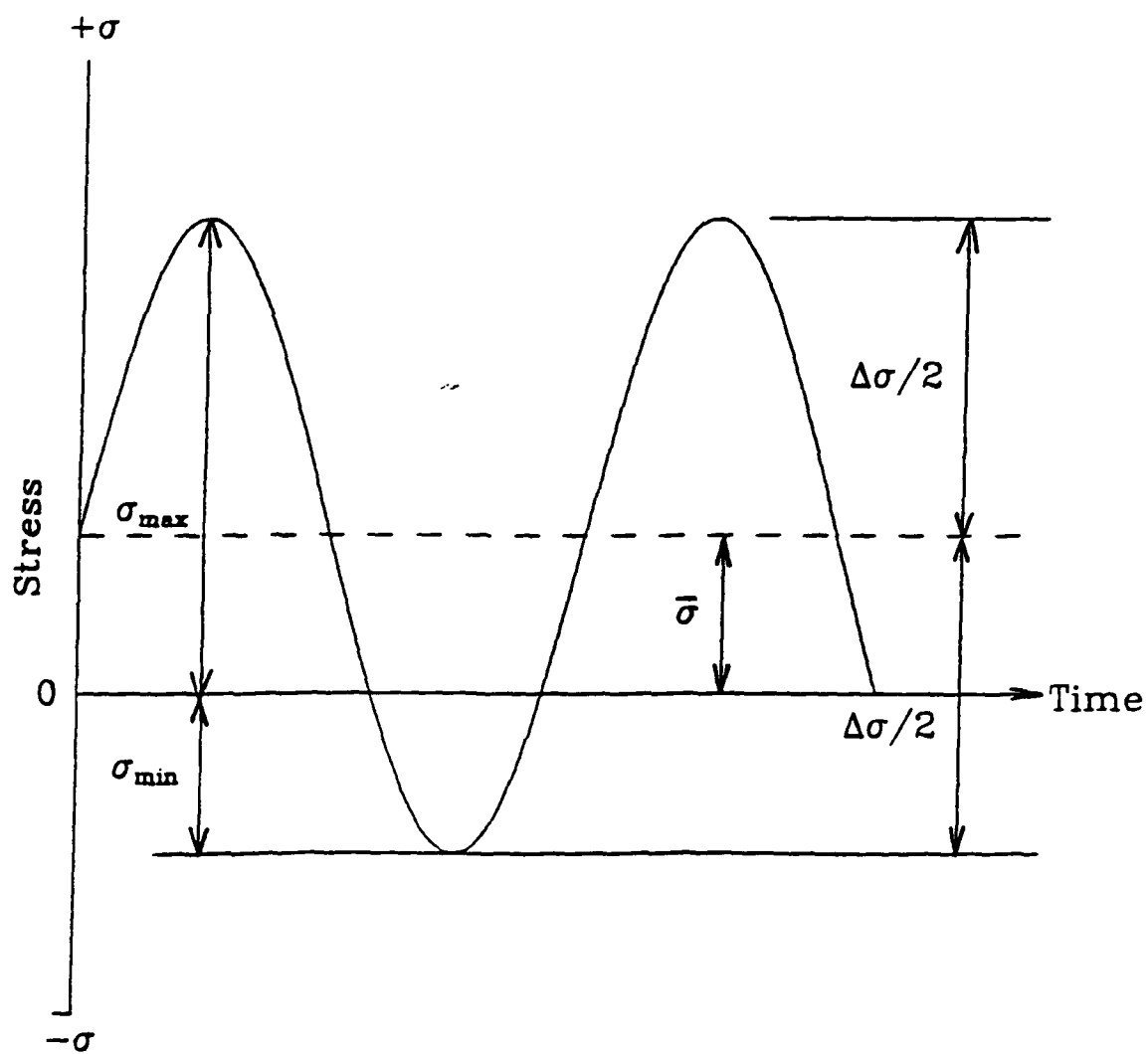
Figure 1. Combination of an Alternating Stress ($\Delta\sigma/2$), and a Constant Stress ($\bar{\sigma}$)

the stress amplitude, σ_a, is simply $\frac{\Delta\sigma}{2}$.

As an early student of Wöhler, Gerber (1874) developed an expression for the endurance limit of a material based upon $\Delta\sigma$ and S_u, where S_u is the static ultimate tensile strength of the material. According to Gerber, the endurance limit may be expressed as,

$$\sigma_{el} = \frac{\Delta\sigma}{2} + \sqrt{S_u^2 - nS_u(\Delta\sigma)} \qquad (2.1)$$

where n is an experimentally determined constant. This equation described cyclic behavior reasonably well with an appropriately determined value of n.

Working independently, Launhardt (1873) and Weyrauch (1880-81) developed the following expressions respectively that, when combined, produced the diagram shown in Figure 2.

$$\sigma_{max} = \sigma_o + r(S_u - \sigma_o) \qquad (2.2)$$

$$\sigma_{max} = \sigma_o - r(\sigma_o - \sigma_{-1}) \qquad (2.3)$$

where r is the range ratio, $\sigma_{min} / \sigma_{max}$, σ_0 is the endurance limit when r = 0, and σ_{-1} is the endurance limit for a complete reversal of stress, r = -1. Goodman developed a similar diagram shown in Figure 3. Goodman (1899) felt that for a minimum stress of zero, the endurance limit was equal to 1/2 of the ultimate tensile strength, and for completely reversed cycling, the endurance limit was equal to 1/3 of the ultimate strength. This diagram was generally found to be conservative.

Johnson (1922), working independently, developed an expression that replaced the curves of the *Launhardt - Weyrauch* diagram with straight lines. When this expression is plotted, the resulting diagram resembles that of the Goodman diagram, and is shown in Figure 4. The expression Johnson used to demonstrate this is shown below.
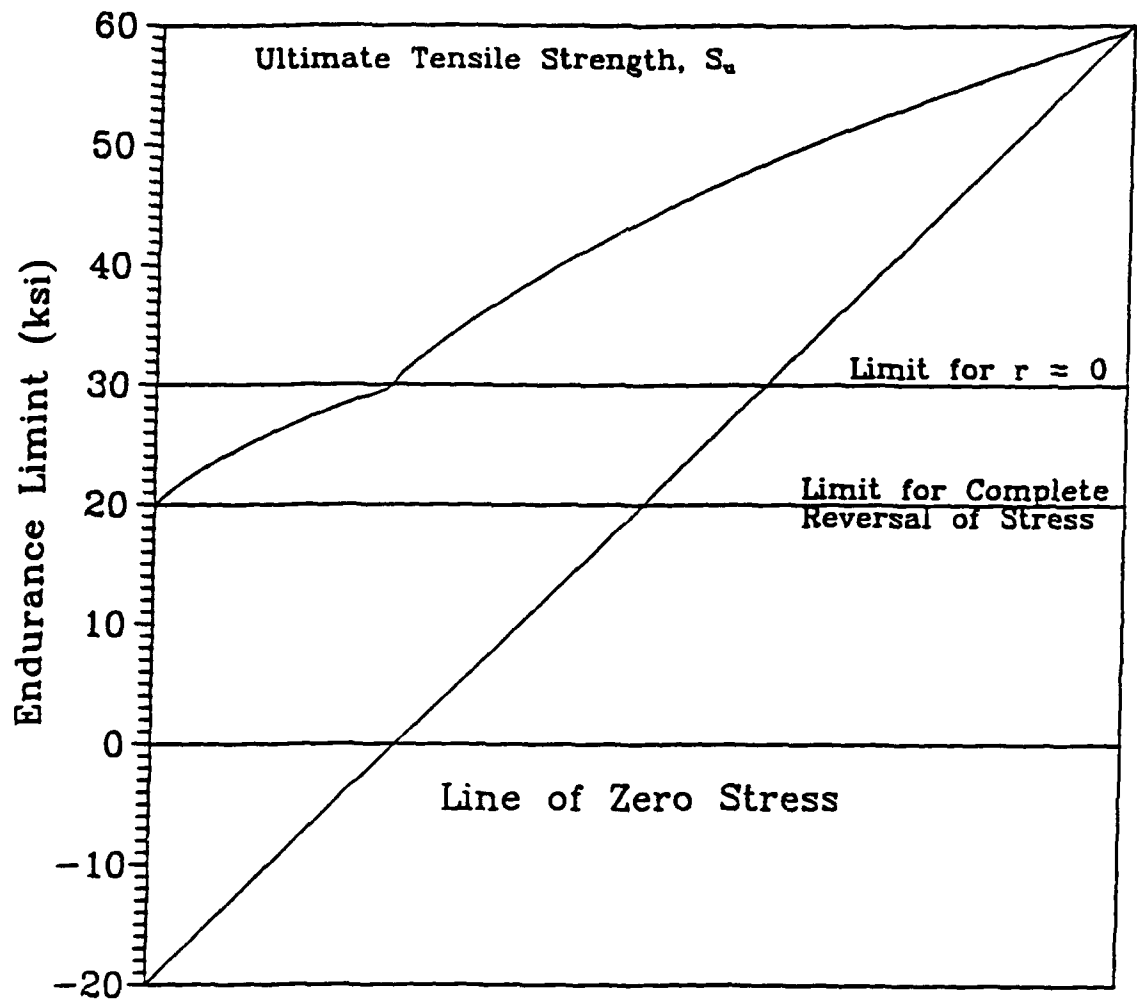
Figure 2. Launhardt - Weyrauch Diagram for Range of Stress
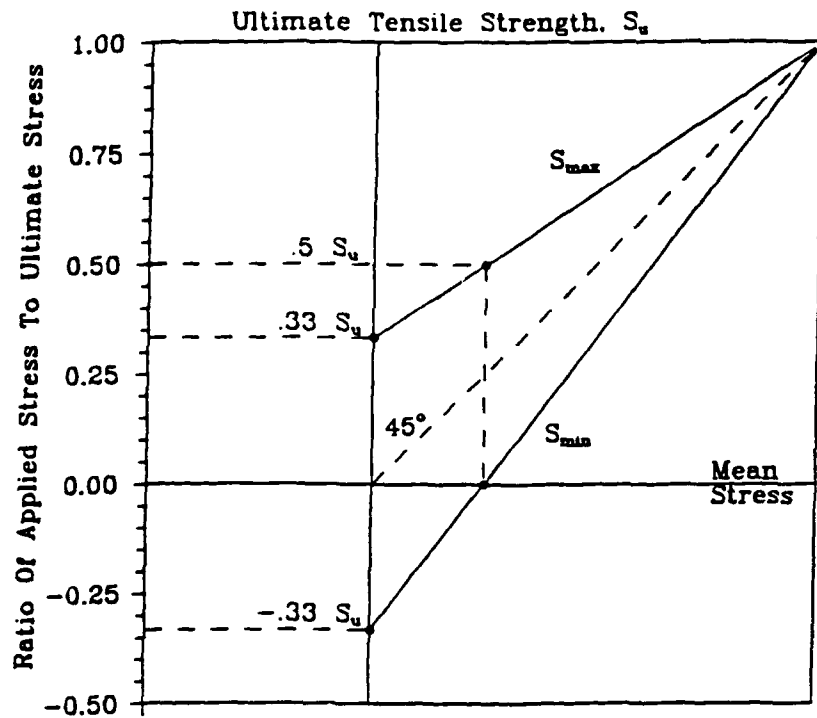
Figure 3. Goodman Diagram for Range of Stress
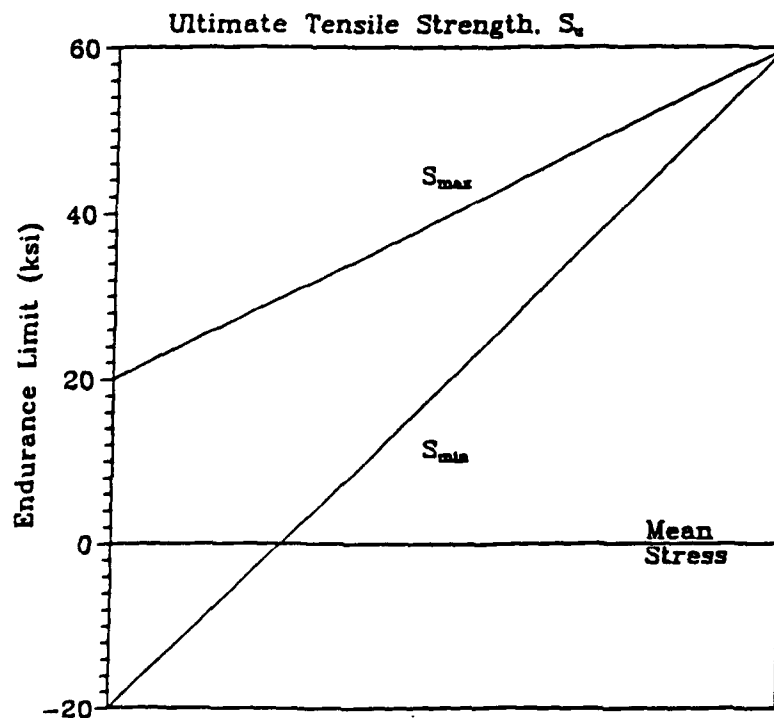
Figure 4. Plot of Goodman - Johnson Formula for Range of Stress

$$\sigma_{max} = \frac{0.5 S_u}{(1 - 0.5r)} \qquad (2.4)$$

The preceding developments were very important for the times in which they were first presented, especially from a design standpoint. Based upon the stress-cycle diagrams of Wöhler, a "safe" level of alternating stress could be determined for a given material and referenced as needed. In addition, the work of Gerber, Launhardt, Weyrauch, Goodman and Johnson helped to determine design criteria for varying stress ranges and amplitudes. There were, however, certain problems associated with these types of analyses. A large number of experiments was required to accurately describe the endurance limit of a material, and this type of testing could take weeks or even months and the end result would still produce a large amount of "scatter" of the data points.

Modern Fatigue Analysis

It has long been the desire of many researchers and engineers to develop simple relationships concerning fatigue for the purpose of design. Studies attempting to provide theses types of relationships have been well documented by many authors. Only a brief summary of the more pertinent works will be discussed.

During the 1930's, a gradual shift in thinking occurred in the area of fatigue studies. Experiments that utilized strain as the independent variable were becoming more and more prevalent. This was a logical step due to the fact that strain is an actual measurable physical quantity while the concept of stress is somewhat more abstract. The determination of the exact instantaneous cross sectional area is difficult, if not impossible. Hence, the shift from stress controlled to strain controlled experiments .

During this period, separating the total strain into elastic and plastic components by subtracting the quantity σ/E from the total applied strain became common practice. Figure 5 shows a typical hysteresis loop that has been subdivided into its respective
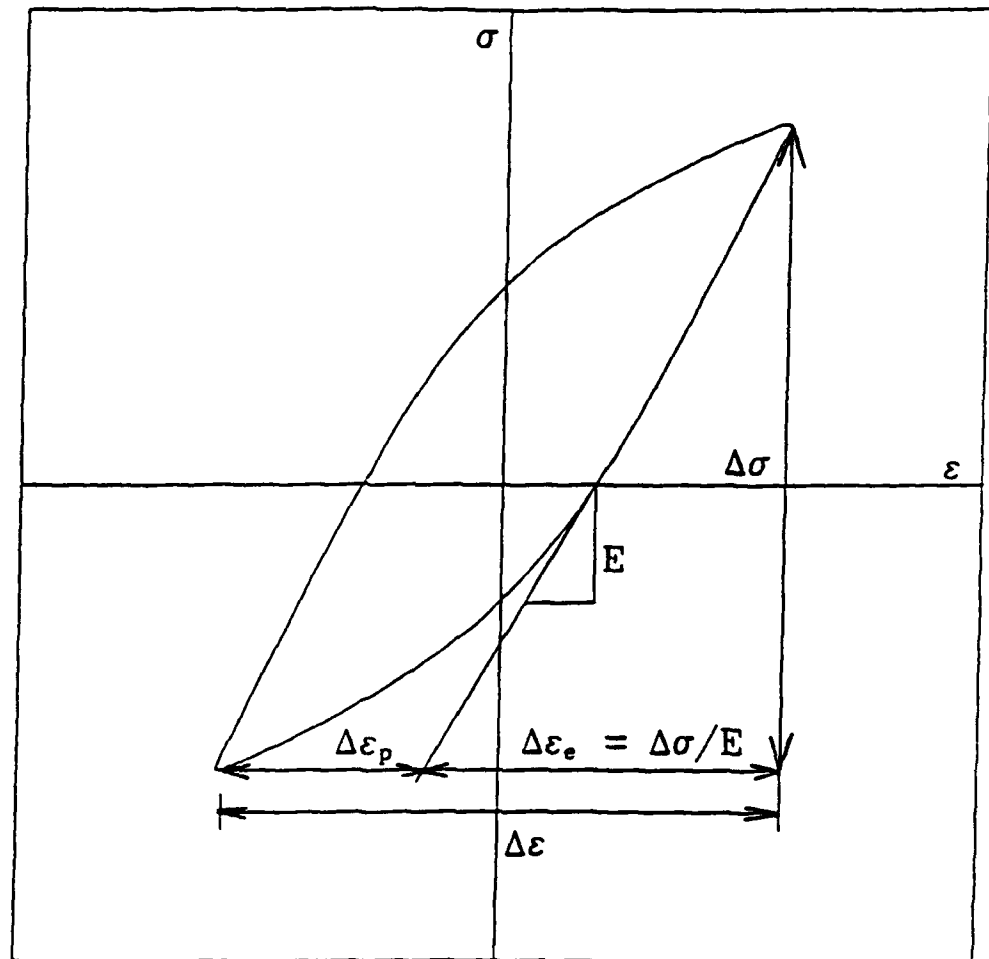
Figure 5. Typical Hysteresis Loop Showing Elastic - Plastic Strain Division

elastic and plastic components. The reason for this strain division lies in the belief that it was only the plastic strain that was associated with cyclic damage. The first step in employing this type of analysis was to determine material parameters from the monotonic true stress - true strain diagram. Halford (1963) and Mitchell (1978) describe simple procedures for determining the strain hardening exponent, n, true fracture strength, σ_f, true fracture ductility, ε_f, and the strength coefficient, K, from monotonic tensile stress - strain experiments. These parameters are utilized in determining the power law relationship, shown below, that is an attempt to describe a material's monotonic behavior.

$$\varepsilon_t = \varepsilon_e + \varepsilon_p = \frac{\sigma}{E} + \left(\frac{\sigma}{K}\right)^{1/n} \tag{2.5}$$

where E = Young's modulus of elasticity, and K = the strength coefficient, $\sigma_f / \varepsilon_f^n$ (intercept at $\varepsilon_p = 1$).

It is easily seen from equation (2.5) that the total strain is composed of two components, elastic and plastic. The material parameters just mentioned have similar counterparts that are associated with what is known as the cyclic stress - strain curve. The cyclic stress - strain curve can be obtained in several ways. One procedure for determining this diagram is to plot many different stabilized hysteresis loops from different strain cycled experiments of varying strain amplitudes on the same diagram and then connect the tips of the loops. The locus of these loop tips forms the cyclic stress - strain curve. This was the procedure used to construct the cyclic stress - strain curves shown in Figures 6 and 7. The counterparts described above are determined from the cyclic stress - strain curve in much the same way as those of the monotonic stress - strain curve, and are differentiated from those of the monotonic stress - strain diagram with the use of a prime symbol. These parameters are then used in the expression for cyclic strain shown below
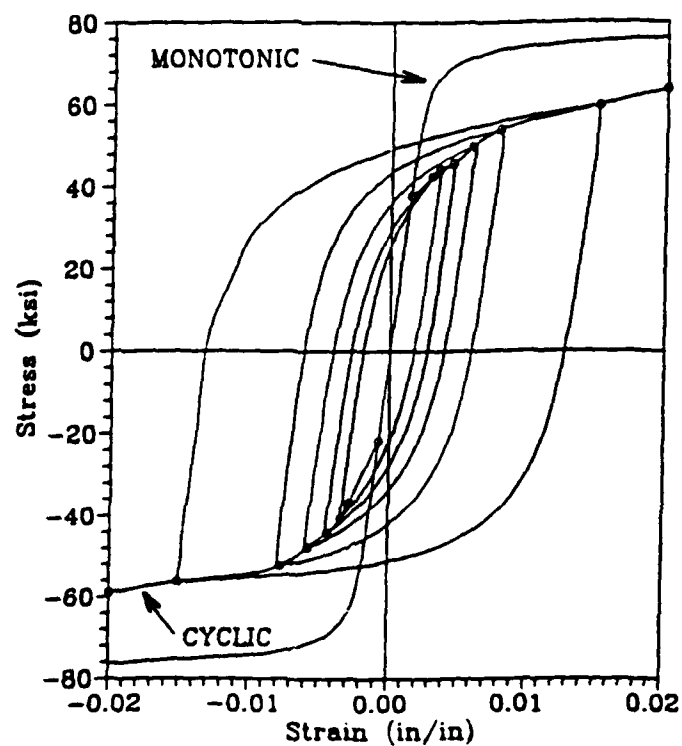
Figure 6. Cyclic and Monotonic Stress - Strain Curves
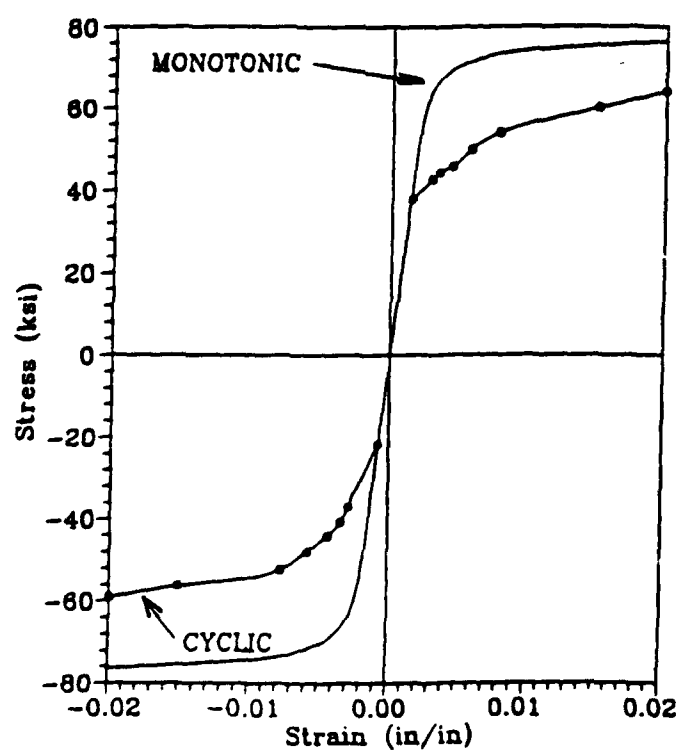
Figure 7. Cyclic and Monotonic Stress - Strain Curves Shown Separately

$$\epsilon_t = \frac{\sigma}{E} + (\frac{\sigma}{K'})^{1/n'}, \tag{2.6}$$

where K' = the cyclic strength coefficient, (intercept at $\epsilon_f' = 1$), and n' = the cyclic strain hardening exponent.

Fatigue - Life Behavior

The first approach to be discussed in this section is based on stress amplitude. The difference between this approach and that of Wöhler (1860-71) is that in determining the fatigue strength behavior, the logarithm of true stress is plotted versus the logarithm of reversals to failure, $2N_f$. A plot of this type will yield a reasonably straight line. An example of this approach is shown in Figure 8. The expression representing this curve was first given by Basquin (1910) as,

$$\frac{\Delta \sigma}{2} = \sigma_f'(2N_f)^b, \tag{2.7}$$

where σ_a = the true stress amplitude, σ_f' = fatigue strength coefficient (stress intercept at one reversal), and b = the slope of the line. In addition, Morrow (1964) developed a similar expression to account for the effects of mean stress on fatigue life. He proposed that the stress amplitude could be represented by

$$\frac{\Delta \sigma}{2} = (\sigma_f' - \overline{\sigma})(2N_f)^b \tag{2.8}$$

where all variables have been previously defined. The problem that arises with this type of approach is the development of a universal method for accurately determining the constant, σ_f'. A number of different methods proposed by different authors have been compared by Landgraf (1970). Each of these methods yields a certain amount of scatter which tends to call into question any claimed universality.

While the approach presented by Basquin (1910) seemed to represent data fairly
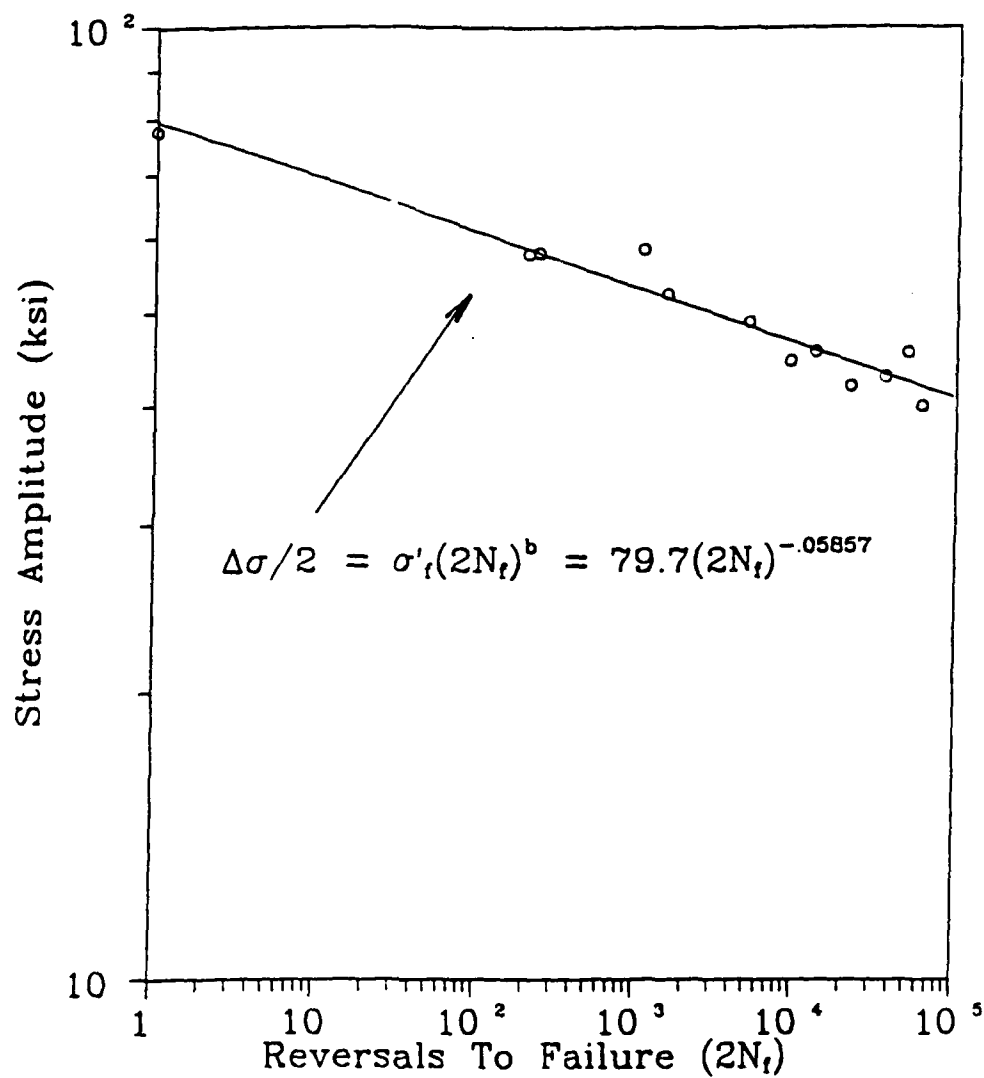
Figure 8. Fatigue Strength Properties, $\Delta\sigma/2$ vs $2N_f$

well, the trend turned, once again, toward strain controlled experiments. Landgraf (1970) provides a description of work performed independently by Manson and Coffin in which an expression similar to equation (2.7) is developed. The emphasis is again on the plastic component of the total strain. This expression is

$$\frac{\Delta \varepsilon_p}{2} = \varepsilon_f'(2N_f)^c \tag{2.9}$$

where ε_f' = the fatigue ductility coefficient, and c = the slope of the line taken from the graph of $\Delta \varepsilon_p/2$ vs $2N_f$. A diagram displaying this approach is shown in Figure 9. A problem similar to that of determining σ_f' is encountered while attempting to accurately determine ε_f'. Landgraf (1970) also provides a comparison of these methods.

By combining equations (2.7) and (2.9), an expression that relates the total strain amplitude to the summation of its respective elastic and plastic components is obtained. This expression may be shown to be,

$$\frac{\Delta \varepsilon_t}{2} = \frac{\Delta \varepsilon_e}{2} + \frac{\Delta \varepsilon_p}{2} = (\sigma_f'/E)(2N_f)^b + \varepsilon_f'(2N_f)^c, \tag{2.10}$$

and is referred to as the strain - life relation. Figure 10 displays the respective strain components as well as the total strain plotted as a function of reversals, $2N_f$. By noting where the curve representing the elastic strain amplitude meets the curve representing the total strain amplitude, it is seen that this approach, if useful at all, is only appropriate in the low cycle fatigue range (i.e. N_f less than 10^5).

Energy Concepts

Energy considerations have been an integral part of many different disciplines for many years. The underlying concept in this approach is, in essence, nothing more than the Law of the Conservation of Energy which states that energy can neither be created nor destroyed, but, instead, transferred from one system to another, or converted from
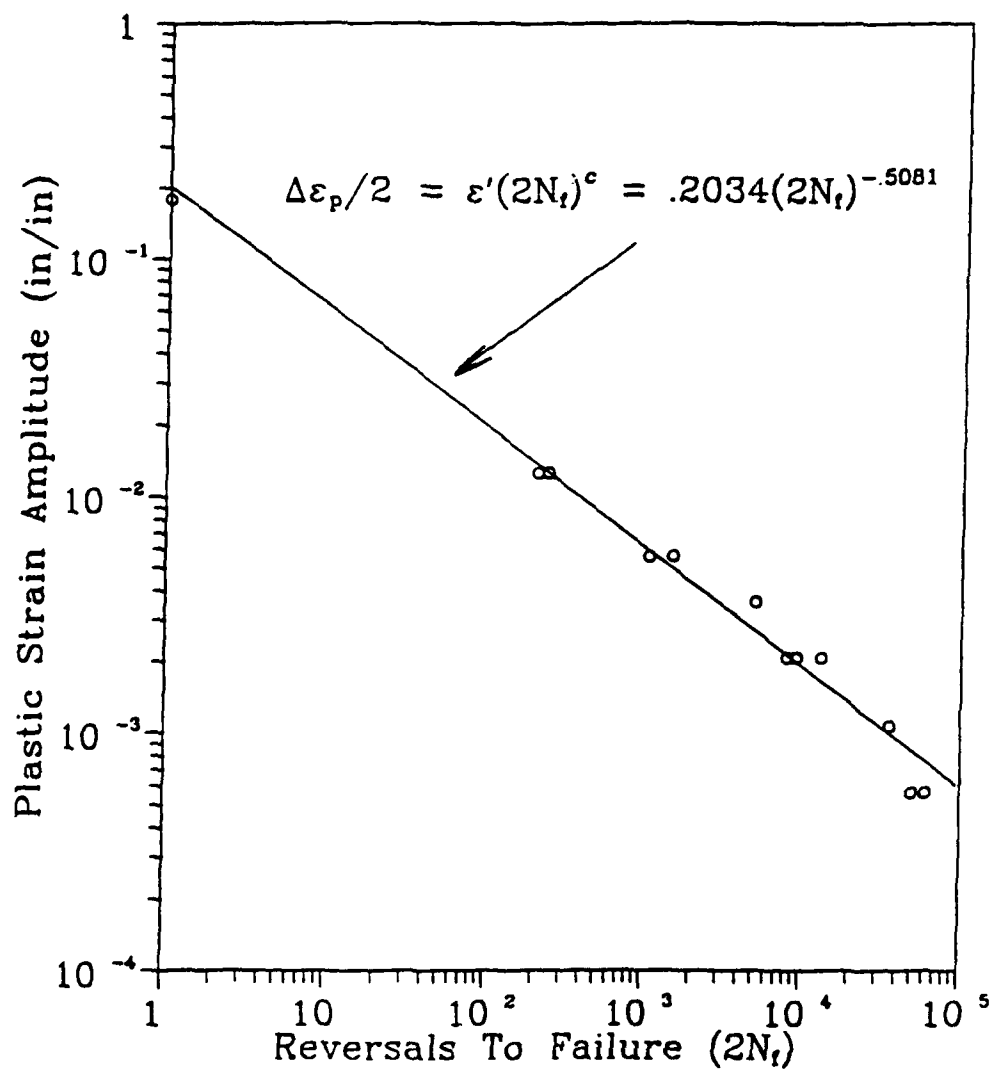
Figure 9. Fatigue Ductility Properties, $\frac{\Delta \varepsilon_p}{2}$ vs $2N_f$
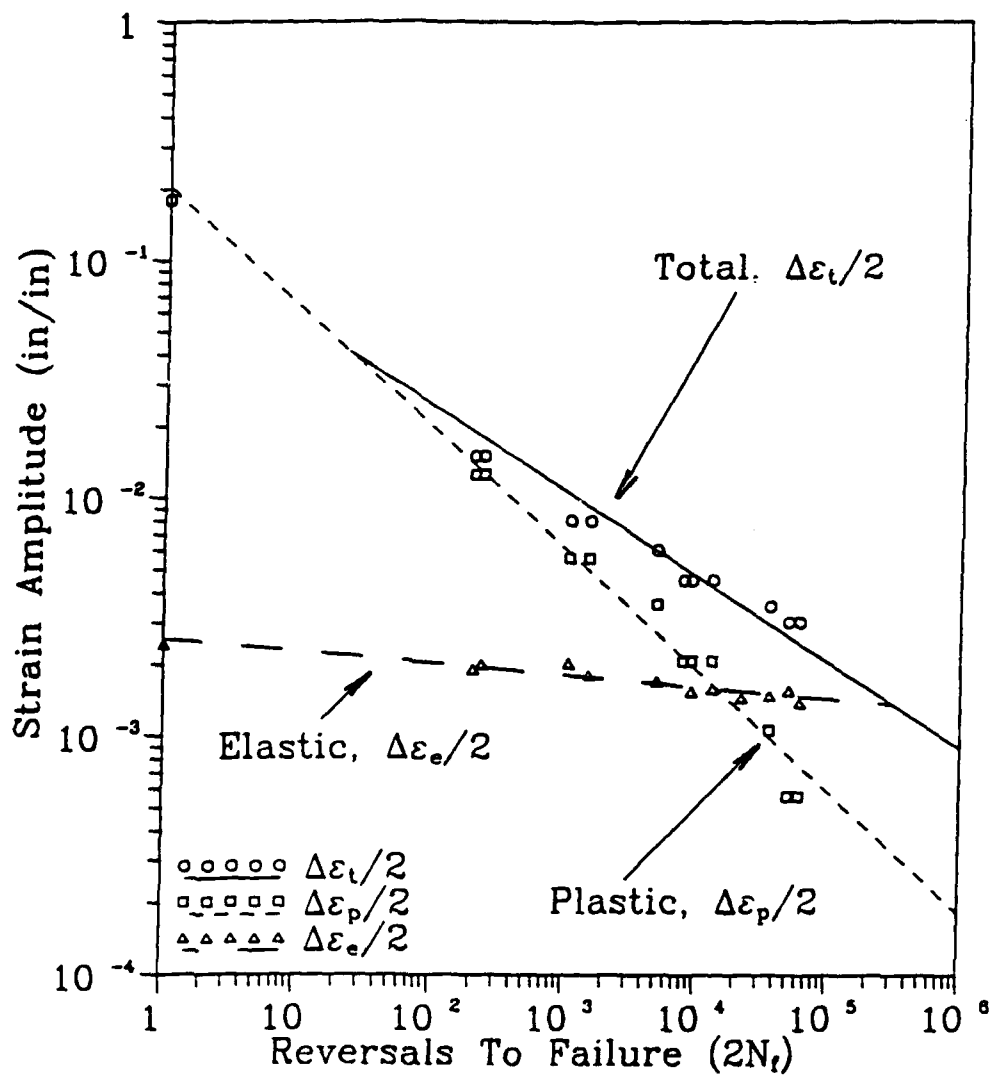
Figure 10. Strain Amplitude vs Reversals to Failure: Strain - Life Relation

one form to another. This forms the fundamental concept of energy considerations in fatigue studies.

The initial step in beginning this type of analysis is the integration of stress - strain hysteresis loops, the area of which has units of $\frac{(kip\ inch)}{inch^3}$. This quantity has sometimes been defined as a material's toughness. These units are those of strain energy per unit volume, or strain energy density. Feltner and Morrow (1961) and Halford (1966) felt that it was only the plastic strain energy that contributed to any accumulation of damaging energy in fatigue. Feltner and Morrow (1961) define the plastic strain energy per cycle as

$$\Delta W = 2 \int_0^{\Delta \varepsilon_p} \sigma\, d\varepsilon_p \qquad (2.11)$$

where ΔW = the plastic strain energy lost in one cycle, $\Delta \varepsilon_p$ = the total true strain excursion, and σ = the instantaneous true stress. By assuming that the plastic strain energy per cycle is very nearly a constant, the total cumulative plastic strain energy to failure, which is also referred to as the fatigue toughness, may be taken to be,

$$W_p = N_f\, \Delta W = 2N \int_0^{\Delta \varepsilon_p} \sigma\, d\varepsilon_p \qquad (2.12)$$

where W_p = the cumulative plastic strain energy at failure, and N_f = the number of cycles to failure. If the derivative of the term on the right side of equation (2.7) is taken with respect to σ and substituted into equation (2.12), integrated with appropriate limits of integration, and further manipulated, then the following expression results,

$$\log_{10} \sigma_a = k - (\frac{n}{1+n})\log_{10} N_f \qquad (2.13)$$

where n = the strain hardening exponent, N_f = the number of cycles to failure, and k

= a constant determined from total plastic strain energy to failure, W_p, the strain hardening exponent, n, and K, the stress intercept at $N_f=1$. This expression mathematically describes the relationship between the logarithm of true stress amplitude and the logarithm of the number of cycles to failure. This method was fairly accurate for predicting stress versus number of cycles to failure diagrams for intermediate cycle ranges. It can not, however, predict the almost horizontal regions in very low cycle fatigue, or in regions near the endurance limit.

Halford (1966) compiled data from over 190 experiments performed by many researchers and found a general trend in which the total plastic strain energy to failure increased to the $1/3$ power of N_f. He has also shown many relationships between the exponents, b and c, of the strain - life relation in equation (2.10), and the cyclic strain hardening exponent, n'. One such relationship determines the slope of the plastic strain amplitude versus the logarithm of reversals to failure to be approximately equal to -0.58. Tavernelli and Coffin (1959) have reported the value of this slope to be equal to -1/2. Both of these values are in agreement with that of Figure 9.

Cumulative Damage

Perhaps the most notable attempt at predicting how damage accumulates during cyclic loading was proposed by Miner (1945). Miner's law of cumulative damage is usually expressed as,

$$\sum_{i=1}^{K} \frac{n_i}{N_i} = 1 \qquad (2.14)$$

where n_i = the number of cycles at the ith stress amplitude, N_i = the number of cycles to cause failure at the ith stress amplitude, and K = the total number of different stress amplitudes. Failure occurs when the sum of the K cycle ratios is equal to 1. Equation (2.14) was originally derived by Miner (1945) with the use of an energy approach, in

which a linear variation of the ratio of energy per cycle to total energy to failure was assumed. It has also been suggested by Feltner and Morrow (1961) and Martin (1961) that the total energy required to fracture a specimen under monotonic tension is equal to the amount of damaging energy required to cause failure in fatigue. To give this notion proper magnitude, Halford (1966) compares the thermal energy required to melt iron with the total energy accumulated over a fatigue life of 500,000 cycles. He explains that the equivalent thermal energy lost over 500,000 cycles is more than nine times the energy required to melt the steel. An obvious conclusion drawn by Martin (1961) is "that total hysteresis energy cannot be equated to fatigue damage."

CHAPTER III

THE FATIGUE MODEL

The purpose of this research was to investigate a model for metal fatigue first proposed by Guralnick (1975) that utilizes an analogy between the incremental collapse of structures and the fatigue failure of metals. The plastic collapse, shakedown, and incremental collapse of structures has been investigated by many researchers; for example, Symonds (1952), Neal (1956), Popov and McCarthy (1960), Cohn, Ghosh, and Parimi, (1972), Guralnick (1973), Popov and Bertero (1973), Popov and Petersson (1978), Guralnick, Singh, and Erber (1984), and Guralnick, Erber, Soudan, and He (1988) to name but a few. These authors, and many others, have provided a great deal of information about the manner in which structures fail under both monotonic and cyclic loadings. The fatigue model previously proposed by Guralnick (1975) and presented herein shows the direct analogy between what may be termed the progressive failure of structures categorically described as failure by incremental collapse, and the fatigue failure of metals under completely reversed or alternating loadings, and loadings of varying amplitude. At first, this may seem to be a very bold analogy, but the following arguments will clearly describe its correlations as well as its pertinent differences.

Comparison Between the Progressive Failure of Structures and the Fatigue of Metals

The discussion of these comparisons must begin at the most elemental level. The previously discussed work of Ewing and Rosenhain (1899), and Ewing and Humfrey (1903), is of particular importance in this respect. As a structure is loaded to a particular level, there are discrete points at which "plastic hinges" form. The formation of a plastic hinge is directly analogous to the formation of slip bands in a metal. Rather than considering these areas as slip bands or dislocations, the model depicts them as

regions of "microplasticity" of the same relative scale as that of a plastic hinge in a structure. In the case of the structures, the number and position of the plastic hinges themselves is of prime importance. In general, the number of plastic hinges required to form a collapse mechanism is,

$$N_c = s + 1 \qquad (3.1)$$

where N_c is the number of plastic hinges present at collapse, and s is the degree of statical indeterminacy of the structure. It is important to note that it is possible for more than N_c plastic hinges form in a structure during a given complete load cycle. However, it is only when these N_c plastic hinges are arranged, or organized into a specific configuration that collapse occurs. It is also interesting to note that the collapse mechanism for a structure loaded monotonically to failure is not necessarily the same mechanism of failure under cyclic loading. Likewise, when a critical number of microplastic regions organize themselves into a particular configuration, or network in a metal, failure occurs. Since, for all practical purposes, there can be infinitely many microplastic configurations sufficient to cause failure, the actual positioning and or physical location of these microplastic zones is not known. Figure 11 displays a reproduction of a micrograph of the distorted surface of a mild steel specimen just after yield has been reached presented by Nadai (1931). This figure clearly displays a certain degree of organization. One might argue that comparing a large structure to a material is incongruous. In physical terms this may be so, but for the purpose of understanding a given material's phenomenological response it is a reasonable approach. An example of this type of approach is the application of a finite element mesh to model a continuous solid. The finite element mesh bears a strong resemblance to the lattice-like structure of a rigid frame building.

Many ferrous metals are composed of crystals, which in turn, form grain structures. These grain structures are oftentimes very regular throughout a solid, and
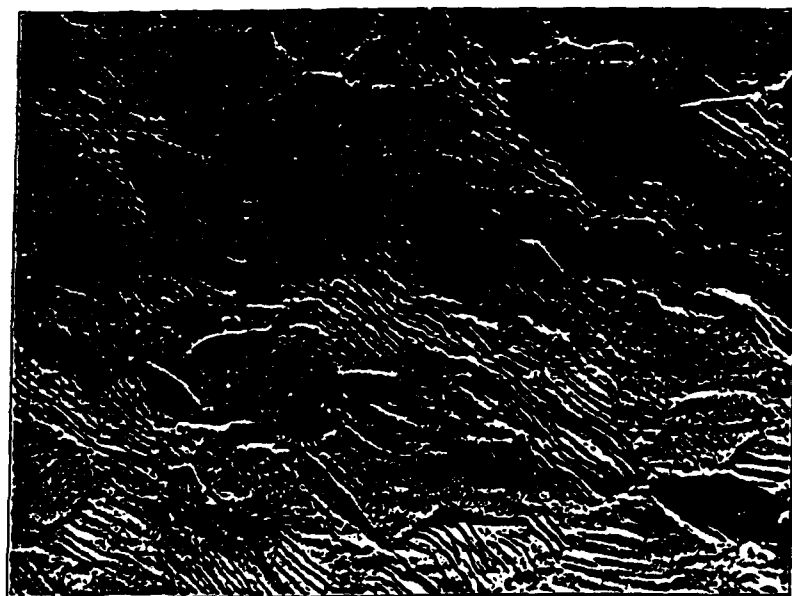
Figure 11. Micrograph of an "Organized" Steel Surface After Yielding

only possess irregularities along grain boundaries. Of course, a material composed of literally millions and millions of grains cannot possess the same degree of regularity that a real structure does. However, by considering complex structures known as the "squared square" (SQ-SQ) and the "squared rectangle" (SQ-RECT) some type of interpolation between a completely regular structure (crystal lattice) and a completely random structure (amorphous solids) may be inferred. The SQ-SQ is the smallest known dissection of a square into non-congruent squares (Fig. 12), and, similarly, the SQ-RECT (Fig. 13) is the smallest known dissection of a rectangle into non-congruent squares. Analyses of these types of structures was given by Guralnick and Erber (1990) and He (1990).

One of the strongest correlations, and the main body of this research, has been the relation through the concept of energy conservation discussed in Chapter II. Work by Guralnick (1973), Guralnick (1975), Guralnick, Singh, and Erber (1984), and Guralnick, Erber, Stefanis, and Soudan (1986) have shown that the failure of structures under cyclic loading can be fully described by means of energy methods. The most important aspect behind an analysis of this kind is that if the total irrecoverable energy, or "hysteresis energy" absorbed by a structure is unbounded, then the structure must ultimately fail. Stated another way, if the hysteresis energy loss per cycle becomes a constant, then over the course of a supposedly infinite life, the total hysteresis loss must also become infinite. This is, of course, impossible; therefore, the structure must fail under a finite number of cycles. If, however, then the hysteresis loss per cycle becomes zero as the number of cycles increases toward infinity, the total hysteresis loss is finite and the structure will not fail. In the notation used by Guralnick, Erber, Soudan, and Stefanis, (1988)
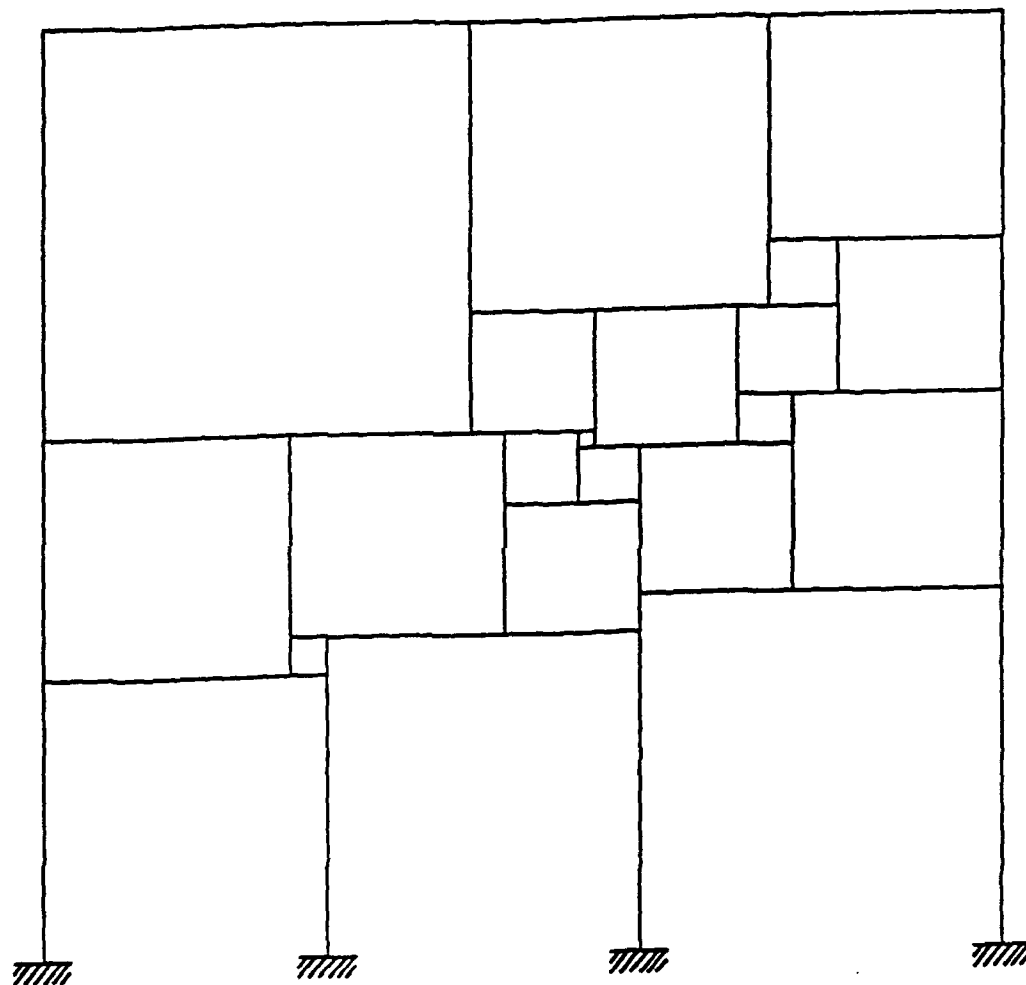
Figure 12. Complex Structure: Squared Square (SQ-SQ)
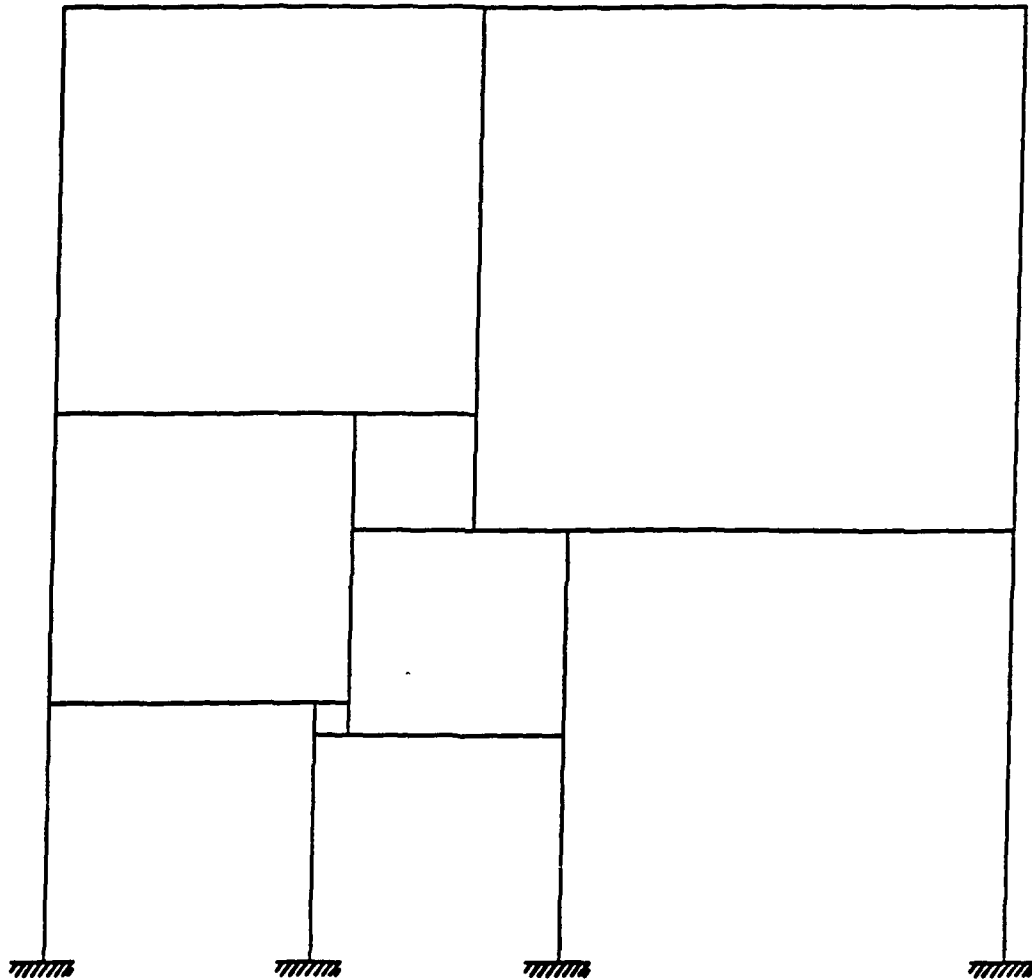
Figure 13. Complex Structure: Squared Rectangle (SQ-RECT)

$$U_T(W_{max}, n) = \sum_{i=1}^{n} U_i(W_{max}), \tag{3.2}$$

where

$$U_i(W_{max}) = \sum_{j=1}^{J(i)} \sum_{k=1}^{K(i)} \Delta U_{ijk}(W_{max}), \tag{3.3}$$

in which $\Delta U_{ijk}(W_{max})$ is the energy absorbed by the kth plastic hinge of the jth program step of the ith load cycle, $U_i(W_{max})$ is the total energy absorbed in the ith load cycle, and $U_T(W_{max}, n)$ is the total energy absorbed by the structure over a lifetime of n load cycles. In other words, if

$$\lim_{i \to \infty} U_i(W_{max}) = k, \tag{3.4}$$

where k is some finite constant, then

$$\lim_{n \to \infty} U_T(W_{max}, n) = \infty, \tag{3.5}$$

and the structure must ultimately fail. Conversely, if

$$\lim_{i \to \infty} U_i(W_{max}) = 0, \tag{3.6}$$

and the infinite series (3.2) converges, then

$$\lim_{n \to \infty} U_T(W_{max}, n) = c \tag{3.7}$$

where c is some finite number, and the structure will not fail.

The amount of energy absorbed by a structure is readily calculated and is equal to the summation of the products of the magnitudes of the fully plastic moments and the corresponding rotations of the members at the positions of the respective plastic hinges. This computation yields the actual quantity of irrecoverable energy imparted to the

structure at specific locations. On the other hand, the energy associated with the area of a stress - strain hysteresis loop is an energy density as described in Chapter II. This is logical because the phenomenon of fatigue is a process that occurs within a continuum.

By employing the approach outlined above, Guralnick (1973) was able to replicate load values corresponding to W_a, the load at which a structure will fail due to alternating plasticity, W_s, the load below which failure will not occur, and W_c, the plastic collapse load. These are just three of the values that may be used to construct what is known as the incremental collapse envelope shown in Figure 14. The resemblance between this diagram and those of Goodman, Johnson, Launhardt and Weyrauch is remarkable.

Research Approach

The approach utilized by Guralnick, et al., is very similar to the methods utilized throughout the course of this research. As an initial starting point, the assumption was made that to every load cycle upon a specimen there is associated a corresponding finite amount of irrecoverable energy, as shown by Sih (1985). Figure 15 displays a graph of stress versus strain as an example. The amount of total energy is represented by the area OAB. However, upon unloading the energy corresponding to the area of the triangle ABC is recovered. Therefore, the total irrecoverable energy is represented by the dotted area OAC. A similar procedure is used to describe the energy absorbed in one closed* hysteresis loop, and is characterized by

$$\Delta U_i(\varepsilon) = \oint \sigma \, d\varepsilon, \tag{3.8}$$

where $\Delta U_i(\varepsilon)$ is the hysteresis energy lost in the ith cycle, σ is the unit stress, and $d\varepsilon$ is

---

*Although hysteresis loops may appear to be closed, they are in reality not closed.
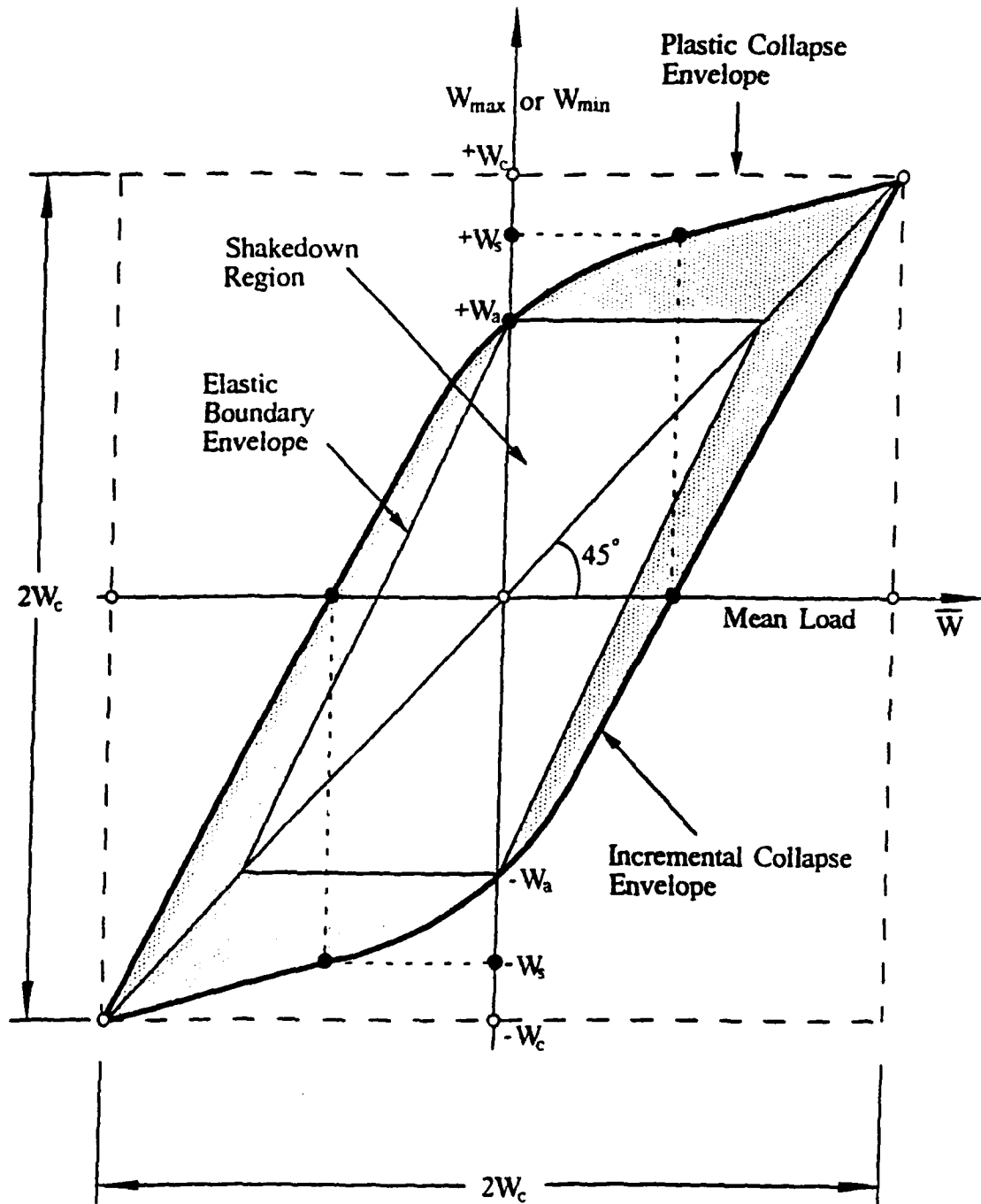
Figure 14. Incremental Collapse Envelope for Structural Frameworks
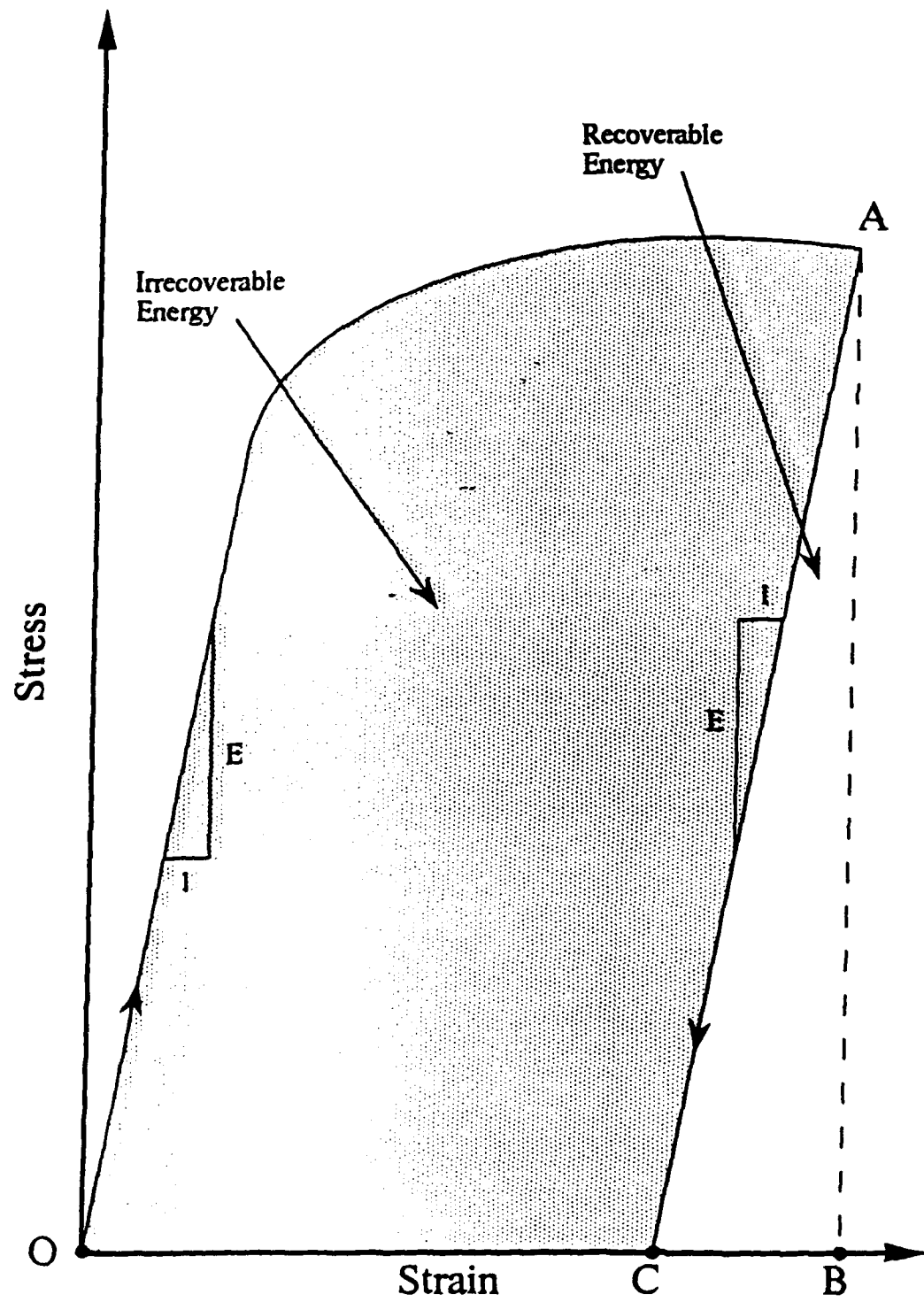
Figure 15. Schematic Showing Total, Recoverable, and Irrecoverable Energy

a differential amount of strain.

It has been well established that only a small fraction of the energy absorbed during a specimen's life actually accumulates as damage. In the opinions of Halford (1966), Morrow (1964) and other authors, only the plastic strain energy contributes to any accumulation of damage. As mentioned in Chapter II, Ewing and Humfrey reported the formation of slip bands at stress levels below the yield stress. This suggests that there is some amount of damaging energy associated with stress and strain levels below the elastic limit. In light of this observation, the choice was made to concentrate on the total energy absorbed by the specimen rather than just the plastic contribution. Therefore, equation (3.8) represents the total irrecoverable hysteresis loss per cycle irrespective of any division into elastic or plastic portions.

The quantity $\Delta U_i(\varepsilon)$ is analogous to the quantity $U_i(W_{max})$ defined by Guralnick (1988) in all ways but one. The difference between the two quantities is that $U_i(W_{max})$ is composed of actual discrete amounts of energy absorbed in the formation of the individual plastic hinges. This is where the analogy between a structure and a metal fails because it is not possible to look into the metal while it is being tested. This is an example of the traditional "black box" problem in which the input is known and the output is known, but one can only infer what happens inside. This is exactly why a structural model is so attractive. With a structure, it is possible to determine the energy imparted to the structure, and the energy actually absorbed by the structure at each and every plastic hinge. Since the "input" side and the "output" side of the so called black box is very similar to the "input" and "output" sides of the structure, it is a reasonable assumption that what happens inside the black box corresponding to the metal is also similar to the known behavior of the real structure.

Using the link established above, an energy criterion for metal fatigue may now be developed. As stated earlier, there is some quantity of irrecoverable energy, $\Delta U_i(\varepsilon)$,

associated with each load cycle. This quantity, $\Delta U_i(\varepsilon)$, will be referred to as the hysteresis loss per cycle, and, except for early cycles (virgin and near virgin state) and near failure, it is essentially a constant with that is dependent upon $\Delta\varepsilon/2$. By summing the hysteresis loss per cycle over the life of a specimen, the total hysteresis loss to failure is,

$$U_f(n,\varepsilon) = \sum_{n=1}^{N_f} \Delta U_i(\varepsilon),\qquad(3.9)$$

where $U_f(n,\varepsilon)$ is the total cumulated energy at failure for a given strain amplitude, and N_f is the number of cycles to failure. Clearly, if $\Delta U_i(\varepsilon)$ becomes a constant and i increases to infinity, then $U_f(n,\varepsilon)$ must also increase to infinity as shown below. If

$$\lim_{i\to\infty} \Delta U_i(\varepsilon) = c \qquad(3.10)$$

where c is some finite constant, then

$$\lim_{n\to\infty} U_F(n,\varepsilon) = \infty. \qquad(3.11)$$

In reality, of course, this cannot happen because the specimen will ultimately fail at some finite value of $n = N_f$. But, on the other hand, if $\Delta U_i(\varepsilon)$ does not become a constant, but instead goes to zero then

$$\lim_{i\to\infty} \Delta U_i(\varepsilon) = 0 \qquad(3.12)$$

and the infinite series (3.9) converges, then,

$$\lim_{n\to\infty} U_f(\varepsilon,n) = k, \qquad(3.13)$$

where k is some finite amount of energy. This is exactly the same situation as that

occurring in the structure. This development is straightforward and logical, but the problem of the "black box" has not been completely resolved.

Microplastic Organization

To reiterate a conclusion reached by Halford (1966) that was presented in Chapter II, the total amount of mechanical energy absorbed by a specimen through the course of 500,000 cycles, if converted to an equivalent amount of thermal energy, would be more than nine times the energy required to melt the specimen. In the case of a steel specimen cycled to the endurance limit (10 million cycles for steel), the thermal equivalent of the mechanical energy absorbed would be sufficient to vaporize the specimen several times over! This leads to one very simple conclusion; that total hysteresis energy and the energy required to create and sufficiently organize a necessary quantity of microplastic regions accumulate at completely different rates.

The first and most obvious step to take in determining the rate at which microplastic regions organize is to establish some sort of baseline. This means nothing more than determining a situation, if one exists at all, in which hysteresis energy and microplastic organization accumulate at rates that are relatively close to one another. Since these two quantities diverge from one another immediately upon the commencement of load cycling, the only hope of establishing such a baseline is when the cycles to failure, N_f, is a number smaller than or equal to one. This is, of course, the energy associated with a monotonic tension test to failure since the rate of energy loss and the rate of organization must be closest to one another at this point.

There has been some disagreement in the literature as to whether a monotonic tension test to failure occurs at $1/2$ of a cycle or $1/4$ of a cycle. Halford and Morrow (1962) chose N_0 (cycle or reversal number in which energy and organization rates are almost coincident) to be $1/2$ of a cycle, while Coffin and Tavernelli (1959) have chosen
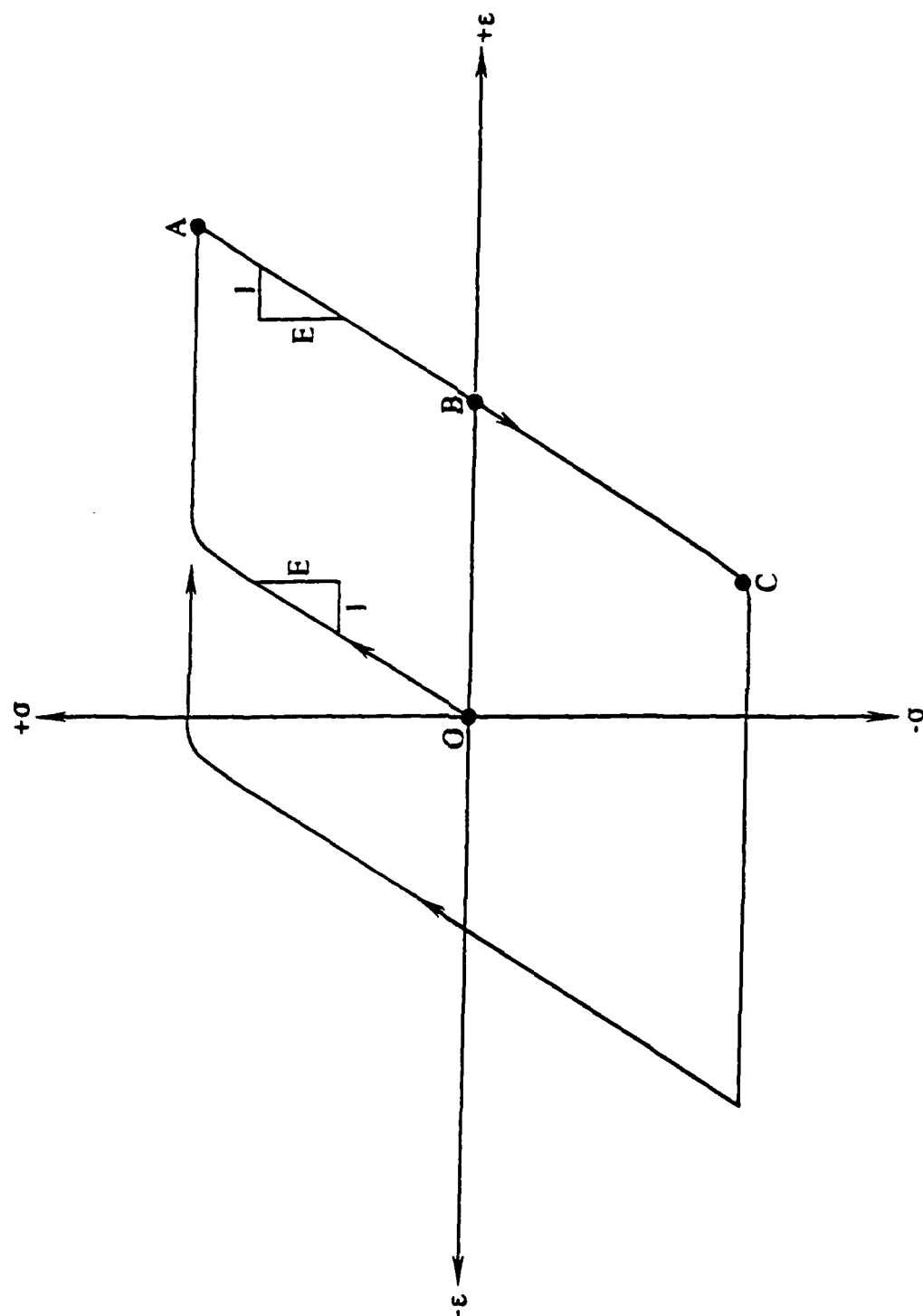
Figure 16. Idealized Fatigue Specimen Failing in One Cycle

N_o to be $1/4$ of a cycle. Rather than arbitrarily setting N_o equal to $1/2$ or $1/4$, N_o may be determined by the following scheme. Shown in Figure 16 is an idealization of a fatigue test that failed in one complete cycle. The curve marked OA is the monotonic stress - strain curve minus some small differential element of stress and strain. The coordinates of points A and B are

$$A(x,y) = (\varepsilon_f - d\varepsilon , \sigma_f - d\sigma),$$

and,

$$B(x,y) = (((\varepsilon_f - d\varepsilon) - (\sigma_f - d\sigma)/E) , 0),$$

respectively. If a specimen were to be subjected to this kind of loading cycle, then it would be damaged to such an extent that it would rupture before it reached point C, and possibly even before it reached point B. In this way, a lower bound for the amount of energy required to cause failure can be established, and is equal to the area OAB (denoted as U_m). In addition, the first order assumption is made that this energy is also equal to the energy required to sufficiently organize a network of microplastic zones, $U_o(\varepsilon)$, or in other terms, the damaging energy required to produce rupture, $U_d(\varepsilon)$. If this is true, then not only is the rate at which total hysteresis energy accumulates, $<\Delta U_i(\varepsilon)>$, strain dependent, but then the damage producing energy rate, $<\Delta U_d(\varepsilon)>$, must also be strain dependent.

Since the damaging energy required to produce rupture is equal to the cumulative energy when N_f is equal to N_o, the situation in which U_m is equal to U_d may be considered as a lower bound on the energy required to sufficiently damage a specimen to cause rupture. If U_d, as a lower bound, is found to be a constant (independent of ε), then failure occurs when $U_d(\varepsilon)$ accumulates to the point where

Halford (1966) suggested that the relationship describing $U_f(\varepsilon, N_f)$ is logarithmic in nature. The heavy solid curve in the lower portion of Figure 17 represents a general

$$\sum_{i=1}^{N_f} U_d(\varepsilon)_i = U_d = U_m.$$ (3.14)

expression for $U_f(\varepsilon, N_f)$ which is shown below,

$$U_f(\varepsilon, N_f) = c(N_f)^b$$ (3.15)

If, as a first approximation, it is assumed that $U_d(\varepsilon)$ accumulates in a linear fashion, then the dashed lines in the lower portion of Figure 17 will represent the accumulated damaging energy that terminates in failure when equation (3.10) is satisfied. The locus of the termination points of the dashed lines, labeled $U_d(\varepsilon) = U_d + F(\varepsilon, N)$, then determines the line of total damaging energy required to cause failure at a given level of strain. This line could be a constant of some very gradually increasing function of strain such that the endurance limit is reached when

$$\sum_{i=1}^{N_f} \Delta U_i(\varepsilon) \leq \sum_{i=1}^{N_f} U_d(\varepsilon)_i = U_d + F(\varepsilon, N),$$ (3.16)

or equivalently,

$$<\Delta U_i(\varepsilon)> \leq <\Delta U_d(\varepsilon)>.$$

In other words, when the average hysteresis loss per cycle is less than the average damagine energy per cycle, $<U_d(\varepsilon)>$, the specimen will not fail. The thin solid lines in this figure show the accumulation of the total hysteresis energy absorbed by the specimen. The difference in slopes between the corresponding $\Sigma \Delta U_d(\varepsilon)$ and $\Sigma \Delta U_i(\varepsilon)$ curves is quite large. It is interesting to notice the vast difference in energy between the heavy solid line and the termination of the dashed lines. This graphical difference represents the amount of energy that is shed harmlessly as heat throughout a specimen's lifetime.
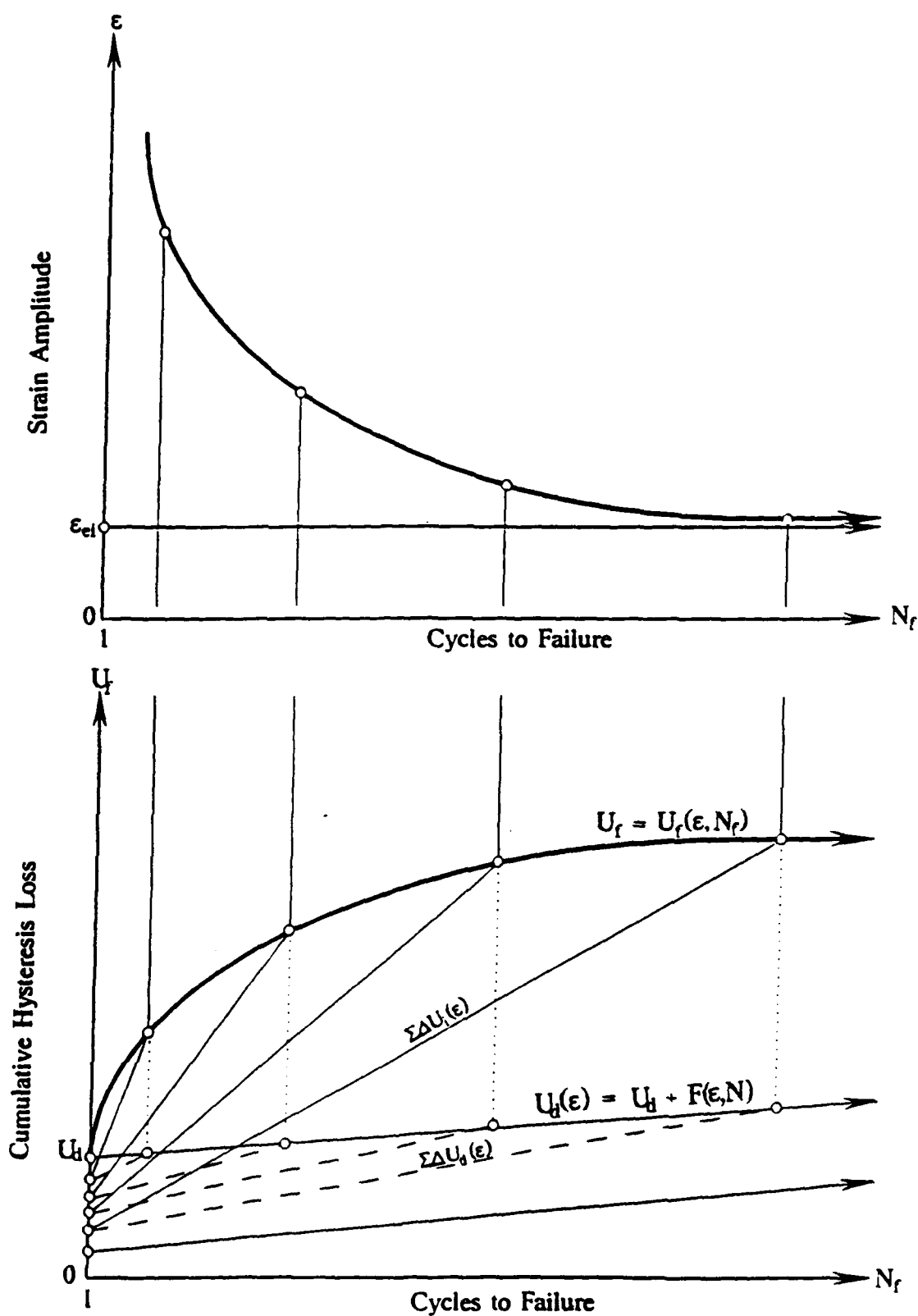
Figure 17. Graphical Representation of the Connection Between Cumulative Energy, Damaging Energy, and Strain Amplitude

CHAPTER IV

EXPERIMENTAL EQUIPMENT AND PROCEDURES

Material and Specimens

The material used throughout the course of this research was AISI 1018 unannealed steel (cold-finished). Since this material is of the gradual yielding type, its stress - strain behavior does not resemble that of the elastic - perfectly plastic material utilized by Neal (1956). Aside from this, it is a commonly used structural material. The chemical composition of the material is shown in Table 1 below. The percentages in Table 1 are consistent with those of the same material provided by The American Society For Metals (II - 1986).

Table 1. Chemical Composition Of Rimmed AISI 1018 Unannealed Steel

Element	Percent By Weight
Carbon	0.16
Manganese	0.75
Phosphorous	0.012
Sulfur	0.016
Silicon	0.04
Nickel	0.04
Chromium	0.04
Copper	0.06
Molybdenum	0.02

The steel was drawn into bar form, from which all specimens were fabricated. From the initial rod stock, ten ASTM Type 2 axial-load tension specimens, shown in Figure 18, and 60 axial-load fatigue specimens, shown in Figure 19, were fabricated. Both types of specimens were machined to ASTM tolerances by turning in a high-speed tracer lathe employing a carbide cutting tool and were meticulously hand polished after turning to remove any surface blemishes or cutting marks visible in a 2X magnifying lens.

Equipment

The fatigue specimens were strain cycled in an MTS series 810 servo valve controlled material testing machine shown in Figure 20. The load cell utilized by the testing machine had a maximum load range of $\pm$ 5.62 kips, which, for the specimens tested, corresponds to a maximum stress of $\pm$ 114.5 ksi. Strain measurements were made with the use of an extensometer that was fabricated from a 3 inch by 1/2 inch strip of 10 gauge steel. The steel strip was bent into a "U" shape, followed by fixing electronic resistance strain gauges configured in a standard "bridge" circuit directly to the back. Calibration was accomplished with a mechanical micrometer and the strain volt meter built directly into the testing machine. The extensometer was calibrated for a maximum full scale strain of $\pm$ 0.022, or $\pm$ 2.2 %.

A common problem associated with fatigue testing has been the procedure and equipment used to mount the specimens in the testing machine. Mounting the specimen in the grips improperly can provide inaccurate results due to back and forth slip, and

bending stresses induced in the specimen by improper alignment. With grips purchased from MTS, and great care while mounting the specimen, these problems were minimized. Diagrams of the grips are provided in Figures 21, 22, and 23.

.750"

.625"

.505"

1"

5/8"

1/16" R

3/8" R

2 - 1/2"

5 - 3/4"

5/8"

3/4" - 10 THD

1"

Figure 18. ASTM Type 2 Axial Load Tension Specimen
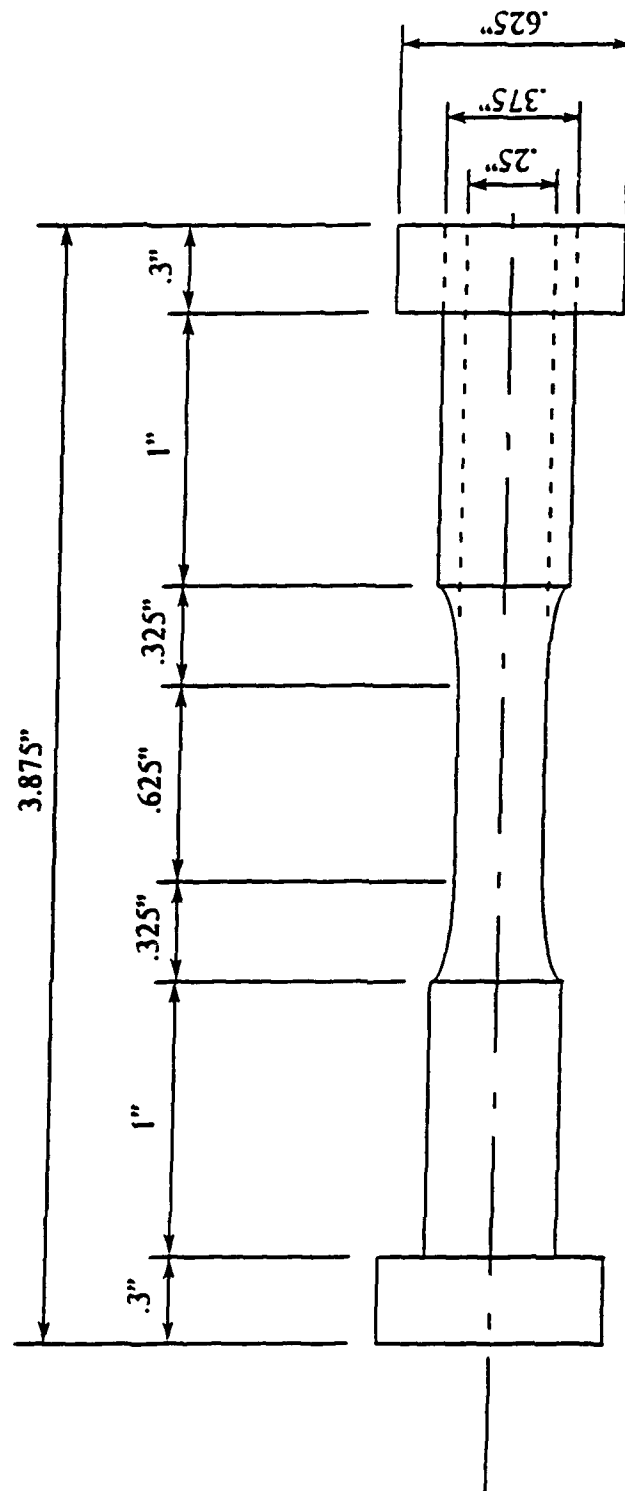
Figure 19. Axial Load Fatigue Specimen
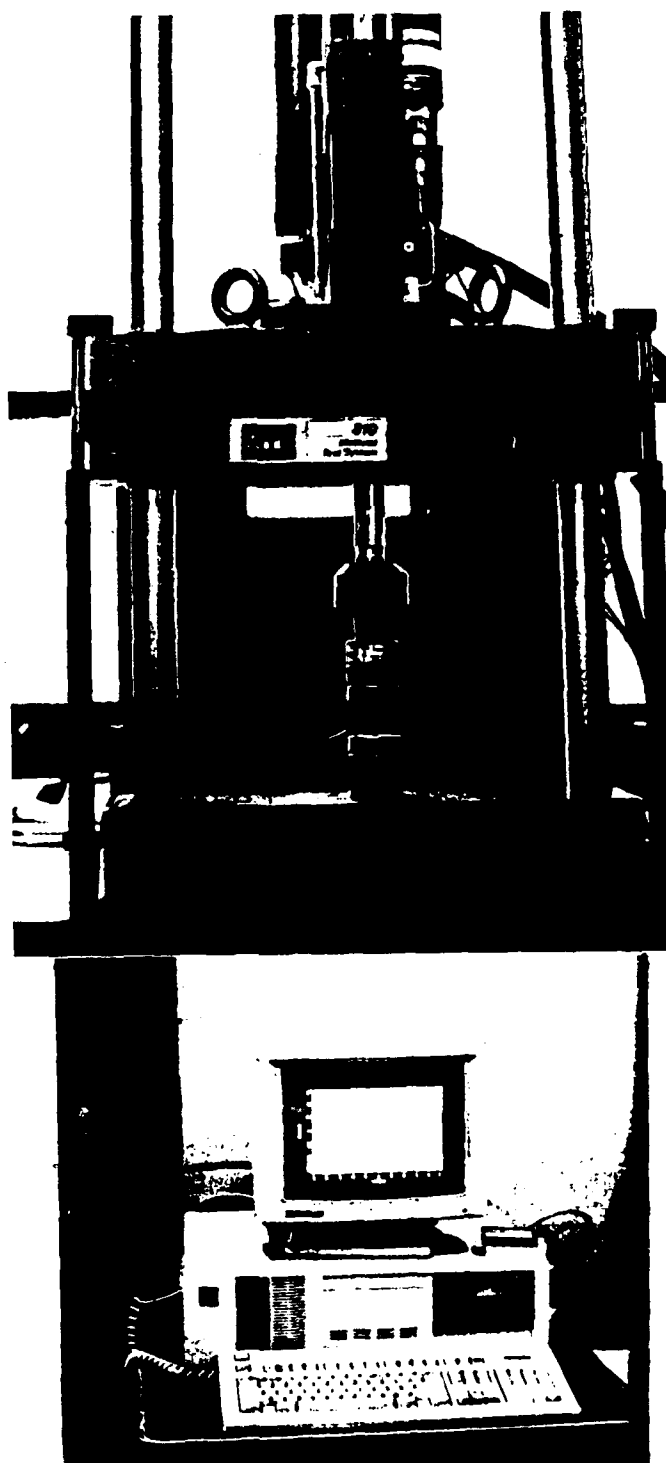
Figure 20. MTS Series 810 Material Test System
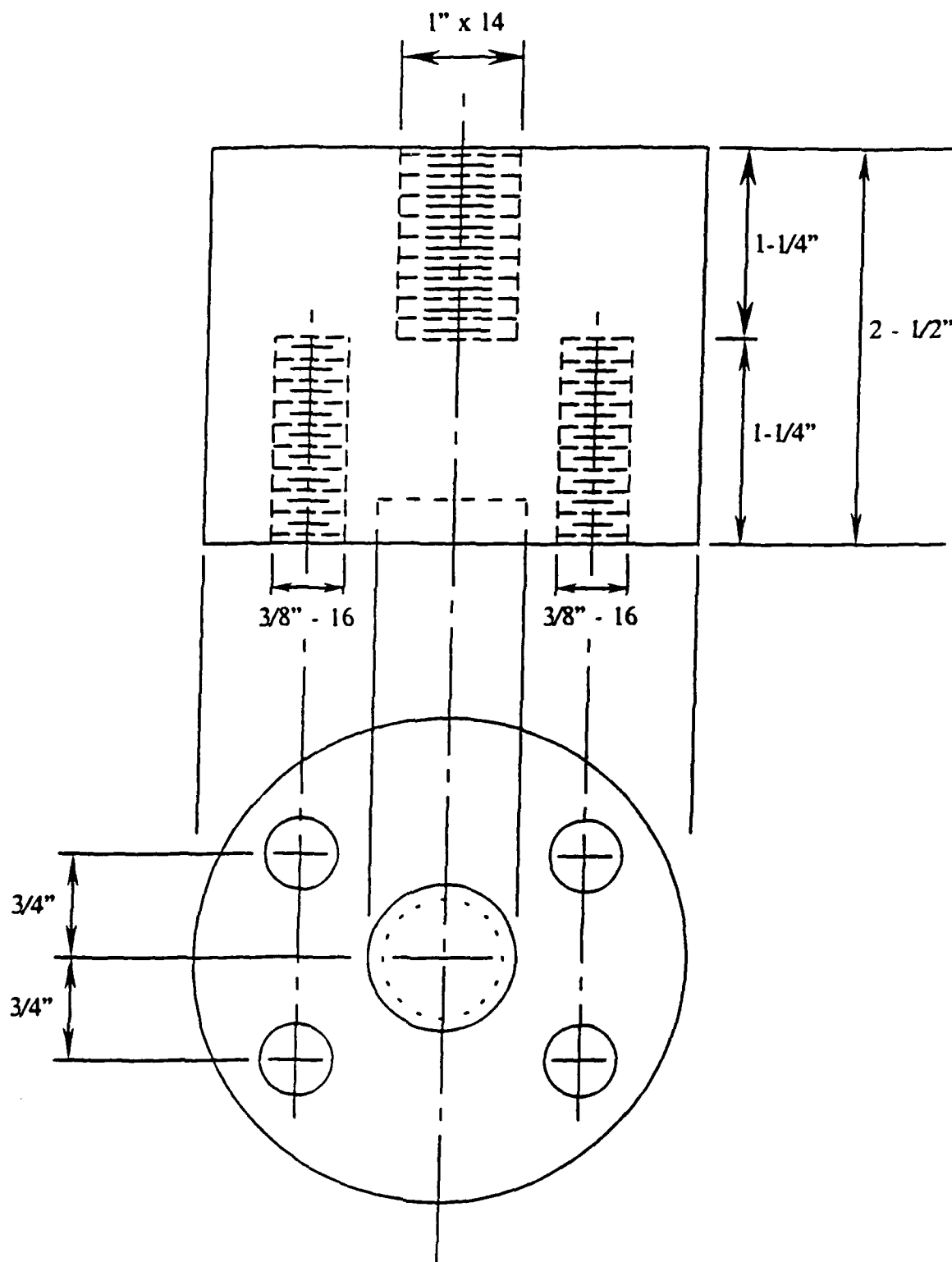
Figure 21. Grip Base Detail Drawing
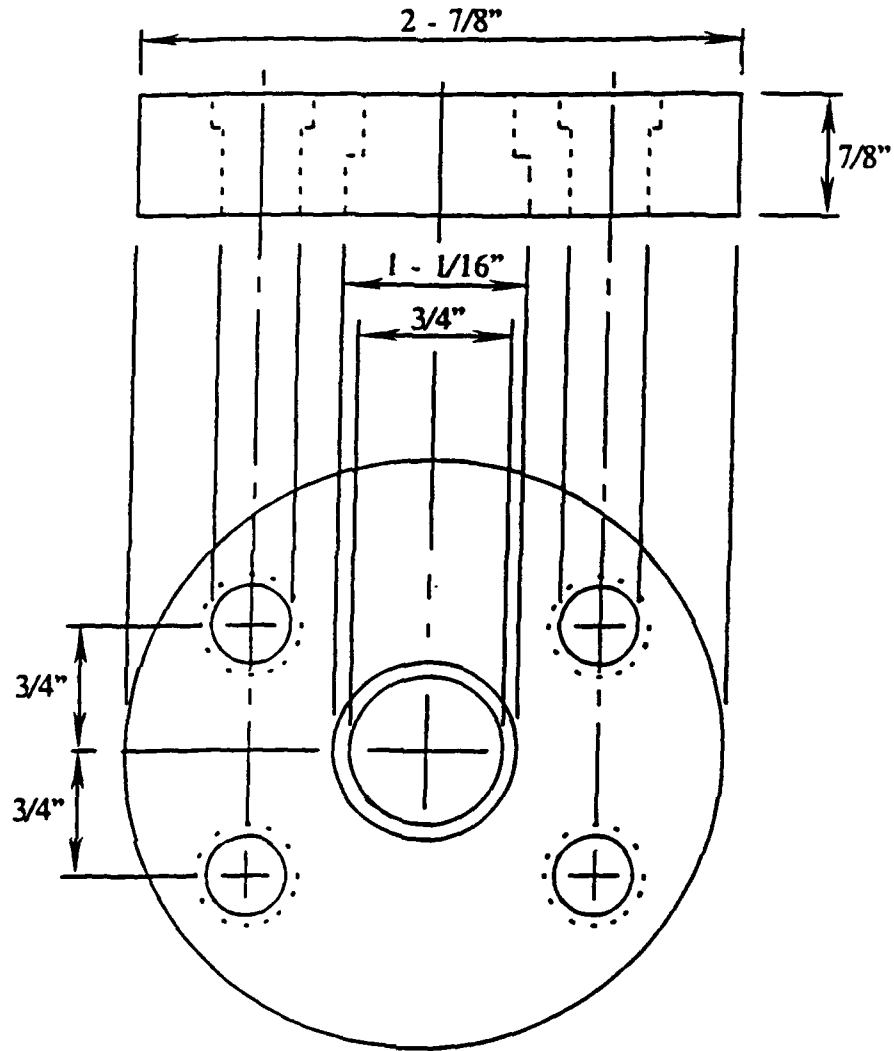
Grip Cap: Side and Bottom View
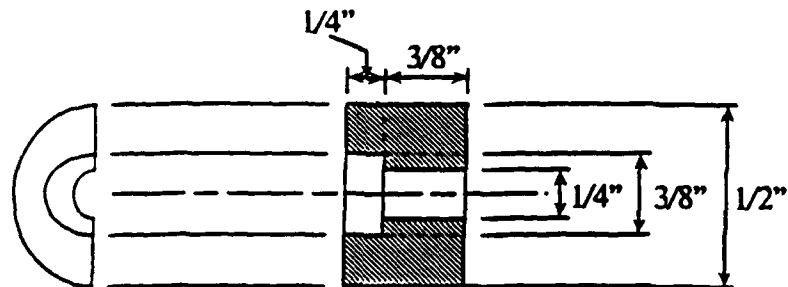
Specimen Retaining Sleeve: Bottom and Inside View

Figure 22. Grip Cap and Specimen Retaining Sleeve
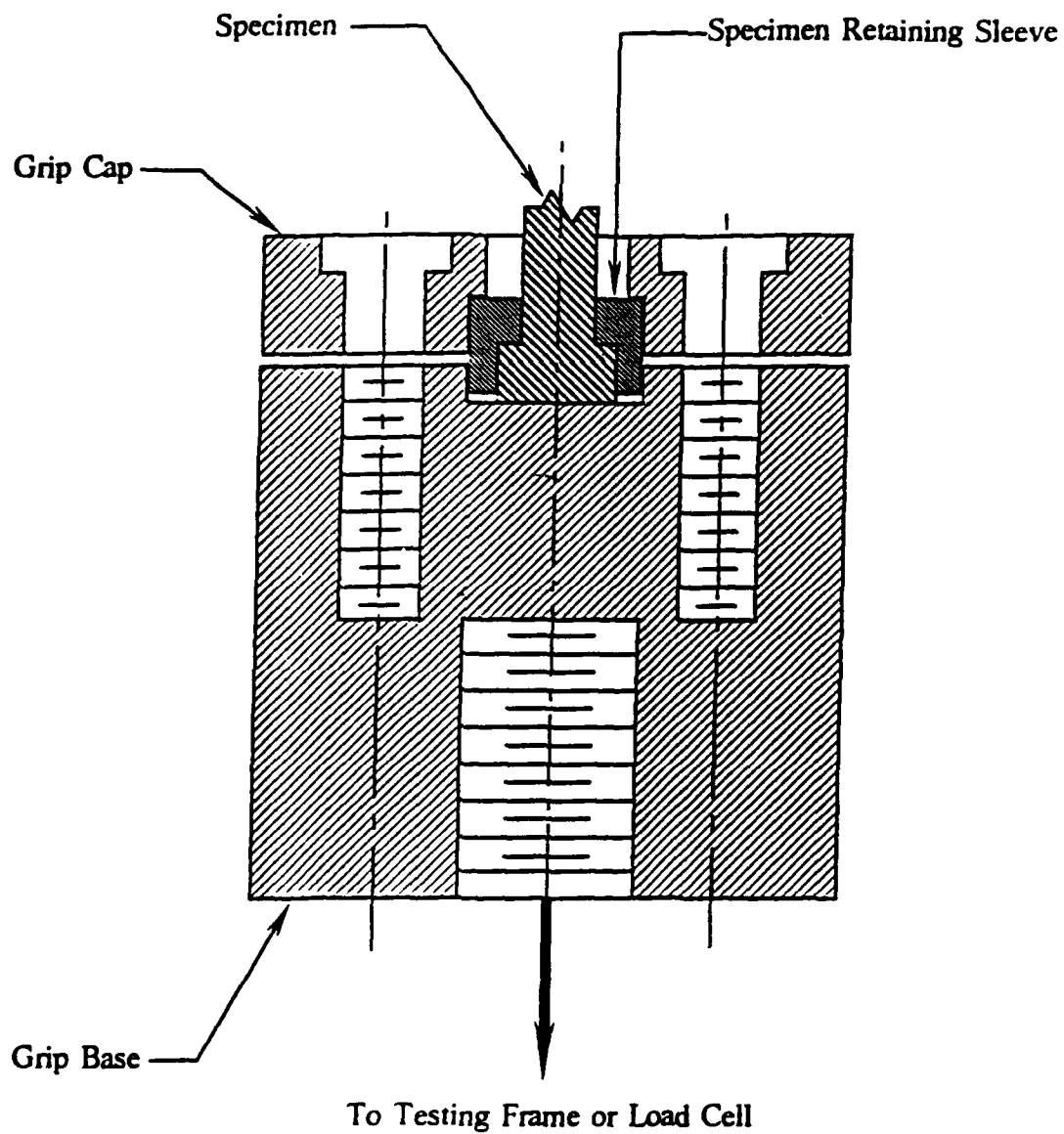
Figure 23. Grip and Specimen Combination Shown in Cross Section

Experimental Preparation

Prior to performing an experiment, the load (strain controlled) program was created. This was accomplished by plotting the desired strain wave form as a function of time. The ordinates of the plot represented the strain to be applied as a percent of the maximum full-scale strain. The slope of the strain wave represented the desired strain rate. The strain rate varied for each individual specimen depending on the maximum and minimum strain levels, but the cycling rate was held constant at 10 seconds per cycle. The strain program was then loaded directly into the MTS machine's microprofiler along with the number of "repeats," or cycles.

To ensure proper alignment of the specimen prior to mounting, a seating stud was fabricated and screwed directly into the load cell. The diameter of the seating stud was identical to that of the retaining clamps used to secure the specimen. By positioning the seating stud in the lower grip base, followed by tightening the lower grip mounting bolt to the machine base, proper alignment was achieved.

This procedure was followed by the actual mounting of the specimen into the upper grip. Great care was exercised to obtain an even pressure distribution across the specimen's "button" end. A feeler gauge was used to measure the space between the grip cap and the grip base. The grip was screwed into the load cell when the space between the grip cap and base was equal on all sides. The load frame cross head was then lowered and the same procedure was followed to mount the bottom of the specimen to the lower grip.

Before mounting the extensometer, small strips of tape were placed on the specimen in the position that the extensometer was to be mounted. The tape was used to eliminate the possibility of scratching the specimen, and minimize the slippage between the specimen and the extensometer. The extensometer was fixed to the specimen with small springs and connected directly to the MTS controller. Upon

completing the specimen and extensometer mounting, the data acquisition system was connected directly to the MTS controllers and the test run. Figure 24 shows a schematic of a typical experiment in process.

Data Acquisition and Post - Processing

With the use of a computer and a digital - analog data acquisition system, stress and strain data for every load cycle was obtained. This proved to be very useful in recognizing gentle trends throughout the lives of the individual specimens. A sampling rate of 100 samples per cycle was used throughout this research and yielded very well defined stress - strain hysteresis loops. Figures 25 and 26 display the same (typical) hysteresis loop plotted with and without the data points being shown, respectively. The smoothness of the curve in Figure 26 was determined to be quite adequate for the purposes of this research. It is interesting to note that Figure 26 is actually constructed with the data points connected by straight line segments.

The data acquisition system provided an excellent means for obtaining data because it allowed for direct reduction of the data with the use of software developed "in house." All post - processing software was developed by S.S. Michels using Microsoft's version 5.0 Fortran 77 compiler.

Equation (3.8) requires the integration of hysteresis loops with respect to a specific direction over a contour surface. The format of the acquired data allowed equation (3.8) to be approximated with the use of the trapezoidal rule shown in equation (4.1).

$$\Delta U_i(\epsilon) = \oint \sigma \, d\epsilon = \sum_{i=1}^{nd} \frac{1}{2} (\sigma_i + \sigma_{i-1}) (\epsilon_i - \epsilon_{i-1}), \qquad (4.1)$$

where nd is the number of data points per cycle which varied between 98 and 102. The summation of trapezoidal areas also made checking the software for accuracy
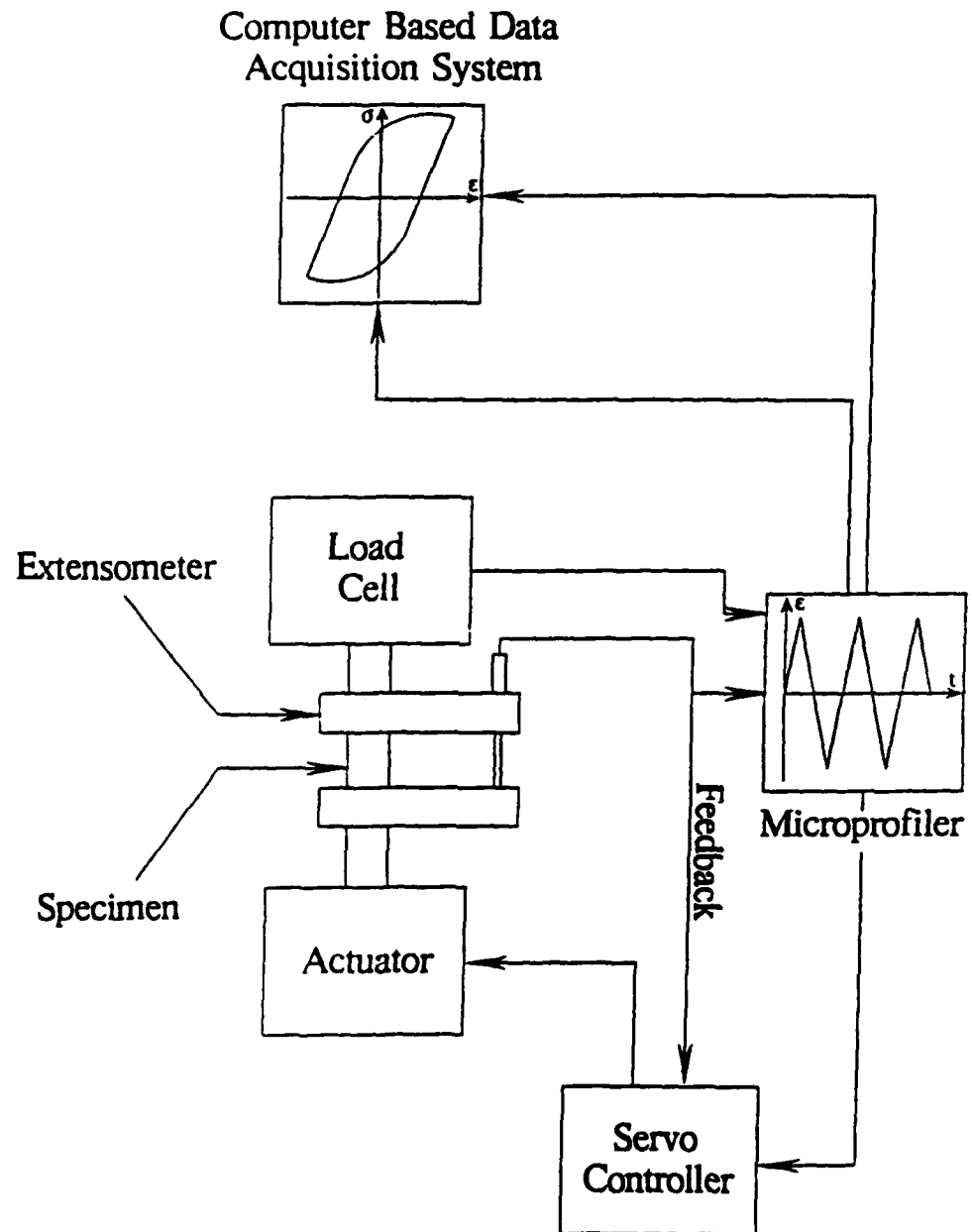
Figure 24. Schematic of Strain Controlled Fatigue Experiment in Progress
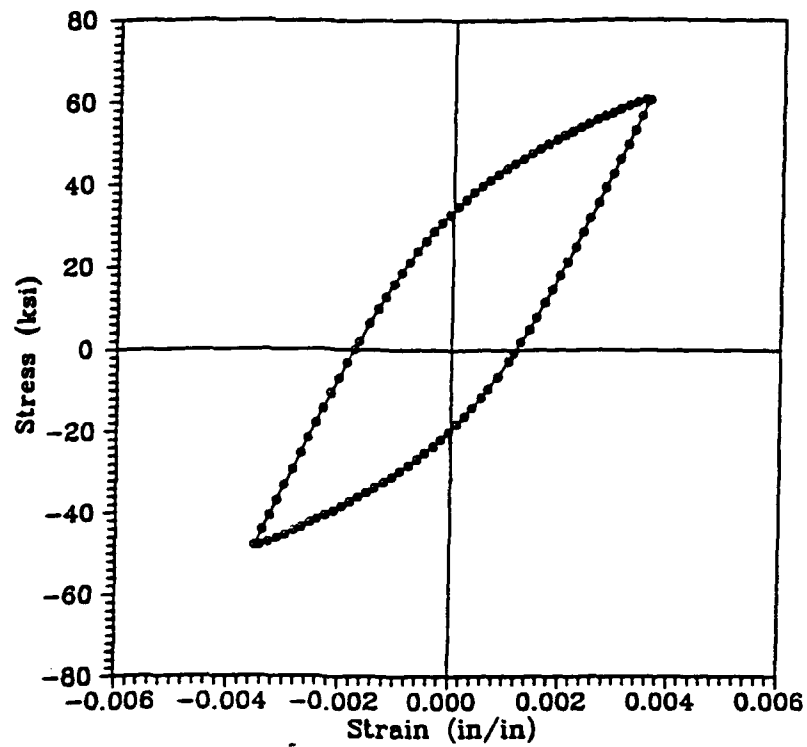
Figure 25. Typical Hysteresis Loop Displayed with Data Points
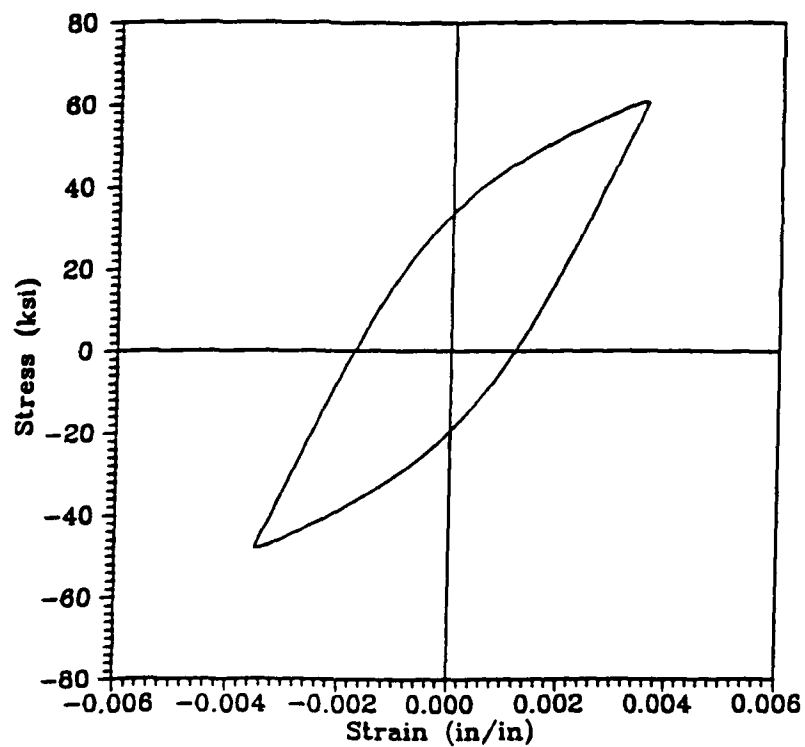
Figure 26. Typical Hysteresis Loop Displayed without Data Points

possible, although very laborious. As an example, the program used to integrate

equation (3.8) is provided in Appendix C.

CHAPTER V

EXPERIMENTAL RESULTS

The principles presented in Chapter III have served as the basis for the experiments performed and the analyses to be presented here. The following material will discuss each type of experiment performed throughout this research, and the results associated with each.

Material Properties

As mentioned previously, ten ASTM Type 2 axial load tension specimens (Fig. 19) were fabricated and loaded to failure. The mechanical properties measured during these ten tests are presented in Table 2. These values are consistent with those provided by The American Society for Metals (II - 1986). All ten specimens exhibited a stress - strain response that was similar to that of Figure 27, and can be categorized as the gradual yielding type. Because the material was of the gradual yielding type, the yield point was measured using the 0.2% offset method and the stress - strain diagrams obtained with the use of an X - Y recorder driven by electronic signals received directly from the load cell and the strain measuring device.

Completely Alternating Cyclic Strain (Two - Sided)

These experiments, which made up the majority of cyclic tests carried to failure, were performed under completely reversed, or alternating strain (mean strain equal to zero and range ratio equal to -1). The endurance limit for this type of experiment, with regard to the structural model, is best characterized by the situation known as alternating plasticity. In all, sixteen specimens were tested under these conditions at varying strain amplitudes. For the sake of completeness, analyses of the type described in Chapter II have been performed. When the approach originally presented by Basquin (1910) is

Table 2. Uniaxial Tensile Properties of Rimmed AISI 1018 Unannealed Steel

Specimen Name	Diameter (inches)	Gage Length (inches)	Yield Strength[**] (psi)	Ultimate Strength (psi)	Elongation (%)	Reduction in Area (%)
AX121	0.505	2.000	70,150	77,090	18.05	61.83
AX122	0.506	2.000	69,620	77,280	18.40	61.74
AX221	0.506	2.000	71,610	78,270	17.95	61.25
AX222	0.506	2.000	72,360	78,570	18.65	61.49
AX321	0.506	2.000	72,110	79,370	17.20	58.75
AX322	0.506	2.000	71,610	79,370	17.25	58.49
AX421	0.506	2.000	67,880	74,490	19.10	61.98
AX422	0.506	2.000	68,130	74,390	18.70	62.47
AX521	0.506	2.000	72,110	79,170	18.40	61.00
AX522	0.506	2.000	72,110	79,170	18.30	61.49
Average			70,769	77,717	18.20	61.05

[**]Yield Strength is obtained at 0.2% offset.
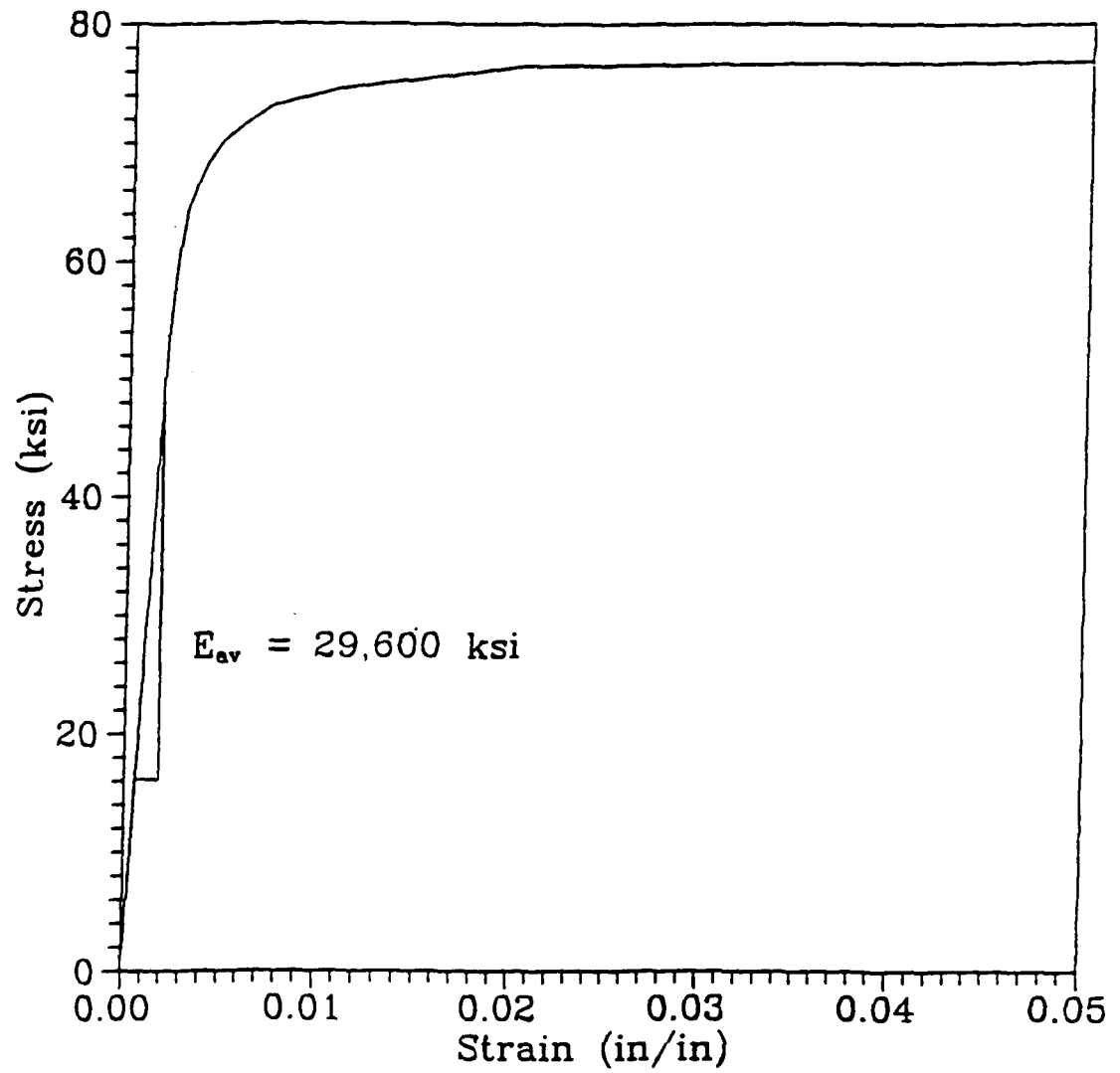
Figure 27. Stress - Strain Diagram for Rimmed AISI 1018 Unannealed Steel

applied to the experiments performed in this research, equations (2.7) and (2.9) take the following form

$$\sigma_a = \sigma_f'(2N_f)^b = 79.7(2N_f)^{-0.05857}, \qquad (5.1)$$

and

$$\frac{\Delta \varepsilon_p}{2} = \varepsilon_f'(2N_f)^c = 0.2034(2N_f)^{-0.5081}, \qquad (5.2)$$

which are graphically displayed in Figures 8 and 9 respectively. The combination of these expressions, known as the strain - life relation, is displayed in Figure 10. The data shown in these figures presents quite a bit of scattering which does not lend much credence to the methods of analysis presented in Chapter II.

As mentioned in Chapter II, the energy associated with an individual hysteresis loop, $\Delta U_i(\varepsilon)$, is essentially a constant. This is true with the exception of the first and last ten to thirty cycles. The hysteresis loss per cycle for specimens that were cycled at high strain amplitudes ($\Delta \varepsilon / 2 > 0.01$) generally decreased from the very first cycle and eventually stabilized after fifteen to twenty cycles. As strain amplitudes were decreased, the hysteresis loss per cycle increased to a peak after four to ten cycles, and then decreased to a stabilized value after an additional ten to fifteen cycles. Finally, at very low strain amplitudes, the hysteresis loss per cycle began at a very low level and increased to a peak fifteen to twenty five cycles later. This peak was followed by a short decrease in hysteresis loss per cycle over a span of zero to five cycles to its respective stabilized value. Figures 28 and 29 display graphs of hysteresis loss per cycle versus cycles for four experiments tested at two different strain amplitudes. These graphs, with the exceptions discussed above, typify results obtained throughout the course of these experiments.

By utilizing equation (4.9), the cumulative hysteresis loss as a function of the
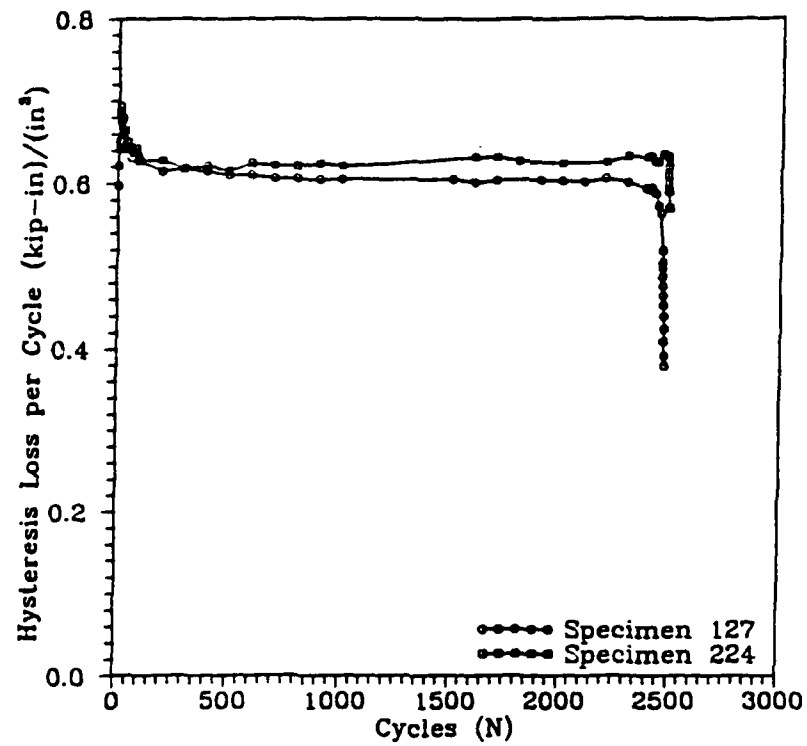
Figure 28. Hysteresis Loss per Cycle vs Cycles $\Delta\varepsilon/2 = 0.006$ in/in
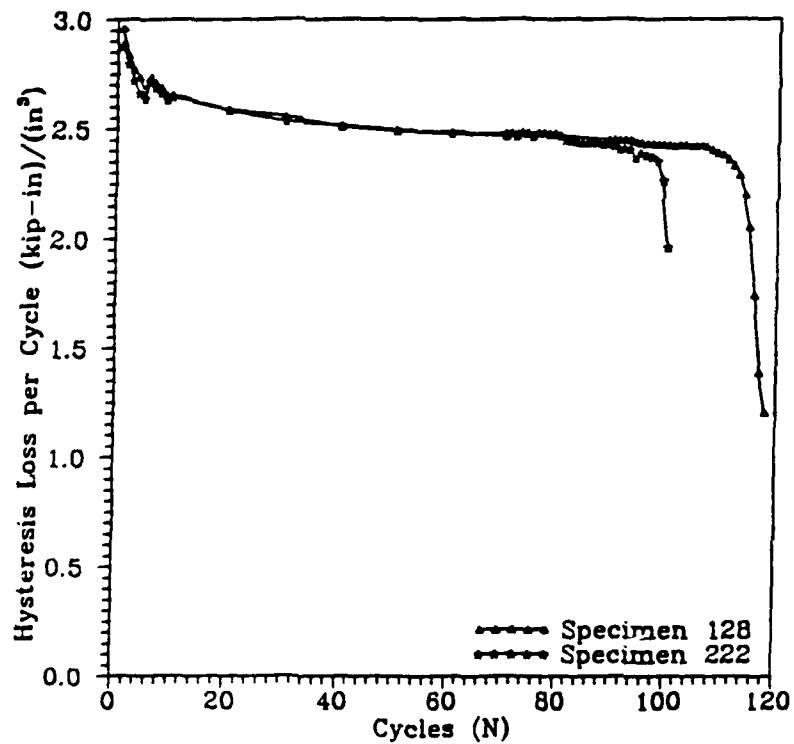
Figure 29. Hysteresis Loss per Cycle vs Cycles $\Delta\varepsilon/2 = 0.015$ in/in

number of cycles is found. Since the hysteresis loss per cycle is essentially a constant throughout the bulk of a specimen's life, it may be displayed as a straight line, the slope of which is equal to the average hysteresis loss per cycle, $<\Delta U_i(\varepsilon)>$. As described in Chapter III, this is the rate at which irrecoverable energy accumulates. The values of $<\Delta U_i(\varepsilon)>$ for the sixteen specimens cycled to failure may be found in the rightmost column of Table 3 in Appendix A. Figures 30 and 31 display the cumulative hysteresis loss per cycle as a function of cycles corresponding to the results shown in Figures 28 and 29 respectively. Figures 30 and 31 were made without showing the actual data points for clarity. It can be seen that, in each case, the curves lie almost directly on top of one another. This provides evidence of reproduceabilty for these experiments.

Although the hysteresis loss per cycle is nearly a constant with respect to the number of cycles, it is, however, not a constant for varying strain amplitudes. The average hysteresis loss per cycle is a monotonically increasing function of strain amplitude. That is

$$< \Delta U_i> = F(\frac{\Delta \varepsilon}{2}).\qquad (5.4)$$

The dependence of the average hysteresis loss per cycle upon $\frac{\Delta \varepsilon}{2}$ is best represented by the tri-linear diagram shown in Figures 32 and 33. As indicated in these figures, the average hysteresis loss per cycle increases as the strain amplitude increases. An important point to notice is the variation of the slopes of the linear portions of the figures. The slopes for the three linear portions of Figures 32 and 33 are

for $0.0009143 < \Delta\varepsilon/2 < 0.0022$, $m = 58.814$

for $0.0022 < \Delta\varepsilon/2 < 0.0055$, $m = 127.795$

for $0.0055 < \Delta\varepsilon/2 < 0.015$, $m = 211.195$

Although an exact interpretation of these differing slopes is not known at this time, one may infer that they are related to different "modes" or mechanisms of failure for varying
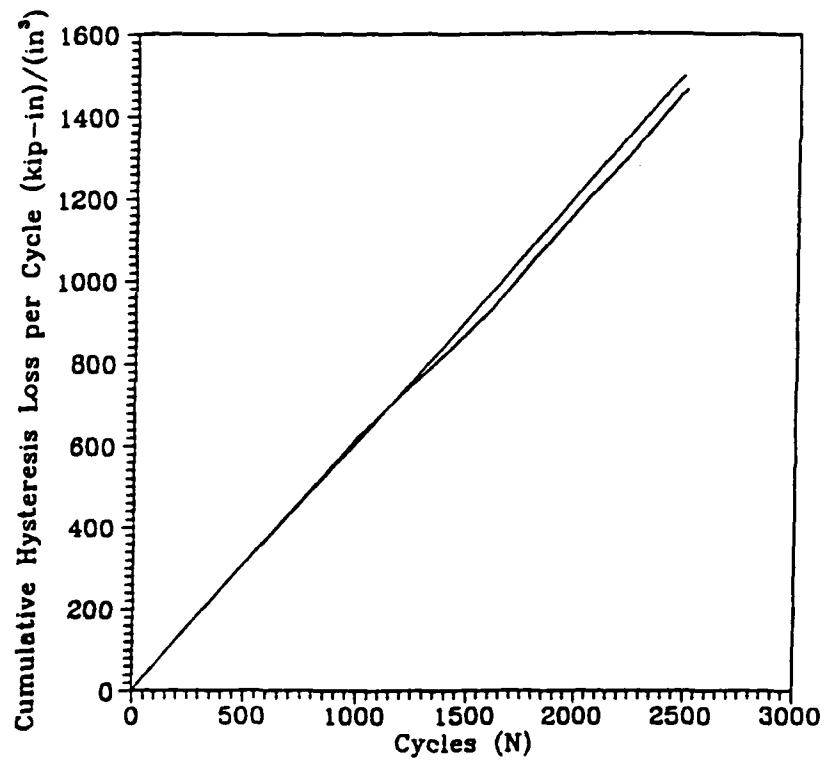
Figure 30. Cumulative Hysteresis Loss Corresponding to Figure 28
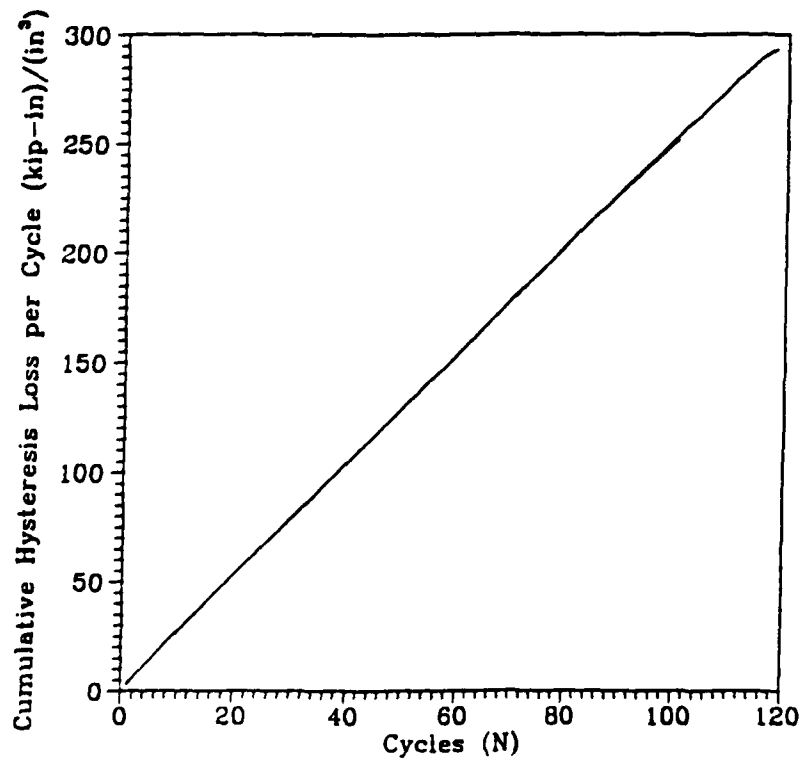
Figure 31. Cumulative Hysteresis Loss Corresponding to Figure 29
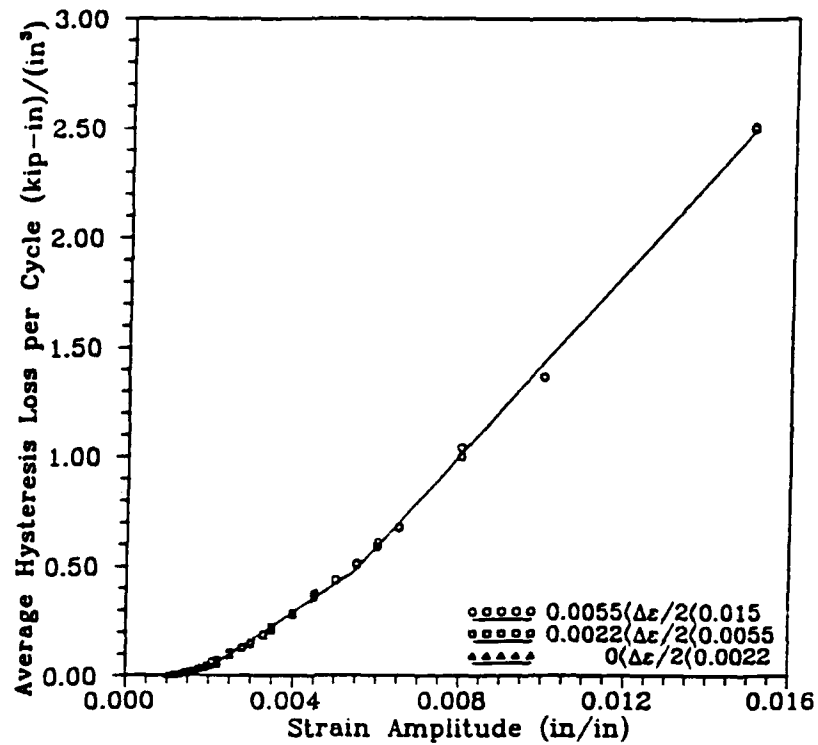
Figure 32. Average Hysteresis Loss per Cycle as a Function of Strain Amplitude
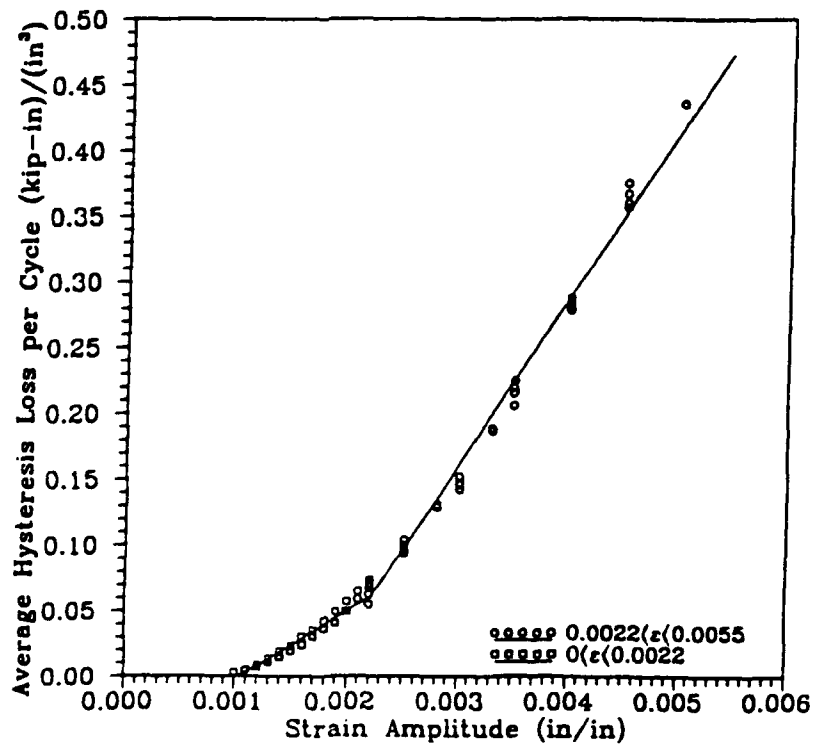
Figure 33. Average Hysteresis Loss per Cycle as a Function of Strain Amplitude: Expanded View

levels of strain amplitude. As in the case of structures, the final collapse mechanism is heavily dependent upon the magnitude of the loads being applied; which has been shown by Neal (1956). Therefore, it is possible that an increase or decrease in the strain amplitude causes a different type of microplastic network to develop, and thus, different rates of microplastic organization and energy accumulation.

An important feature shown in Figure 33 is that the curve with the smallest slope crosses the abscissa at a strain amplitude of

$$\frac{\Delta \varepsilon}{2} = \varepsilon_{th} = 0.0009143$$

where ε_{th} is the threshold of detectable hysteresis. This is the strain at which the average hysteresis loss per cycle becomes zero. Recall from equations (3.12) and (3.13) that as the hysteresis loss per cycle becomes zero, the number of cycles approaches infinity. Therefore, ε_{th} must define the endurance limit of the material for the case of completely alternating strain. If the average value for the yield stress of the material given in Table 2 is divided by the standard value for Young's modulus of elasticity (E = 29,000 ksi), as defined by The American Institute of Steel Construction (1989), the yield strain is found to be

$$\varepsilon_y = \frac{\sigma_y}{E} = \frac{70.769\ ksi}{29,000\ ksi} = 0.00244.$$

Therefore, the strain at which hysteresis can no longer be detected is smaller than the calculated yield strain, and the material, by traditional standards, is still considered to be elastic. Since the material is elastic at $\varepsilon = \varepsilon_{th}$, the stress is readily computed as,

$$\sigma_{th} = E\varepsilon_{th} = 29,000\ ksi(0.0009143) = 26.515 ksi.$$

This value for σ_{th} is 34.12% of the average ultimate strength of the material which is remarkably close to the 1/3 S_u predicted by Goodman for completely alternating stress

in Chapter II.

It is important to note that the data displayed in Figures 32 and 33 are not all taken from specimens that ruptured. Five specimens were subjected to a wide variety of strain amplitudes under what is known as a "staircase" loading program. A staircase pattern of loading consists of cycling a specimen at a specified strain amplitude until its hysteretic response has stabilized, and then increasing or decreasing the strain amplitude to a new level and then it is cycled again. Figure 34 displays a graphical representation of a typical staircase program. This approach was found to be very useful in determining the average hysteresis loss per cycle for many different levels of strain amplitude, and it saved a great deal of time and effort that would otherwise have been expended if the specimens had been cycled to failure. The data acquired using the staircase method are shown in Table 4 of Appendix A.

Both the staircase method and the introduction of overload cycles proved useful in examining the material's response to varying spectra of strain amplitude. During the course of several experiments, specimens were subjected to several cycles of increased strain amplitude, after which the strain amplitude was returned to the original level. An example of several of the hysteresis loops generated during experiments of this kind is shown in Appendix B. Figure 35 displays the hysteresis loss per cycle versus cycles for a specimen that was subjected to a 22% strain amplitude increase for 5 out of every 500 cycles until it failed. The overloads produced a 47.4% increase in hysteresis loss which quickly dissipated upon returning to the original strain amplitude. All data acquired from overload tests were in direct correspondence with specimens tested at the same strain amplitudes without overloads. Therefore, it appears that small overloads of limited duration have little or no effect on the overall response of the material.

If the average hysteresis loss per cycle is plotted as a function of cycles to failure, the diagram shown in Figure 36 results. The data is best represented by the equation
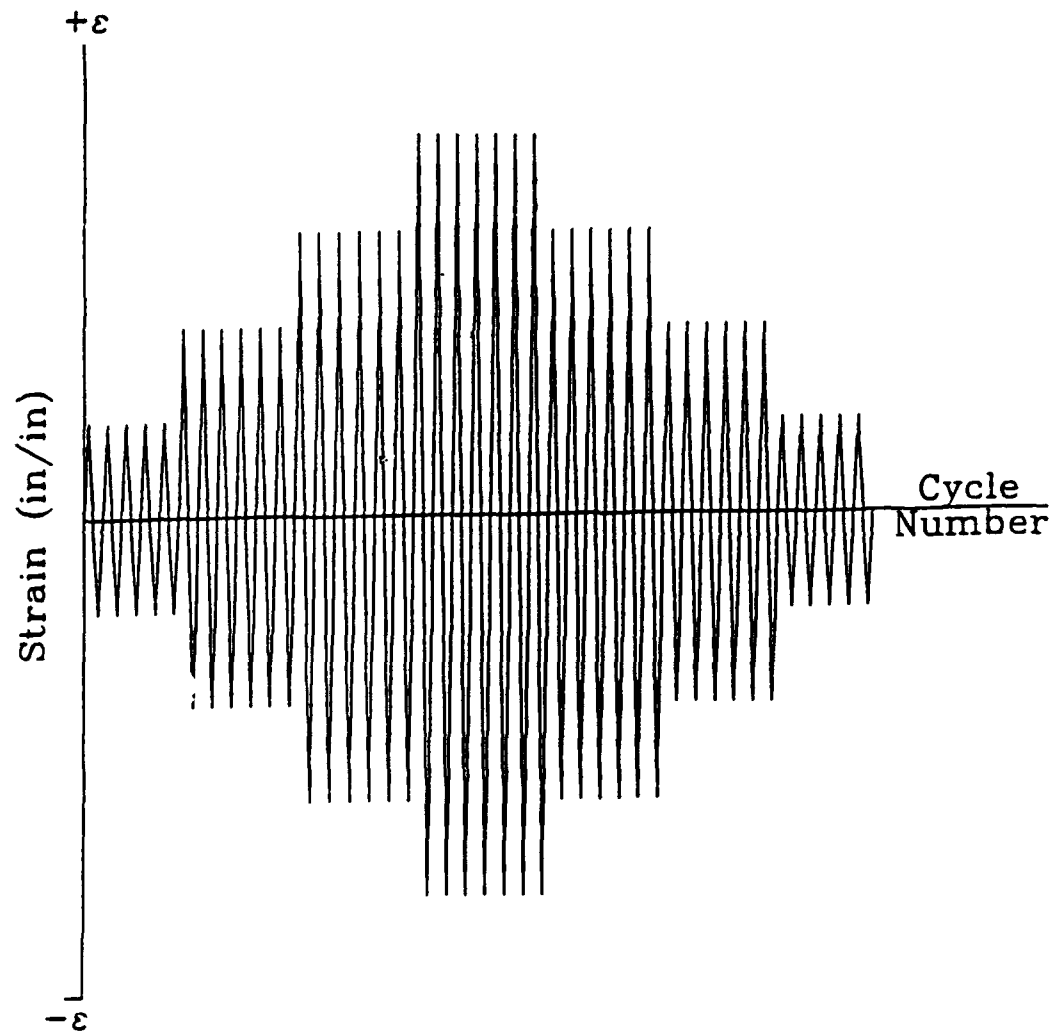
Figure 34. A Typical "Staircase" Loading Program
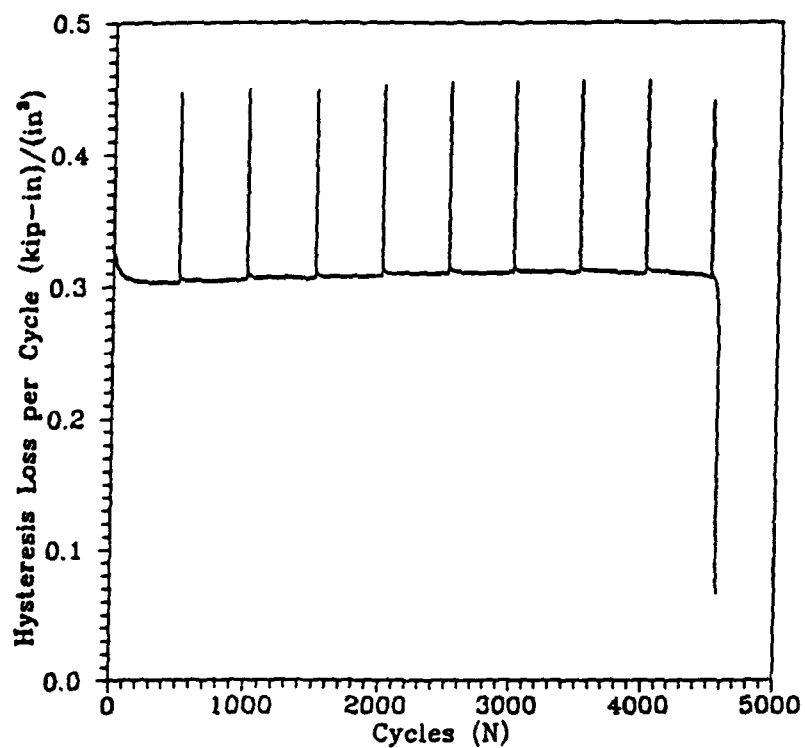
Figure 35. Hysteresis Loss per Cycle vs Cycles for a Specimen Subjected to Overloads

$$\langle \Delta U_i(\varepsilon) \rangle = 32.496(N_f)^{-.6314}$$
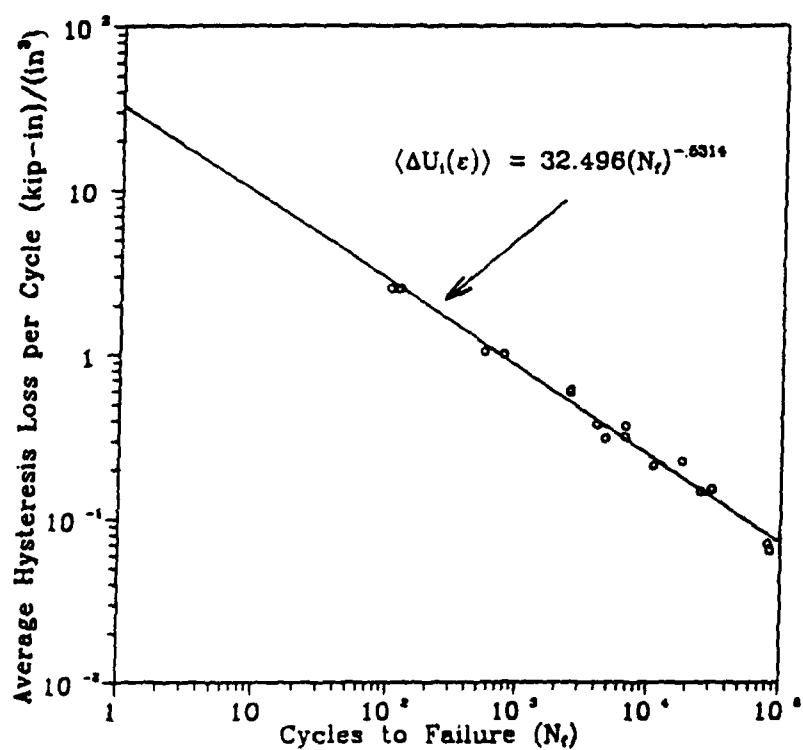
Figure 36. Average Hysteresis Loss per Cycle vs Cycles to Failure

$$<\Delta U_i(\varepsilon)> \ = \ a(N_f)^{-b} \ = \ 32.496(N_f)^{-.5314}. \tag{5.5}$$

Figure 36 further supports the implications of equations (3.12) and (3.13). Solving equation (5.5) for N_f, the following equation results,

$$N_f \ = \ (\frac{a}{<\Delta U_i(\varepsilon)>})^{\frac{1}{b}} \ = \ (\frac{32.496}{<\Delta U_i(\varepsilon)>})^{\frac{1}{.5314}}. \tag{5.6}$$

It is clearly shown by equation (5.6) that as $<\Delta U_i(\varepsilon)>$ approaches zero, N_f approaches infinity. Therefore, it is reasonable to infer that the average hysteresis loss per cycle may be used as an index to help define the endurance limit of a material.

Equation (3.9) is an expression used to determine the cumulative hysteresis loss at failure. Since equation (5.5) is an expression relating the average hysteresis loss to cycles at failure, equation (3.9) should be equivalent to equation (5.5) multiplied by N_f. This is demonstrated by

$$U_f(\varepsilon, N_f) \ = \ N_f <\Delta U_i(\varepsilon, N_f)> \ = \ N_f[32.496(N_f)^{-.5314}]$$

$$= \ 32.496(N_f)^{.4686}. \tag{5.7}$$

This equation is of the form presented as equation (3.15). Figure 37 is a graph of $U_f(\varepsilon, N_f)$ as determined by equation (3.9). The curve of Figure 37 is also of the form of equation (3.15) and is given by

$$U_f(\varepsilon, N_f) \ = \ a(N_f)^b \ = \ 32.636(N_f)^{.4677}. \tag{5.8}$$

The consistency between equations (5.7) and (5.8) is truly remarkable. From Figures 32, 33, and 34 it may be observed that the average hysteresis loss per cycle is dependent on both the strain amplitude and the number of cycles to failure, but it is not intuitively obvious that the cumulative hysteresis loss would have such a strong dependence on the same parameters. A better illustration of this dependence is shown in the three

$$U_f(\varepsilon, N_f) \;=\; 32.636(N_f)^{.4677}$$
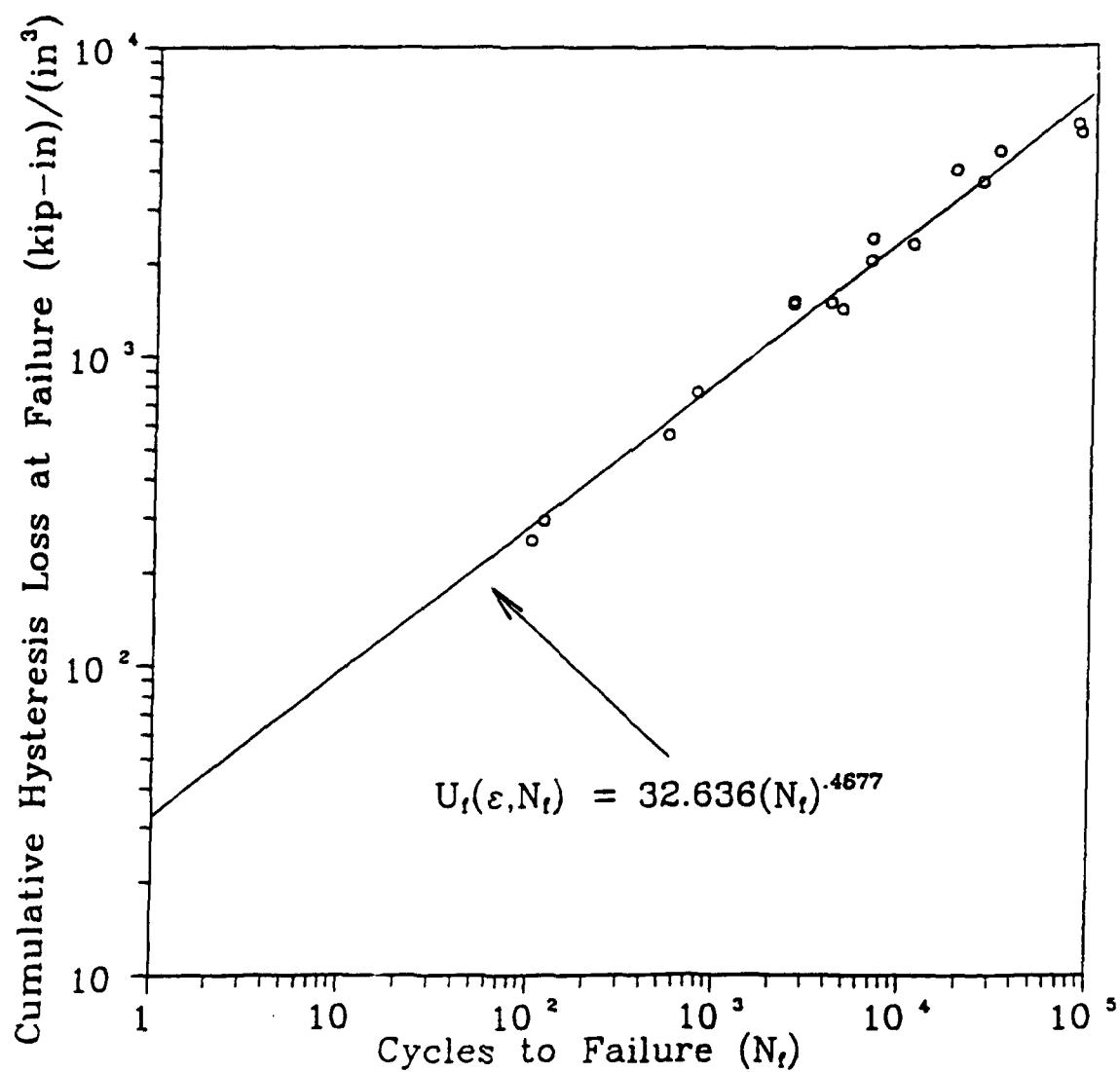
Figure 37. Cumulative Hysteresis Loss at Failure vs Cycles to Failure

dimensional plot of Figure 38. Recall Figure 17 presented in Chapter III. In comparing Figure 17 to Figure 38, one must notice that the upper portion of Figure 17 is identical to the projection of the curve in Figure 38 onto the $\Delta\epsilon/2$ - N_f plane and the lower portion of Figure 17 is identical to the projection of the curve in Figure 38 onto the U_f - N_f plane. Figure 39 displays graphs of both of these projections onto their respective plane surfaces. It is interesting to notice that the material's response to cyclically applied loads when $N_f < 10^4$ differs both qualitatively and quantitatively from the response when $N_f > 10^4$. The value of $N_f = 10^4$ cycles is the traditional separation between low and high cycle fatigue behavior. The fact that the cumulative hysteresis loss increases at such an incredible rate as the strain amplitude decreases and the number of cycles to failure increases confirms Martin's (1961) assertion that the total hysteresis loss cannot itself be equated to fatigue damage. If this were not so, a specimen cycled at a high strain amplitude should "live" longer than a specimen cycled at a low strain amplitude simply because the energy absorbed at the lower strain amplitude would be greater than that of the higher strain amplitude.

Non - Alternating Cyclic Strain (One - Sided)

In this series of experiments, the specimens were cycled between a constant maximum tensile strain and zero. In other words, the strain range was equivalent to the maximum strain, and the strain amplitude was equivalent to one half of the maximum strain. Although the strain range of a one-sided experiment cycled between ϵ_{max} and 0 is one half of the strain range of a two sided experiment cycled between $+\epsilon_{max}$ and $-\epsilon_{max}$, the hysteresis loops appear to be quite different. The difference between one and two-sided hysteresis is best described by the loops in Figure 40. Since these two loops are so different from one another, one might suspect that there can be no correlation between one-sided and two-sided hysteresis. Interestingly enough, this is not true.
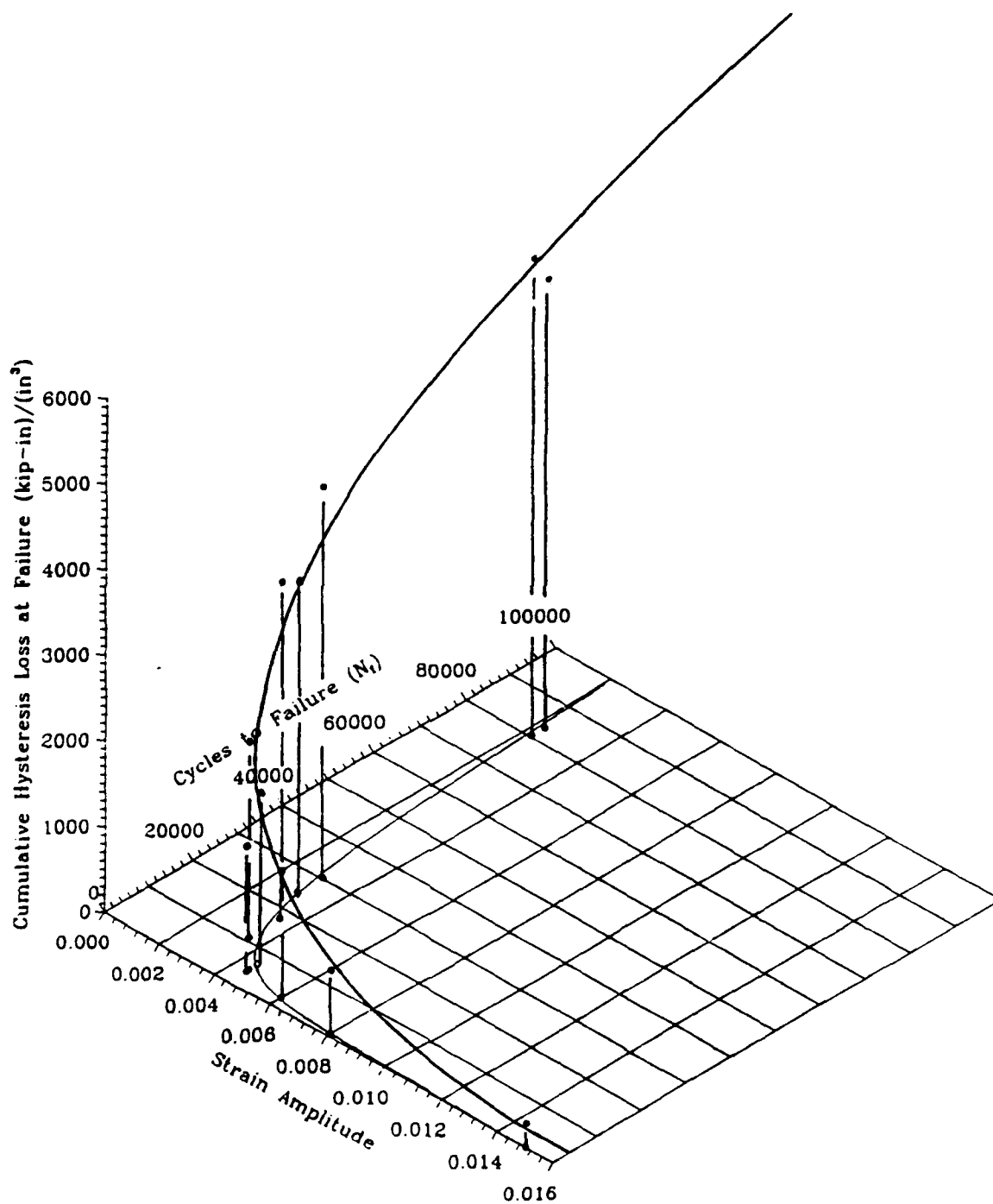
Figure 38. Cumulative Hysteresis Loss at Failure as a Function of $\Delta \epsilon / 2$ and N_f
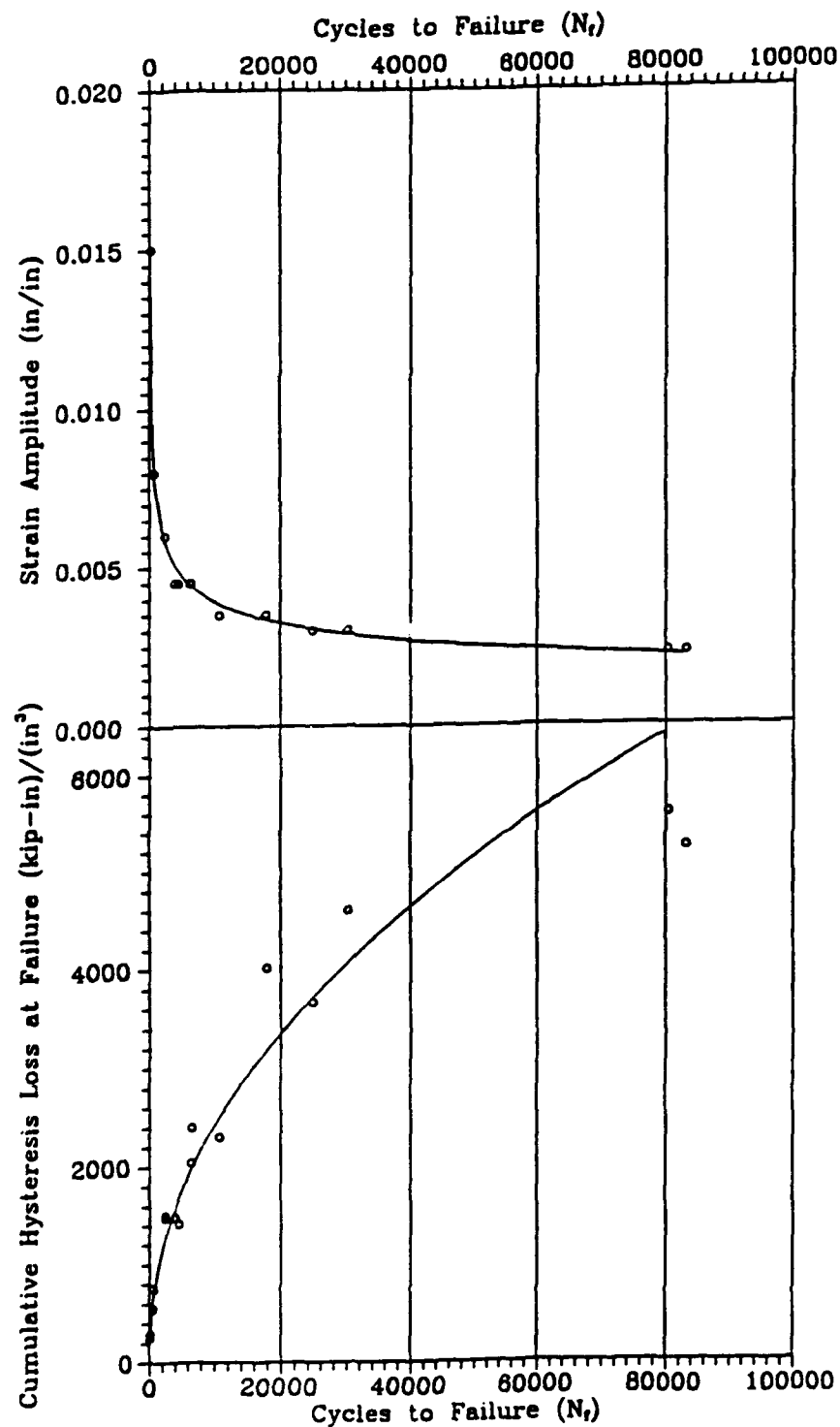
Figure 39. Projections of Figure 38 onto $\Delta\varepsilon/2$ - N_f and U_f - N_f Planes
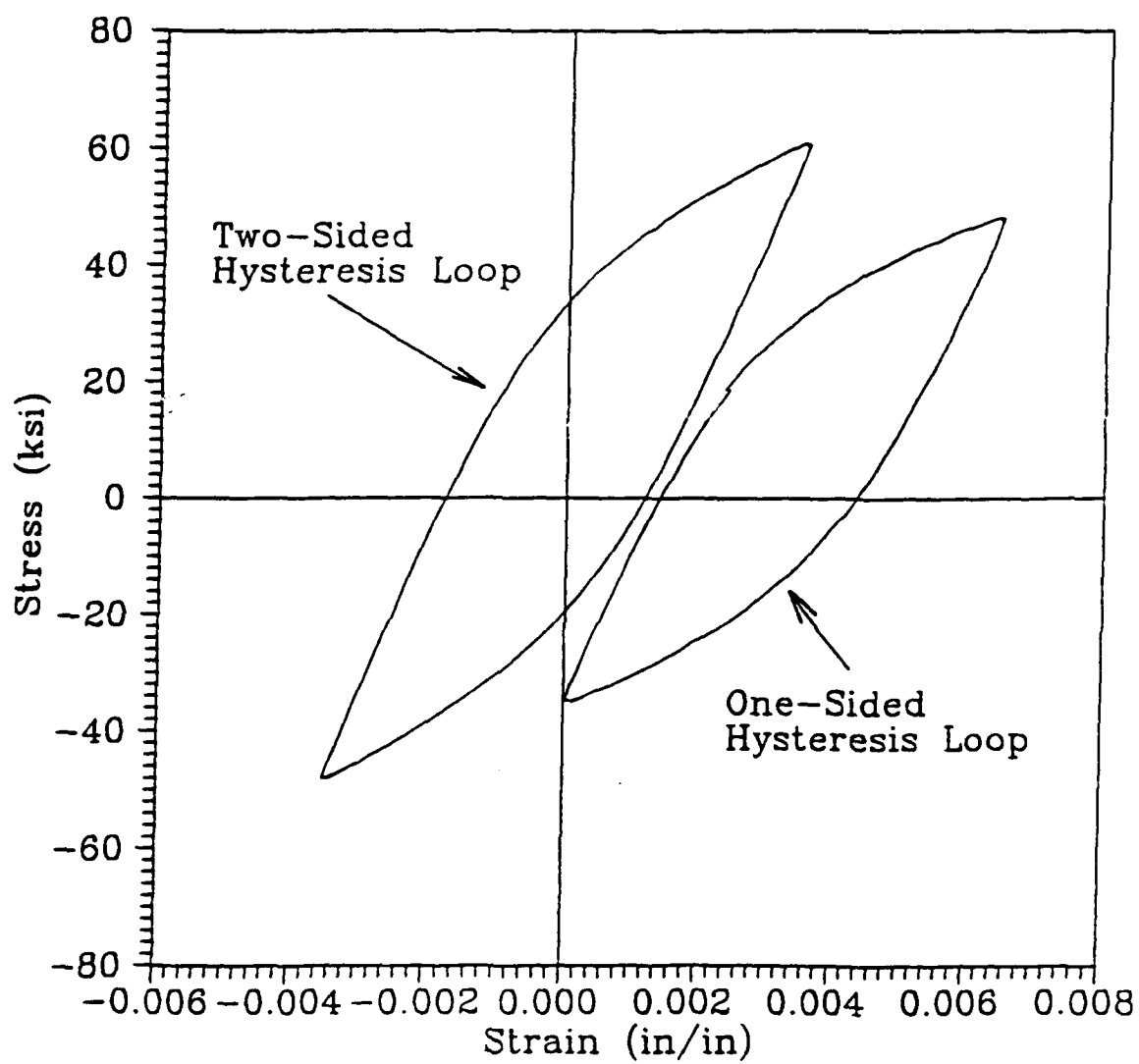
Figure 40. One-Sided and Two-Sided Hysteresis Loops

Shown in Figures 41 and 42 are graphs of average hysteresis loss as a function of cycles to failure and cumulative hysteresis loss at failure as a function of cycles to failure, respectively for the case of one-sided hysteresis. Not only are the equations representing these curves of the same form as those of the two-sided case, but the correspondence between their respective intercepts ($N_f = 1$) and exponents is truly startling. This correspondence leads one to believe that the data from the two series of experiments can be combined.

When the data from the one-sided experiments are combined with the data from the two-sided experiments, the graphs of average hysteresis loss per cycle as a function of cycles to failure and cumulative hysteresis at failure as a function of cycles to failure are obtained. These graphs are presented in Figures 43 and 44 respectively. The data obtained from two-sided experiments are represented by circles and the data obtained from one-sided experiments are represented by squares. The fact that the combination of these two completely different series of experiments leads to a very important discovery in the field of fatigue studies. It appears that the total energy absorbed during the application of constant cyclic loads accumulates in the same fashion regardless of the manner in which the specimen is cycled. With this in mind, it is then possible to reconstruct the three dimensional diagram presented in Figure 38 using the data from both one-sided and two-sided experiments. This graph is shown in Figure 45.

Just as in the case of two-sided fatigue experiments, it is possible to define a threshold value for detectable hysteresis. Figures 46 and 47 are graphs of average hysteresis loss as a function of strain range, $\Delta\varepsilon$. As one might expect, the behavior of the average hysteresis loss for the one-sided case is similar to that of the two-sided case resulting in a tri-linear graph. The slopes for the three linear portions are

for $0.001125 < \Delta\varepsilon < 0.00339$, m = 9.333

for $0.00339 < \Delta\varepsilon < 0.00695$, m = 47.726
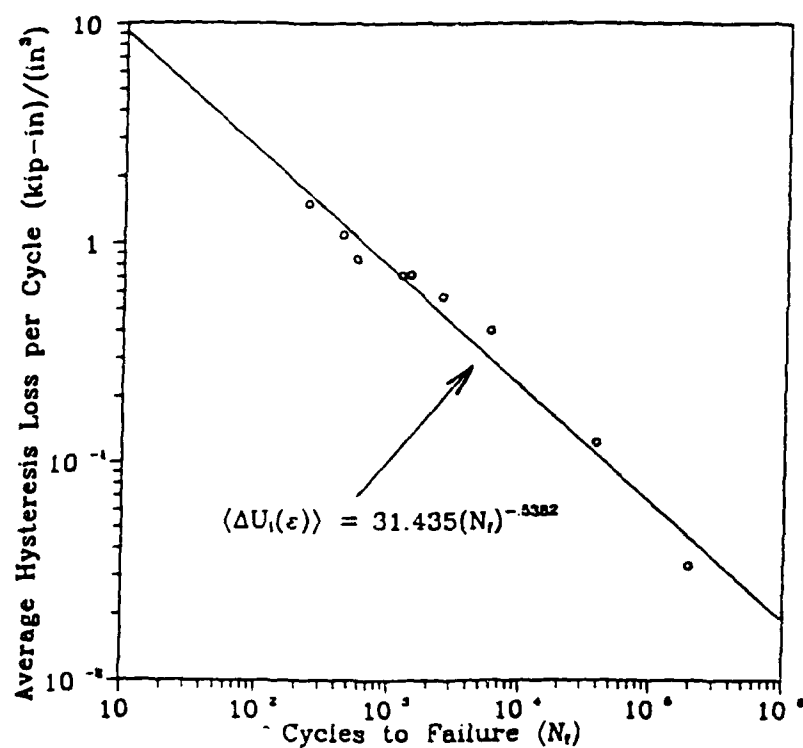
Figure 41. Average Hysteresis Loss per Cycle vs Cycles to Failure: One-Sided Case
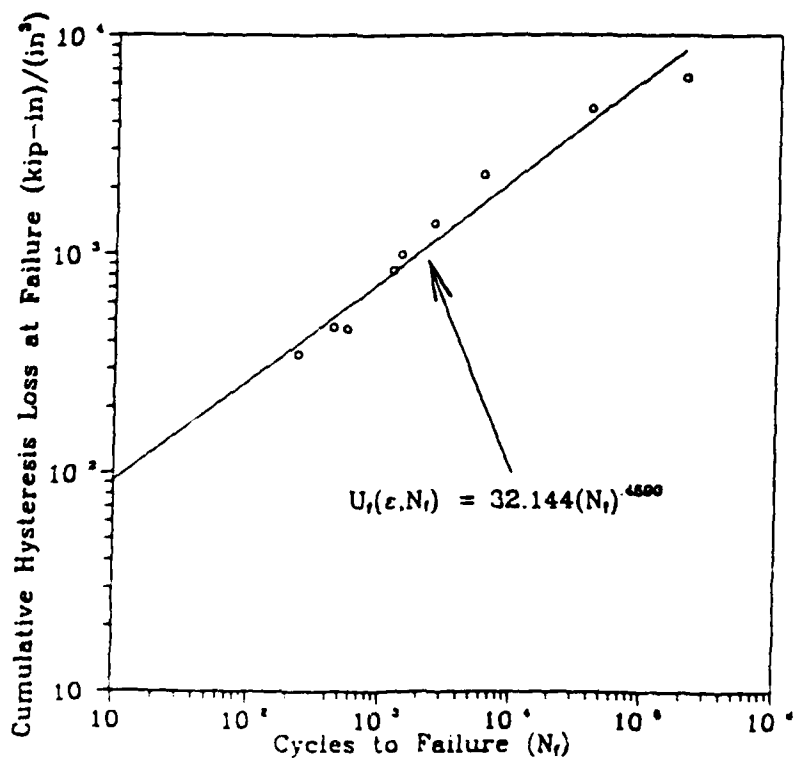
Figure 42. Cumulative Hysteresis Loss at Failure vs Cycles to Failure: One-Sided Case
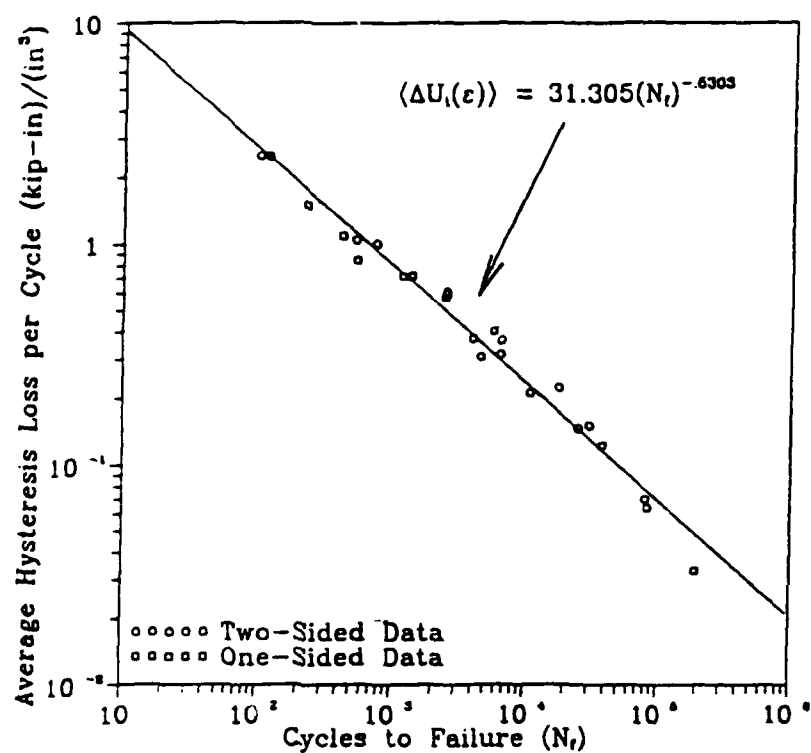
Figure 43. Average Hysteresis Loss per Cycle vs Cycles to Failure: Combined Data
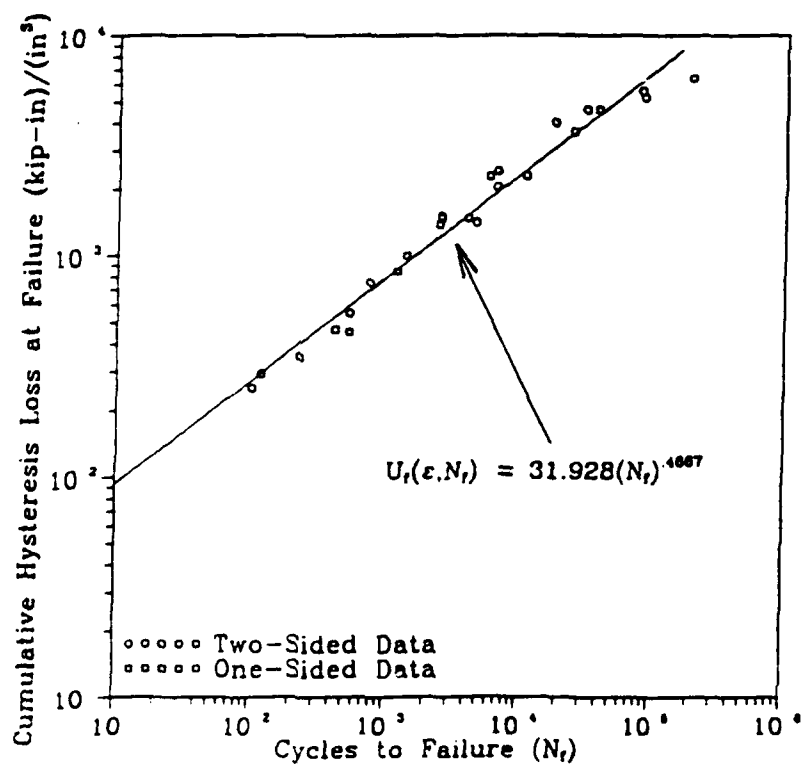
Figure 44. Cumulative Hysteresis Loss at Failure vs Cycles to Failure: Combined Data
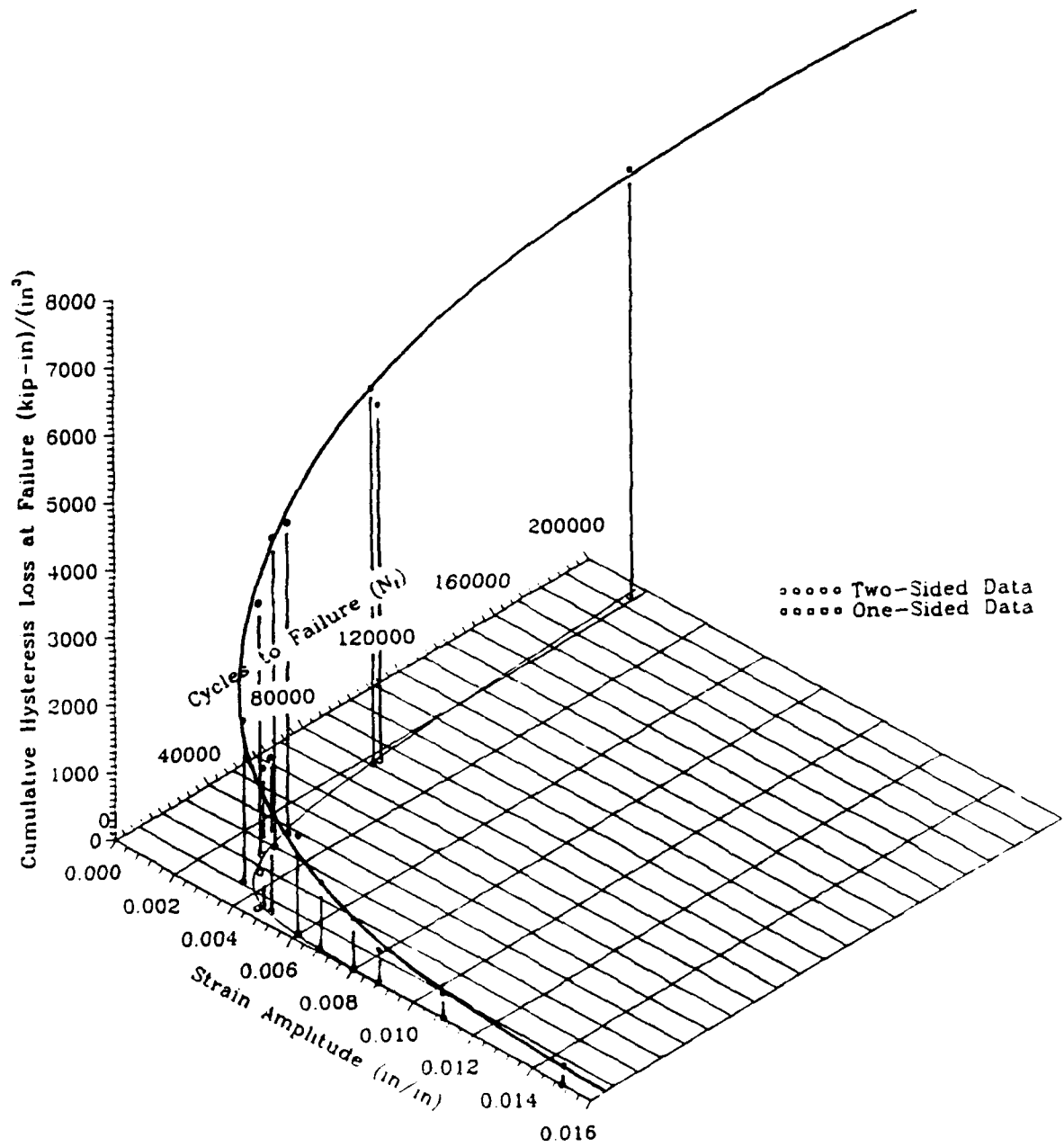
Figure 45. Cumulative Hysteresis Loss at Failure as a Function of $\Delta\epsilon/2$ and N_f: Combined data
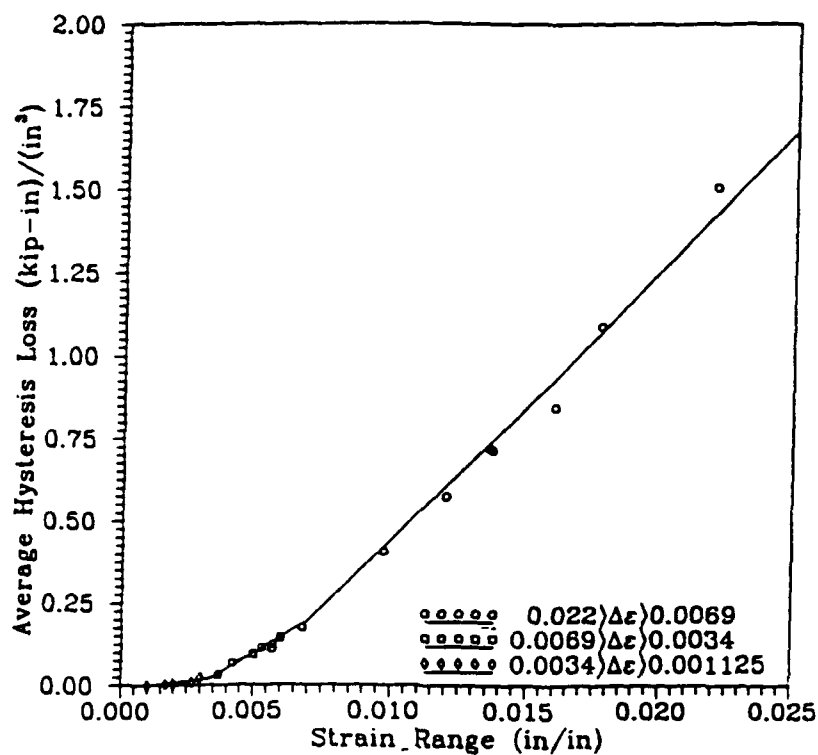
Figure 46. Average Hysteresis Loss per Cycle vs Δε for One-Sided Experiments
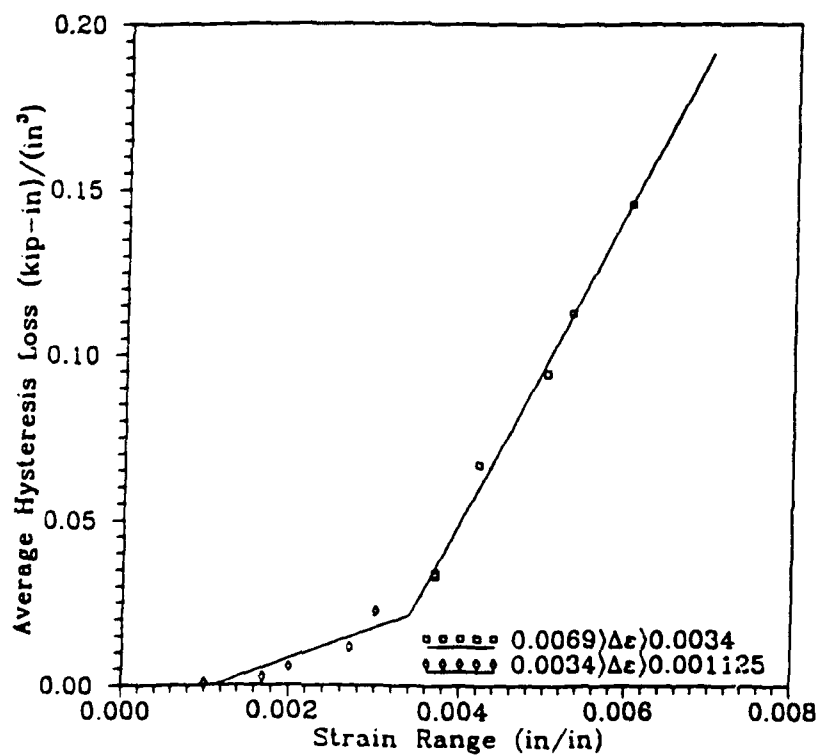
Figure 47. Average Hysteresis Loss per Cycle vs Δε for One-Sided Experiments: Expanded View

$$\text{for} \quad 0.00695 < \Delta \varepsilon < 0.0220, m = 82.192$$

From these slopes and the data shown in Figures 46 and 47, the threshold for detectable hysteresis may be determined, and it has been found,

$$\Delta \varepsilon = \varepsilon_{th} = 0.001125.$$

This value for ε_{th} is also smaller than the yield strain determined previously. Therefore, the corresponding value of threshold stress, σ_{th}, is readily computed as

$$\sigma_{th} = E \varepsilon_{th} = 29000 \; ksi \; (0.001125) = 32.628 \; ksi.$$

Since there is no distinction between the amount of energy absorbed during one-sided and two-sided fatigue experiments, equations (3.12) and (3.13) must be applicable to one-sided hysteresis as well as two-sided hysteresis. Utilizing this fact, the endurance limit for this material when it is subjected to one-sided repeated loading must be defined by

$$\varepsilon_{el}^{(1)} = \varepsilon_{th}^{(1)} = 0.001125$$

where the superscript "(1)" denotes the threshold determined for one-sided fatigue. Likewise, the threshold for the case of two-sided fatigue shall be denoted as

$$\varepsilon_{el}^{(2)} = \varepsilon_{th}^{(2)} = 0.0009143.$$

Recall the Goodman diagram presented in Figure 3. In order to produce a diagram of this type, one must obtain at least five data points. Based upon the previous developments, these five data points exist and are represented as

$$1. \quad \sigma = \sigma_{max} = \sigma_{th}^{(2)} = 26.515 \; ksi$$

$$2. \quad \sigma = \sigma_{min} = -\sigma_{th}^{(2)} = -26.515 \; ksi$$

$$3. \quad \sigma = \sigma_{max} = \sigma_{th}^{(1)} = 32.628 \; ksi$$

$$4. \quad \sigma = \sigma_{min} = 0.0 \; ksi$$

$$5. \quad \sigma = S_u = 77.717 \; ksi$$

Using these five data points and their corresponding values of mean stress, a diagram resembling Figure 3 may be constructed. This diagram is shown in Figure 48.

Derived Cumulative Damage Laws

Recall from Figure 17 and equation (3.16) presented in Chapter III that the accumulated damaging energy was assumed to be a linear function of the form

$$U_d(\varepsilon) = U_d + F(\varepsilon, N).$$

If it is assumed that when $F(\varepsilon, N)$ is equal to zero, $U_d(\varepsilon)$ equals a constant which is equal to the energy associated with a monotonic tension test to failure. The total damaging energy for this material was computed from a diagram similar to the ones shown in Figures 16 and 27, and is

$$U_m = U_d = 13.517 \; \frac{kip-inch}{inch^3}.$$

Hence, the damaging energy per cycle may computed as,

$$<\Delta U_d(\varepsilon)> = \frac{U_d}{N_f}. \tag{5.9}$$

Figures 49 and 50 display graphs of the ratio of damaging energy per cycle to average hysteresis loss per cycle as functions of strain amplitude and cycles to failure respectively. Figures 49 and 50 are best represented by the equations
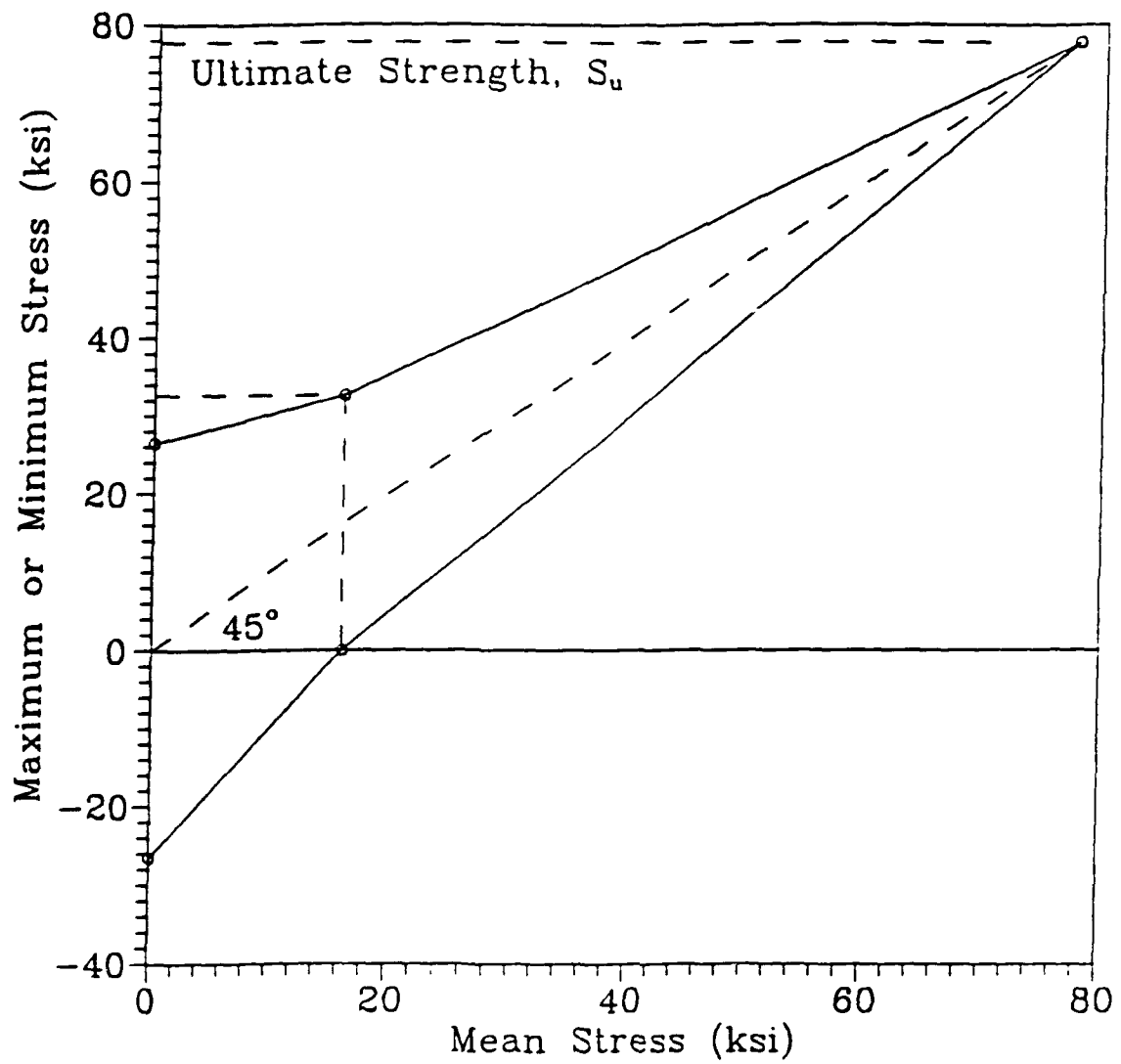
Figure 48. Goodman Type Diagram for Range of Stress: Determined with the Use of Energy Methods

$$\frac{<\Delta U_d(\varepsilon)>}{<\Delta U_i(\varepsilon)>} = 70.435 \left(\frac{\Delta \varepsilon}{2}\right)^{1.701} \tag{5.10}$$

and

$$\frac{<\Delta U_d(\varepsilon)>}{<\Delta U_i(\varepsilon)>} = 0.4285(N_f)^{-.4684} \tag{5.11}$$

respectively. Since it has been assumed that the damaging energy per cycle is the ratio of a constant, U_d, and a number that can grow very large, N_f, then (5.11) implies that

$$\lim_{N_f \to \infty} \frac{<\Delta U_d(\varepsilon)>}{<\Delta U_i(\varepsilon)>} = 0. \tag{5.12}$$

Indeed, Figure 50 and equation (5.11) indicate that the infinite series (5.12) converges as the endurance limit is approached and N becomes infinite.

From these developments, it appears that the initial assumption that the total damaging energy required to cause failure at a given level of strain is equal to a constant is not necessarily correct, and that the total damaging energy required to cause failure may include some unknown strain dependent function. Since the damaging energy per cycle must be some function of strain, the existence of measurable hysteresis energy does not necessarily mean that failure is imminent. In other words, hysteresis energy is a necessary condition required to cause failure, but its existence alone is not sufficient to cause failure. Therefore, the values of $\varepsilon_{th}^{(1)}$ and $\varepsilon_{th}^{(2)}$ may be considered to be lower bounds on the endurance limits for one and two-sided cyclic loading.
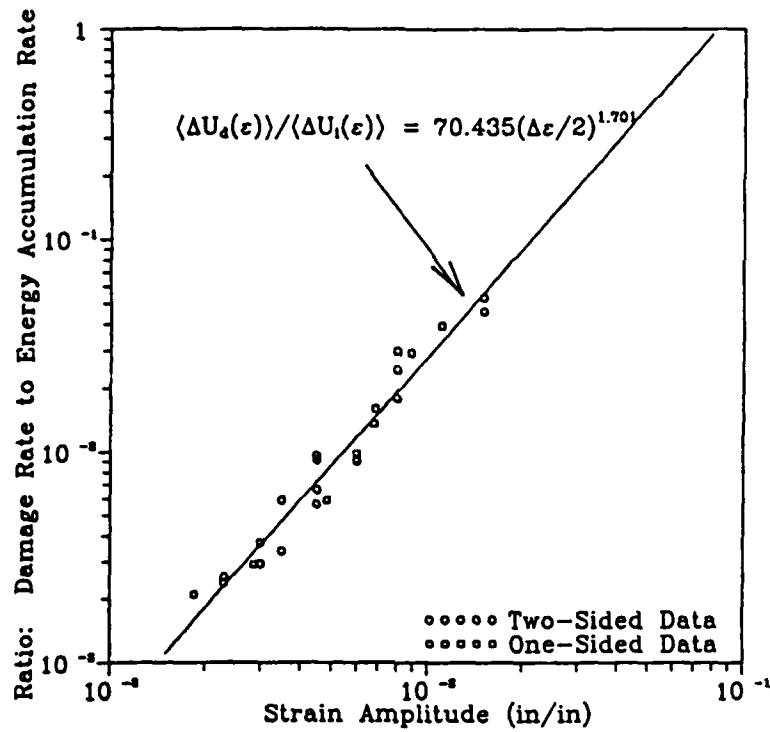
Figure 49. Ratio of Damaging Energy per Cycle to Average Hysteresis Loss per Cycle
vs Strain Amplitude
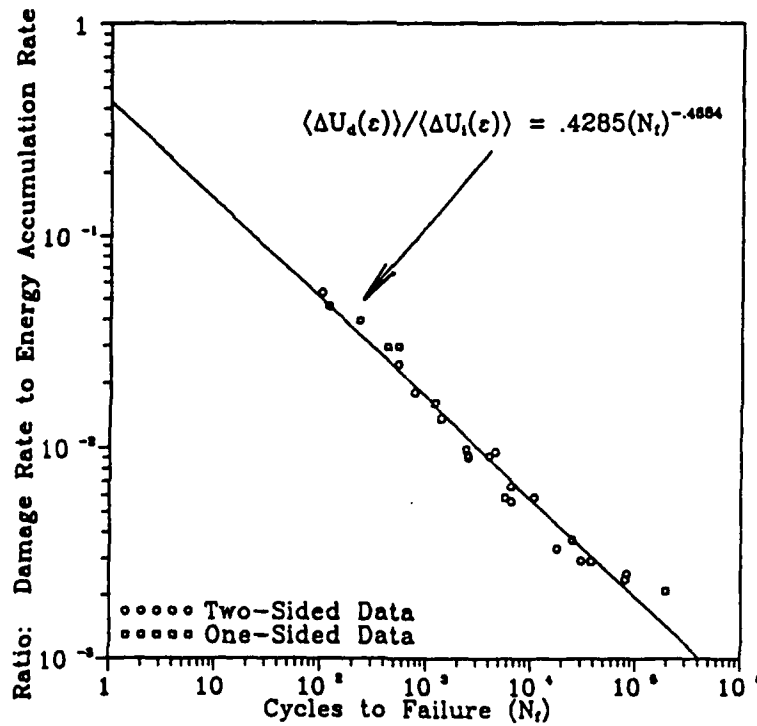
Figure 50. Ratio of Damaging Energy per Cycle to Average Hysteresis Loss per Cycle
vs Cycles to Failure

CHAPTER VI

SUMMARY AND CONCLUSIONS

In this research project, a fatigue model originally proposed by Guralnick (1975) was investigated. Tests were performed on specimens (Figs. 18 and 19) fabricated from AISI 1018 unannealed steel. Several different types of cyclic experiments were performed. The following experiments were performed: Completely alternating (two-sided) constant strain controlled experiments carried to failure; completely alternating (two-sided) strain controlled experiments with the addition of overload cycles carried to failure; completely alternating varying strain controlled ("staircase") experiments cycled for varying durations; non-alternating (one-sided) constant strain controlled experiments carried to failure; and non-alternating (one-sided) varying strain controlled ("staircase") experiments cycled for various durations. All data for these experiments are tabulated in Appendix A.

The results presented in Chapter V have provided valuable insights to the long studied phenomenon known as fatigue. The assumptions made by Feltner and Morrow (1961) and Halford (1966) that the energy associated with one cycle of loading in a constant strain cycled experiment is essentially a constant has been confirmed. In addition, the average hysteresis loss per cycle as a function of maximum strain has been found to vary in a piece-wise linear fashion, thus enabling an estimate for the endurance limit of the material to be made. The use of "staircase" load programs proved to be very useful in this respect. By properly utilizing "staircase" load programs and the energy methods developed in this research, it was found that the endurance limit could be approximated in a relatively small amount of time while using a minimum amount of specimens. This also established a very simple and inexpensive method for determining approximate Goodman type diagrams similar to those described in Chapter I.

It has been found that the average hysteresis loss per cycle and the cumulative hysteresis loss at failure can both be represented by simple power laws related to the number of cycles to failure. These power law relationships are valid regardless of the type of test regime employed so long as maximum and minimum strains are held nearly constant. The addition of overload cycles seems to have little or no effect on the overall hysteresis response of the material provided that the overloads are short in duration and not excessive in magnitude.

One important result of the experiments reported herein, also confirmed by others, is that the total hysteresis energy associated with one cycle is essentially a constant. This means that the accumulated total hysteresis energy is a linear function of the number of cycles of load application for nearly the entire loading history to final rupture. Hence, if the total hysteresis energy may be split into two parts, one part being harmlessly dissipated as heat and the other part causing the accumulation of damage, then the latter part is a constant for each cycle and total damaging energy also accumulates as a linear function of the number of cycles of load application. This result indicates that combining acoustic emission measurements, hysteresis measurements and post-mortem examinations of ruptured specimens may lead to new insights concerning the origin and inception of the fatigue process in metals.

APPENDIX A

TABULATED DATA

Table 3. Two-Sided Specimens Carried to Failure

Specimen Name	Strain Amplitude (in/in)	Cycles to Failure (N_f)	Cumulative Hysteresis Loss at Failure $(kip\text{-}in)/(in^3)$	Average Hysteresis Loss per Cycle $(kip\text{-}in)/(in^3)$
124	0.0035	17,843	4,010.900	0.2248
125	0.0045	6,537	2,400.680	0.3668
127	0.0060	2,472	1,502.440	0.6079
128	0.0150	118	293.846	2.5041
129	0.0080	532	552.329	1.0437
132	0.0030	24,854	3,661.688	0.1473
222	0.0150	101	252.347	2.5182
223	0.0080	754	756.005	1.0028
224	0.0060	2,485	1,469.279	0.5886
225	0.0030	30,276	4,600.180	0.1519
226	0.0045	3,949	1,480.548	0.3750
233	0.0035	10,821	2,301.857	0.2126
323	0.0045	4,560	1,412.978	0.3105
326	0.0045	6,470	2,040.358	0.3165
422	0.0023	80,424	5,585.350	0.0708
426	0.0023	83,277	5,236.276	0.0643

Table 4. Data Acquired Using Staircase Load Program: Two-Sided Case

Specimen Name	Strain Amplitude (in/in)	Cycles Tested	Average Hysteresis Loss per Cycle (kip-in)/(in³)
227A	0.0022	360	0.0626
227B	0.0035	360	0.2250
227C	0.0045	360	0.3595
228A	0.0022	360	0.0684
228B	0.0025	360	0.1039
228C	0.0030	360	0.1423
228D	0.0035	360	0.2060
228E	0.0030	360	0.1457
228F	0.0025	360	0.0970
228G	0.0022	360	0.0710
229A	0.0015	360	0.0059
229B	0.0017	360	0.0197
229D	0.0019	360	0.0408
229E	0.0035	200	0.2194
229F	0.0040	200	0.2874
229G	0.0045	200	0.3602
229H	0.0050	200	0.4357
229I	0.0045	200	0.3566
229J	0.0040	200	0.2839
229K	0.0035	200	0.2156
230A	0.0022	200	0.0551
230B	0.0025	200	0.0941
230C	0.0028	200	0.1290
230D	0.0033	200	0.1888
230E	0.0040	200	0.2805
230F	0.0055	100	0.5115
230G	0.0065	50	0.6789
230H	0.0100	50	1.3673
230I	0.0065	50	0.6754

Table 4. (contiued)

Specimen Name	Strain Amplitude (in/in)	Cycles Tested	Average Hysteresis Loss per Cycle (kip-in)/(in^3)
230J	0.0055	100	0.5049
230K	0.0040	200	0.2783
260L	0.0033	200	0.1866
230M	0.0028	200	0.1304
230N	0.0025	200	0.0999
230O	0.0022	200	0.0736
231A	0.0022	400	0.0708
231B	0.0021	40	0.0649
231C	0.0020	40	0.0571
231D	0.0019	40	0.0493
231E	0.0018	40	0.0425
231F	0.0017	40	0.0357
231G	0.0016	40	0.0303
231H	0.0015	40	0.0236
231I	0.0014	40	0.0194
231J	0.0013	40	0.0137
231K	0.0012	40	0.0090
231L	0.0011	40	0.0049
231M	0.0010	40	0.0033
231N	0.0011	40	0.0050
231O	0.0012	40	0.0075
231P	0.0013	40	0.0108
231Q	0.0014	40	0.0149
231R	0.0015	40	0.0194
231S	0.0016	40	0.243
231T	0.0017	40	0.0306
231U	0.0018	40	0.0366
231V	0.0019	40	0.0432
231W	0.0020	40	0.0499

Table 4. (continued)

Specimen Name	Strain Amplitude (in/in)	Cycles Tested	Average Hysteresis Loss per Cycle (kip-in)/(in^3)
231X	0.0021	40	0.0591

Table 5. One-Sided Specimes Carried to Failure

Specimen Name	Strain Range (in/in)	Strain Amplitude (in/in)	Cycles to Failure (N$_f$)	Cumulative Hysteresis Loss at Failure (kip-in)/(in^3)	Average Hysteresis Loss per Cycle (kip-in)/(in^3)
331	0.0220	0.01100	229	349.006	1.5066
332	0.0177	0.00885	423	464.740	1.0937
423	0.0097	0.00485	5,684	2,286.833	0.4035
424	0.0057	0.00285	37,655	4,594.810	0.1232
425	0.0037	0.00185	194,729	6,387.100	0.0331
428	0.0136	0.00680	1,376	997.778	0.7211
429	0.0160	0.00800	538	453.540	0.8480
430	0.0137	0.00685	1,179	849.750	0.7150
431	0.0120	0.00600	2,406	1,375.058	0.5726

Table 6. Data Acquired Using Staircase Load Program: One-Sided Case

Specimen Name	Strain Range (in/in)	Strain Amplitude (in/in)	Cycles Tested	Average Hysteresis Loss per Cycle (kip-in)/(in^3)
432-1	0.0057	0.00285	250	0.1092
432-1	0.0037	0.00185	250	0.0340
432-1	0.0027	0.00135	250	0.0115
432-1	0.0017	0.00085	250	0.0024
432-1	0.0007	0.00035	250	0.0004
432-2	0.0060	0.00300	250	0.1414
432-2	0.0050	0.00250	250	0.0942
432-2	0.0030	0.00150	250	0.0225
432-2	0.0020	0.00100	250	0.0056
432-2	0.0010	0.00050	250	0.0009
432-3	0.0042	0.00210	250	0.0667
432-3	0.0053	0.00265	250	0.1127
432-3	0.0068	0.00340	250	0.1741

Table 7. Ratios of Damaging Energy per Cycle to Average Hysteresis Loss per Cycle

Specimen Name	Strain Amplitude (in/in)	Ratio of Damaging Energy per Cycle to Average Hysteresis Loss per Cycle
124	0.0035	0.003369
125	0.0045	0.005637
127	0.0060	0.008995
128	0.0150	0.045740
129	0.008	0.024340
132	0.0030	0.003692
222	0.0150	0.053140
223	0.0080	0.017877
224	0.0060	0.009241
225	0.0030	0.002939
226	0.0045	0.009127
233	0.0035	0.005875
323	0.0045	0.009547
326	0.0045	0.006599
422	0.0023	0.002374
426	0.0023	0.002526
331	0.0110	0.039180
332	0.00885	0.028220
423	0.00485	0.005893
424	0.00285	0.002914
425	0.00185	0.002094
428	0.00680	0.013620
429	0.0080	0.029630
430	0.00685	0.016035
431	0.0060	0.009811

APPENDIX B

SUPPLEMENTARY FIGURES
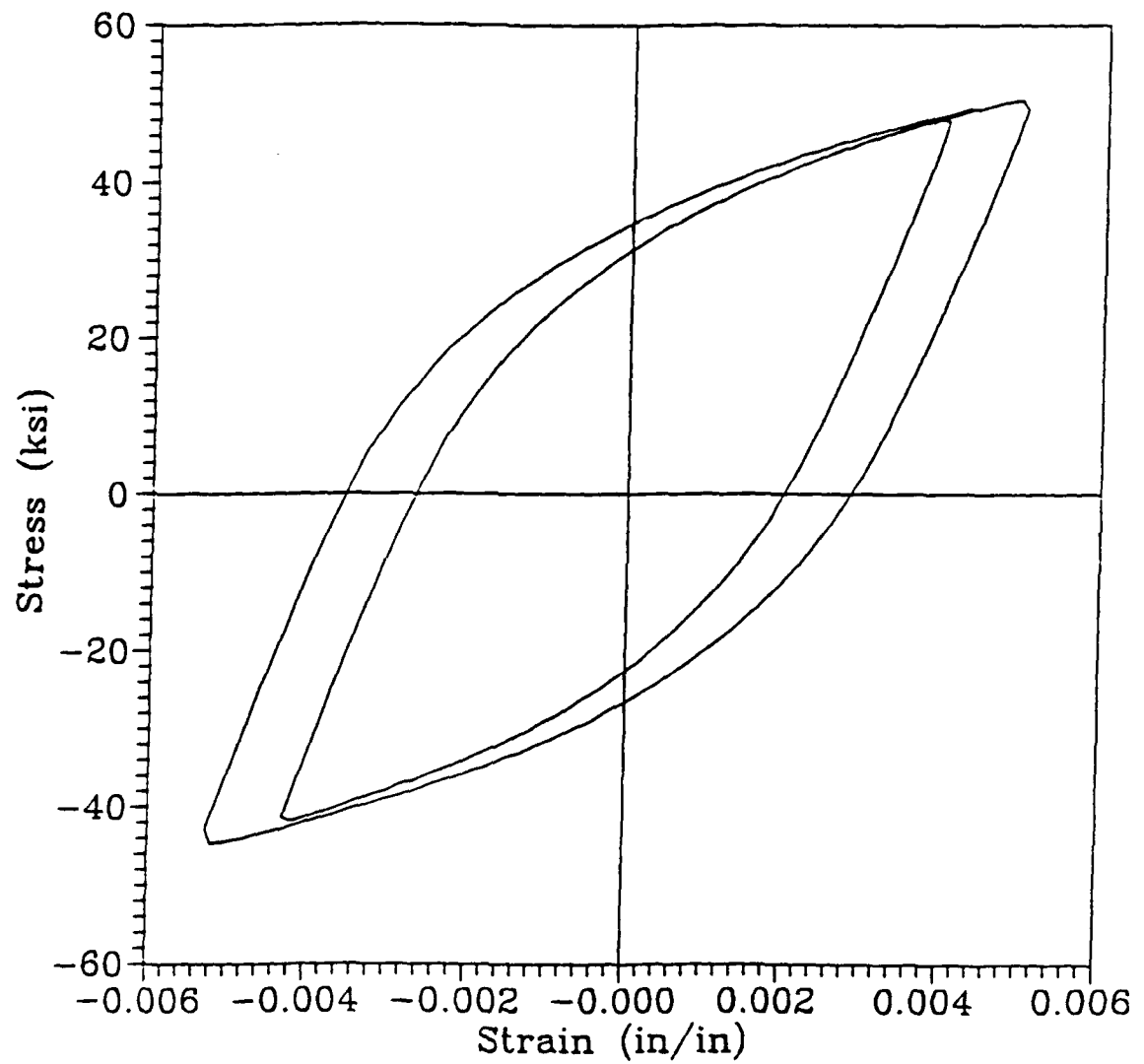
Figure 51. Hysteresis Loops for a Specimen Subjected to Overloads
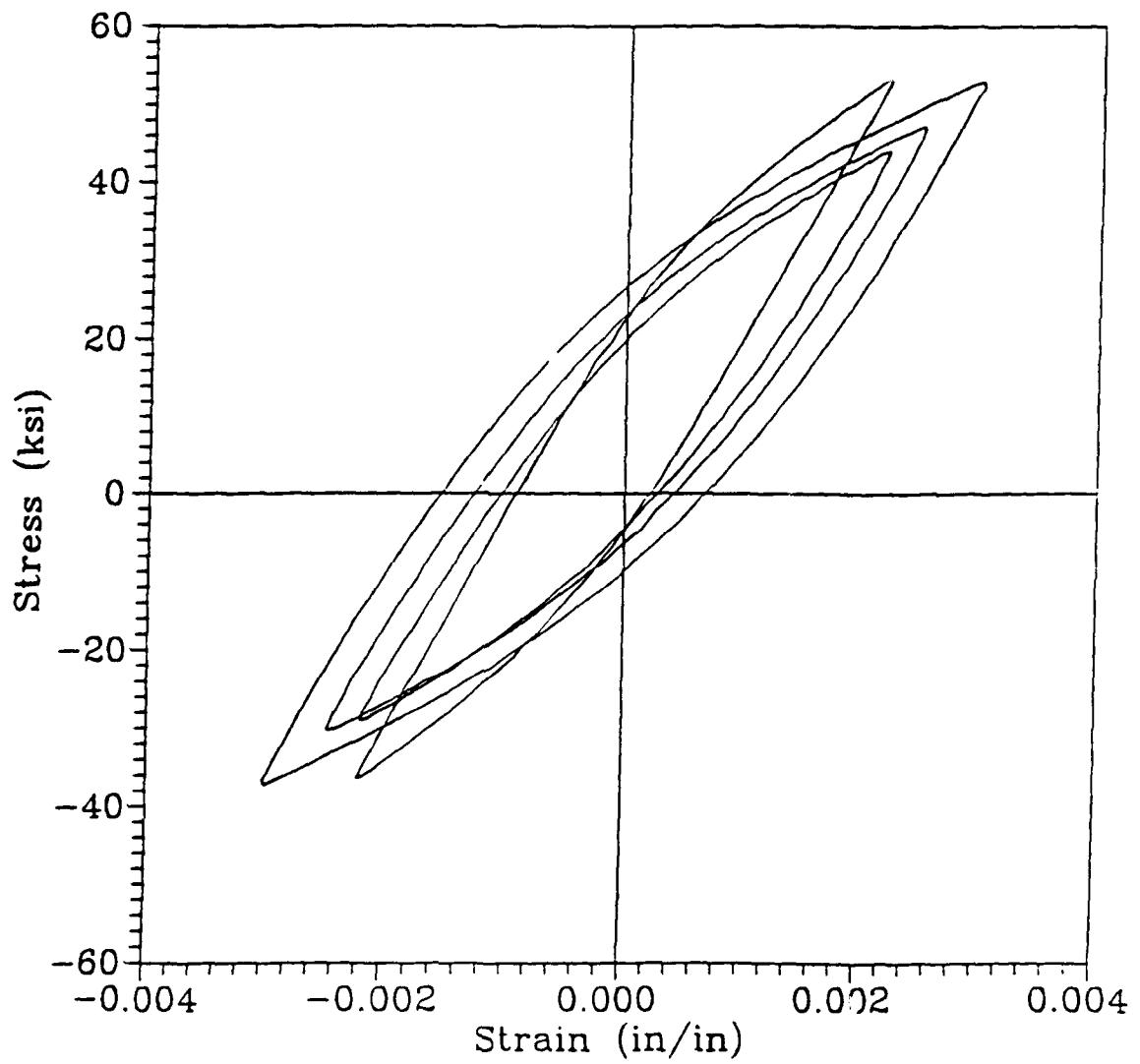
Figure 52. Typical Hysteresis Loops from a Staircase Load Program
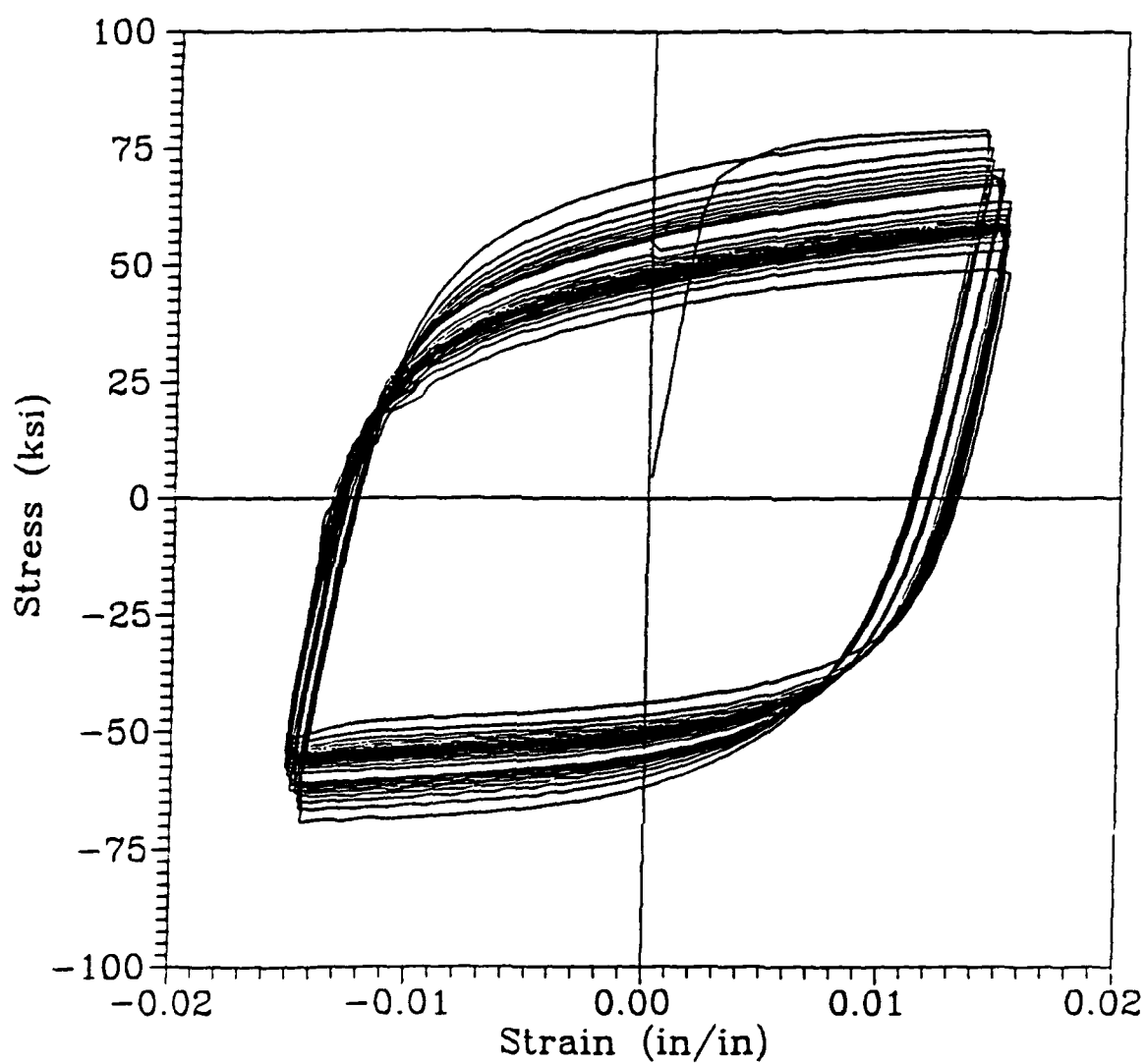
Figure 53. Typical Strain Controlled Fatigue Experiment Displaying Strain Softening
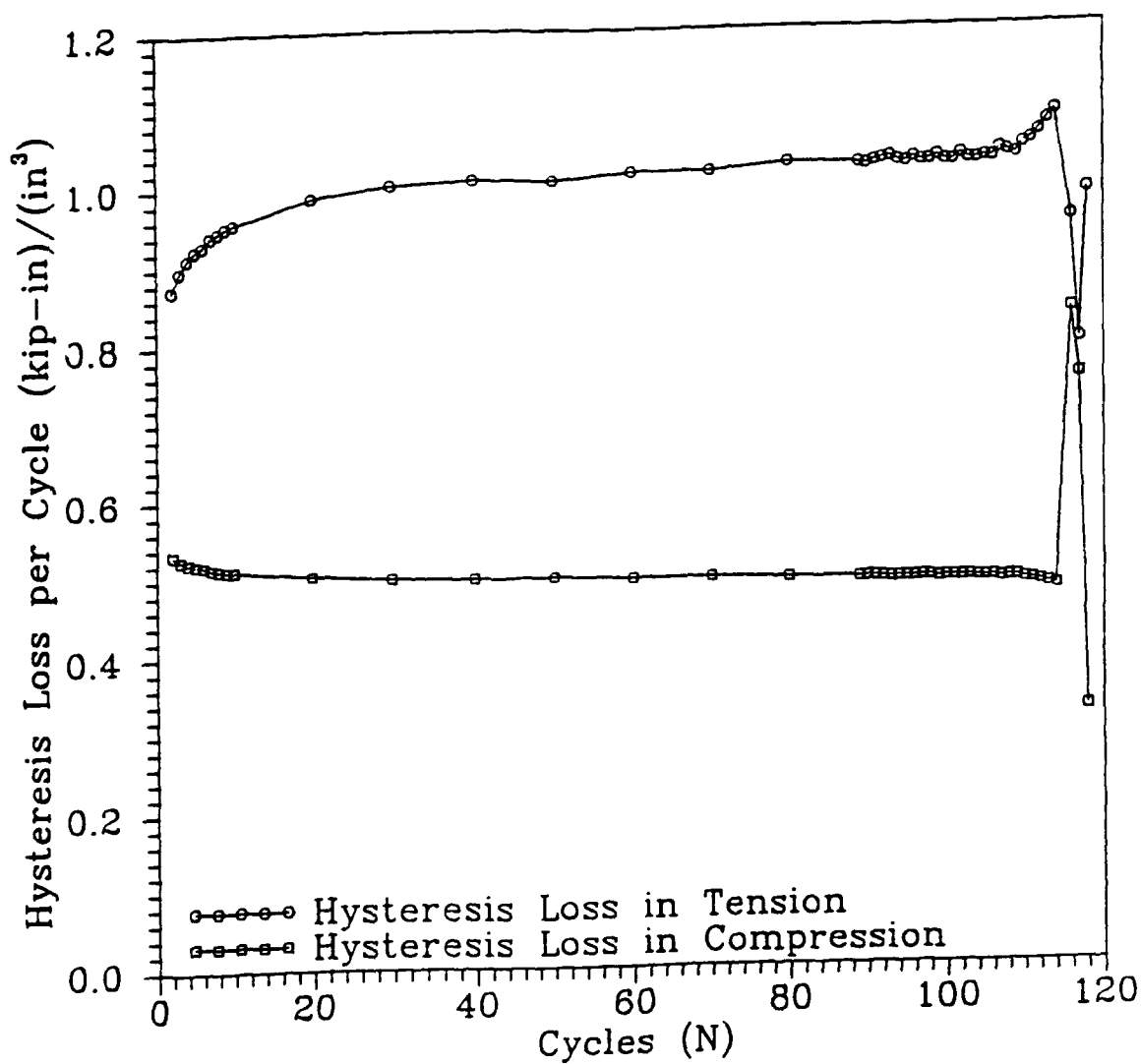
Figure 54. The Difference Between the Hysteresis Loss in Tension and Compression for Specimen Subjected to a Large Strain Amplitude
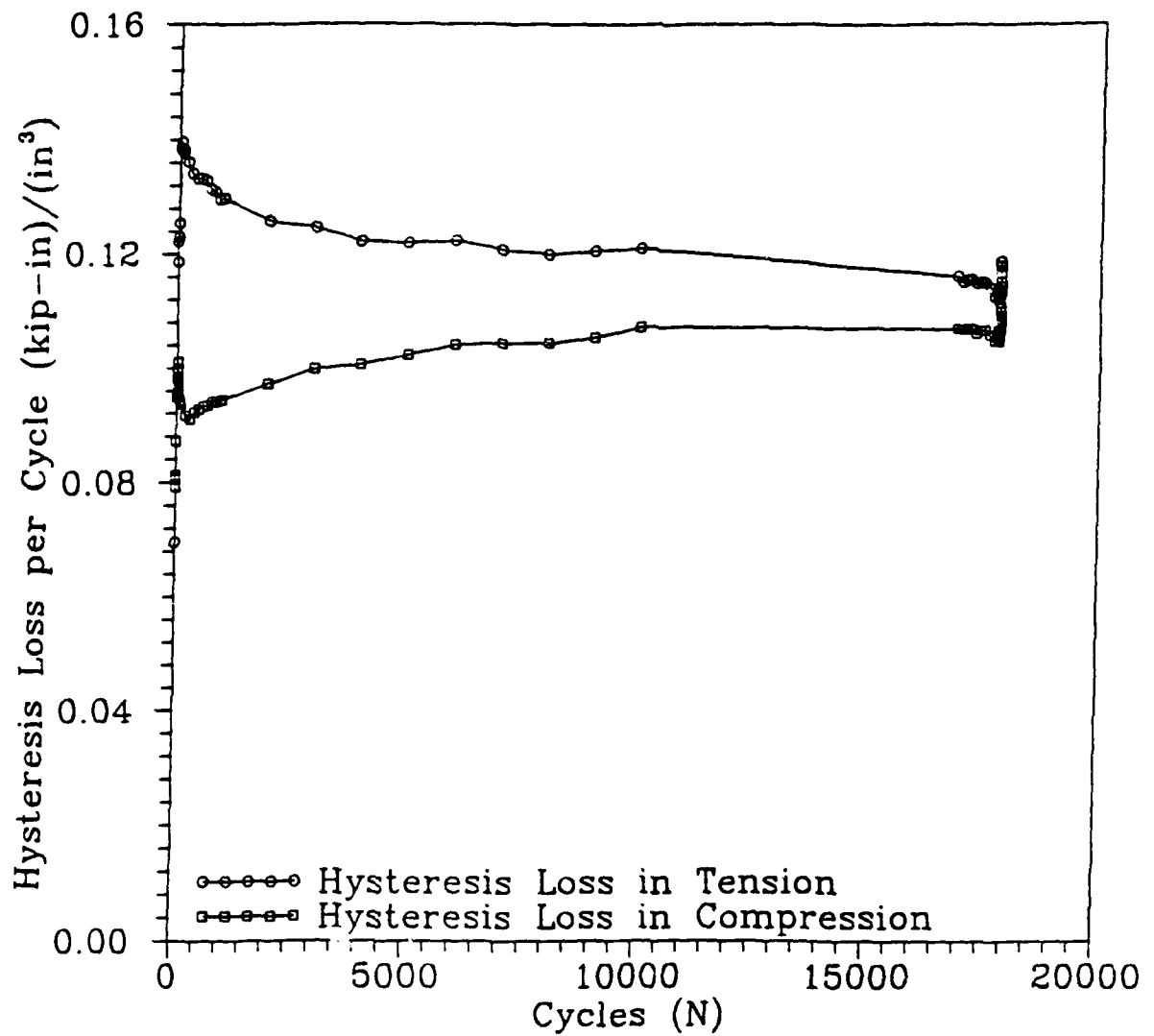
Figure 55. The Difference Between the Hysteresis Loss in Tension and Compression for a Specimen Subjected to a Small Strain Amplitude

APPENDIX C

PROGRAM USED TO EVALUATE EQUATION (3.8)

```
C
C       THIS PROGRAM USES SIMPSON'S TRAPEZOIDAL RULE TO
C       APPROXIMATE THE AREA ENCLOSED BY HYSTERESIS LOOPS
C       IT ALSO CALCULATES THE CUMULATIVE ENERGY WHICH IS THE
C       SUMMATION OF ALL OF THE RESPECTIVE HYSTERESIS LOOP
C       AREAS, A RUNNING AVERAGE OF EVERY 10 HYSTERESIS LOOP
C       AREAS, A RUNNING DIFFERENCE BETWEEN EVERY HYSTERESIS
C       LOOP AREA, AND A RUNNING AVERAGE OF EVERY 10
C       POSITIVE AND NEGATIVE DIFFERENCES RESPECTIVELY
C
C       VARIABLES USED:
C               STRS:  A ONE DIMENSIONAL ARRAY USED TO STORE ALL
        C                STRESS VALUES ASSOCIATED WITH ONE HYSTERESIS LOOP
C
C               STRN: A ONE DIMENSIONAL ARRAY USED TO STORE ALL
        C                STRAIN VALUES ASSOCIATED WITH ONE HYSTERESIS LOOP
C
C               AREA:  THE INDIVIDUAL AREA OF A HYSTERESIS LOOP
C
C               CUMAREA:  A REAL VALUE USED TO STORE THE
C               CUMULATIVE HYSTERESIS-ENERGY
C
C               AREA10:  THE SUMMATION OF 10 HYSTERESIS LOOPS USED
C               IN CALCULATING THE AVERAGE OF EVERY 10 LOOPS
C
C               DIFFM:  THE SUMMATION OF 10 NEGATIVE DIFFERENCES
C
C               DIFFP:  THE SUMMATION OF 10 POSITIVE DIFFERENCES
C
C               AVGM:  THE AVERAGE OF 10 SUCCESSIVE NEGATIVE CDIFFERENCES
C
C               AVGP:  THE AVERAGE OF 10 SUCCESSIVE POSITIVE
C               DIFFERENCES
C
C               STRSEND:  THE INTERPOLATED VALUE OF STRESS USED TO CCLOSE THE
LOOP
C
C               STRNEND:  THE INTERPOLATED VALUE OF STRAIN USED
          C              TO "CLOSE" THE LOOP
C
C               CYCNO:  THE COUNTER USED TO COUNT CYCLES
C
C               COUNT10:  THE COUNTER USED TO COUNT FOR THE
          C              AVERAGE OF EVERY 10 LOOPS
C
C               COUNTP:  THE COUNTER USED TO COUNT FOR THE 10
C               POSITIVE DIFFERENCES
C
C               COUNTM:  THE COUNTER USED TO COUNT FOR THE 10
C               NEGATIVE DIFFERENCES
C
CCCCCCCCCCCCCCCCCCCCCCCCCCCCCCCCCCCCCCCCCCCCCCCCCCCCCC
```

```
      $DEBUG
      DOUBLE PRECISION STRS,STRN,CUMAREA,AREAI,AREA,AREA10,AVG10
      DOUBLE PRECISION DIFFM,AVGP,AVGM,STRSEND,STRNEND,DIFFP
         INTEGER*4 I
         INTEGER ND,CYCNO,CYCNOI,COUNT10,COUNTM,COUNTP
         CHARACTER*12 INP,OUT
         CHARACTER*3 END
         CHARACTER*1 REPLY
         DIMENSION STRS(150),STRN(150)
C
C        ENTER THE NAME OF THE DATA FILE YOU WISH TO EVALUATE
C
         WRITE(6,*)'ENTER THE NAME OF THE INPUT FILE.'
         READ(5,1)INP
1        FORMAT(A12)
C
C        ENTER THE NAME OF THE DATA FILE YOU WISH TO CREATE
C
         WRITE(6,*)'ENTER THE NAME OF THE OUTPUT FILE.'
         READ(5,2)OUT
2        FORMAT(A12)
C
C        THE FIRST SIX LINES OF EVERY ORIGINAL DATA FILE CONTAINS
C        SIX LINES OF ASCII CHARACTERS.  A REPLY OF 'Y' CAUSES THE
C        PROGRAM TO SKIP OVER THEM TO GET TO THE DATA
C
         WRITE(6,*)'DO YOU WANT TO KEEP THE FIRST SIX LINES OF DATA? (Y FOR
       + YES, N FOR NO)'
         READ(5,3)REPLY
3        FORMAT(A1)
         OPEN(5,FILE=INP)
         OPEN(6,FILE=OUT)
C
C        ZERO ALL VARIABLES
C
         AREA=0.0D0
         CUMAREA=0.0D0
         CYCNO=0
         ND=0
         DIFFP=0.0D0
         DIFFM=0.0D0
         AREA10=0.0D0


C
C        BEGIN THE MAIN LOOP TO EVALUATE ALL CYCLES
C
      DO 10 I=1,50000,1
C
C        COUNTER IS A SUBROUTINE USED TO DETERMINE WHAT CONSTITUTES A
C        CYCLE AND THE INTERPOLATED VALUE OF STRSEND AND STRNEND
C
```

```
C      LOOPAREA IS THE SUBROUTINE USED TO EVALUATE THE AREA OF THE LOOP
C      USING TRAPEZOIDS
C
       CALL COUNTER(STRS,STRN,ND,CYCNO,END,REPLY,STRNEND,STRSEND)
       IF(END.EQ.'END')GOTO 99
       CALL LOOPAREA(STRS,STRN,ND,AREA,STRSEND,STRNEND,CYCNO)
       IF(CYCNO.EQ.1)THEN
            CUMAREA=AREA
            AREAI=AREA
            CYCNOI=CYCNO
            COUNT10=COUNT10+1
            AREA10=AREA
            WRITE(6,6)
6    FORMAT(1X,'AREA',19X,'LOOP',7X,'AVERAGE',5X,'AVERAGE +',4X,'AVERAG
     +E -')
            WRITE(6,7)
7    FORMAT(1X,'DIFFERENCE',3X,'CYCLE # ',3X,'AREA',7X,'AREA (10)',3X,'D
     +IFFERENCE',3X,'DIFFERENCE')
            WRITE(6,8)CYCNO,AREA
8           FORMAT(1X,14X,I5,3X,F9.6)
        ELSE
            CUMAREA=CUMAREA+AREA
            AREA10=AREA10+AREA
            RUNDIFF=(AREA-AREAI)/AREAI
            COUNT10=COUNT10+1
            IF(COUNT10.EQ.10)THEN
                AVG10=AREA10/DBLE(10)
            END IF
            IF(RUNDIFF.LT.0)THEN
                COUNTM=COUNTM+1
                DIFFM=DIFFM+RUNDIFF
            END IF
            IF(RUNDIFF.GT.0)THEN
                COUNTP=COUNTP+1
                DIFFP=DIFFP+RUNDIFF
            END IF
            IF(COUNT10.EQ.10)THEN
                IF(COUNTP.EQ.10)THEN
                    AVGP=DIFFP/DBLE(10)
                    IF(COUNTM.EQ.10)THEN
                        AVGM=DIFFM/DBLE(10)
                        WRITE(6,9)RUNDIFF,CYCNO,AREA,AVG10,AVG
     +P,AVGM
9    FORMAT(1X,F9.6,5X,I5,3X,F9.6,2X,F9.6,4X,F8.6,4X,F9.6)
                        DIFFP=0.0D0
                        DIFFM=0.0D0
                        AREA10=0.0D0
                        COUNT10=0
                        COUNTP=0
                        COUNTM=0
                    ELSE
                    WRITE(6,11)RUNDIFF,CYCNO,AREA,AVG10,AV
```

```
         +GP
   11    FORMAT(1X,F9.6,5X,I5,3X,F9.6,2X,F9.6,4X,F8.6)
                           DIFFP=0.0D0
                           AREA10=0.0D0
                           COUNT10=0
                           COUNTP=0
                    END IF
                 ELSE IF(COUNTM.EQ.10)THEN
                    AVGM=DIFFM/DBLE(10)
                    WRITE(6,12)RUNDIFF,CYCNO,AREA,AVG10,AVGM
   12    FORMAT(1X,F9.6,5X,I5,3X,F9.6,2X,F9.6,16X,F9.6)
                    AREA10=0.0D0
                    DIFFM=0.0D0
                    COUNT10=0
                    COUNTM=0
                 ELSE
                    WRITE(6,13)RUNDIFF,CYCNO,AREA,AVG10
   13    FORMAT(1X,F9.6,5X,I5,3X,F9.6,2X,F9.6)
                    AREA10=0.0D0
                    COUNT10=0
                 END IF
              ELSE
                 IF(COUNTP.EQ.10)THEN
                    AVGP=DIFFP/DBLE(10)
                    IF(COUNTM.EQ.10)THEN
                       AVGM=DIFFM/DBLE(10)
                       WRITE(6,14)RUNDIFF,CYCNO,AREA,AVGP,AVG
         +M
   14    FORMAT(1X,F9.6,5X,I5,3X,F9.6,15X,F8.6,4X,F9.6)
                           DIFFM=0.0D0
                           DIFFP=0.0D0
                           COUNTP=0
                           COUNTM=0
                       ELSE
                          WRITE(6,15)RUNDIFF,CYCNO,AREA,AVGP
   15    FORMAT(1X,F9.6,5X,I5,3X,F9.6,15X,F8.6)
                          DIFFP=0.0D0
                          COUNTP=0
                       END IF
                    ELSE IF(COUNTM.EQ.10)THEN
                       AVGM=DIFFM/DBLE(10)
                       WRITE(6,16)RUNDIFF,CYCNO,AREA,AVGM
   16    FORMAT(1X,F9.6,5X,I5,3X,F9.6,27X,F9.6)
                       COUNTM=0
                       DIFFM=0.0D0
                    ELSE
                       WRITE(6,17)RUNDIFF,CYCNO,AREA
   17    FORMAT(1X,F9.6,5X,I5,3X,F9.6)
                    END IF
                 END IF
                 CYCNOI=CYCNO
                 AREAI=AREA
```

```
              END IF
   10    CONTINUE
   99    WRITE(6,*)CUMAREA
         CLOSE(5)
         CLOSE(6)
         STOP
         END


         SUBROUTINE LOOPAREA(STRS,STRN,ND,TOTAREA,STRSEND,STRNEND,CYCNO)
         DOUBLE PRECISION STRS,STRN,AREA,TOTAREA,STRSEND,STRNEND,Y
         INTEGER*4 CYCNO
         DIMENSION STRS(ND),STRN(ND)
         TOTAREA=0.0
         AREA=0.0
         DO 10 I=1,ND-1,1
            IF(I.EQ.1.AND.CYCNO.EQ.1.AND.STRN(I).GT.0.D0)THEN
               AREA=STRN(I)*STRS(I)*.5D0
               TOTAREA=AREA+((STRS(I+1)+STRS(I))*.5D0*(STRN(I+1)-STRN
     +(I)))
               GOTO 10
            ELSE IF(I.EQ.1)THEN
               Y=(((STRS(I+1)-STRS(I))/(STRN(I+1)-STRN(I)))*(0.D0-ST
     +RN(I)))+STRS(I)
               AREA=(Y+STRS(I+1))*.5D0*STRN(I+1)
               TOTAREA=TOTAREA+AREA
               GOTO 10
            ELSE
            END IF
            AREA=(.5*(STRS(I+1)+STRS(I)))*(STRN(I+1)-STRN(I))
            TOTAREA=TOTAREA+AREA
   10    CONTINUE
         Y=(((STRSEND-STRS(ND))/(STRNEND-STRN(ND)))*(0.D0-STRN(ND)))+STRS(N
     +D)
         TOTAREA=TOTAREA+(.5D0*(Y+STRS(ND)))*(0.0D0-STRN(ND))
         RETURN
         STOP
         END

         SUBROUTINE COUNTER(STRS1,STRN1,J,CYCCOUNT,END,REPLY,STRNEND,STRSEN
     +D)
         DOUBLE PRECISION STRS1,STRN1,STRS2,STRN2,STRNEND,STRSEND
         INTEGER CYCCOUNT,I,J
         CHARACTER*3 END
         CHARACTER*1 REPLY
         CHARACTER*50 BOGUS
         DIMENSION STRS1(150),STRN1(150),STRS2(20),STRN2(20)

         IF(REPLY.EQ.'Y')GOTO 15
         IF(CYCCOUNT.EQ.0)THEN
            DO 10 I=1,6,1
               READ(5,3)BOGUS
```

```
3           FORMAT(A50)
10      CONTINUE
    END IF
15   DO 30 J=1,90,1
            READ(5,*,END=99)STRS1(J),STRN1(J)
30   CONTINUE
    CYCCOUNT=CYCCOUNT+1
    J=J-1
    DO 40 K=1,20,1
        READ(5,*,END=99)STRS2(K),STRN2(K)
        IF(STRN2(K).GE.STRN1(J).AND.STRN2(K).LE.0.)THEN
            J=J+1
            STRN1(J)=STRN2(K)
            STRS1(J)=STRS2(K)
        ELSE
            STRNEND=STRN2(K)
            STRSEND=STRS2(K)
            BACKSPACE 5
            BACKSPACE 5
            GOTO 101
        END IF
40   CONTINUE
99   END='END'
101  RETURN
    STOP
    END
```

BIBLIOGRAPHY

American Institute of Steel Construction (1989), <u>Manual of Steel Construction, Allowable Stress Design</u>, 9th ed., AISC, Chicago, Ill., pp. 5-202, 1989.

Albert (1896), <u>Stahl u. Eisen</u>, 1896, pp.437.

American Society for Metals (I - 1986), <u>Atlas of Fatigue Curves</u>, 2nd printing, Carnes Publishing Services Inc., May, 1986, pp. 43.

American Society for Metals (II - 1986), <u>Metals Handbook</u>, 9th ed., Vol. 1, Carnes Publication Services Inc., 1986, pp. 125, 223, 241.

Basquin, O. (1910), "The Exponential Law of Endurance Tests," <u>Proceedings of the American Society for Testing and Materials</u>, Vol. 10, 1910, pp. 625 - 630.

Coffin, L. and Tavernelli, J. (1959), "The Cyclic Straining and Fatigue of Metals," <u>Transactions of the Mettalurgical Society</u>, American Institute for Mining Engineering, Vol. 215, Oct, 1959, pp. 794 - 806.

Cohn, M., Ghosh, S., and Parimi, S. (1972), "Unified Approach to Theory of Plastic Structures," <u>Journal of the Engineering Mechanics Division, Proceedings of the American Society of Civil Engineers</u>, Vol. 98, No. EM5, Oct, 1972, pp. 1133 - 1157.

Ewing, Sir J. and Rosenhain, W. (1899), "Experiments in Micro-metallurgy - Effects of Strain," <u>Proceedings of the Royal Society of London</u>, Vol. 65, 1899, pp. 85.

Ewing, Sir J. and Humfrey, J. (1903), "Fracture of Metals Under Repeated Alternations of Stress," <u>Philosophical Transactions of the Royal Society of London</u>, Vol. 200A, 1903, pp. 241.

Feltner, C. and Morrow, J. (1961), "Microplastic Strain Hysteresis Energy as a Criterion for Fatigue Fracture," <u>Journal of Basic Engineering, Series D, Transactions of the American Society of Mechanical Engineers</u>, Vol. 83, March 1961, pp. 15 - 22.

French, H. (1933), "Fatigue and The Hardening of Steels," <u>Transactions of the ASST</u>, Oct, 1933, pp. 899 - 946.

Gerber, W. (1874), "Relation Between the Superior and Inferior Stresses of a Cycle of Limiting Stress," <u>Zeit. Bayerischen Arch. Ing.-Vereins</u>, 1874.

Goodman, J. (1899), <u>Mechanics Applied to Engineering</u>, Longmans, Green and Co., London, England, 1899.

Guralnick, S. (1973), "Incremental Collapse Under Conditions of Partial Unloading," <u>International Association for Bridge and Structural Engineering</u>, Vol. 33 Part II, 1973.

Guralnick, S. (1975), "An Incremental Collapse Model for Metal Fatigue," International Association for Bridge and Structural Engineering, Vol. 35 Part II, pp. 634 - 650, 1975, pp. 634 - 650.

Guralnick, S., Singh, S., and Erber, T. (1984), "Plastic Collapse, Shakedown and Hysteresis," Journal of Structural Engineering, Vol 110, No. 9, Sept, 1984, pp. 2103 - 2119.

Guralnick, S., Erber, T., Stefanis, J., and Soudan, O. (1986), "Plastic Collapse, Shakedown, and Hysteresis of Multistory Steel Sturctures," Journal of Structural Engineering, Vol. 112, No. 12, Dec., 1986, pp. 2610 - 2627.

Guralnick, S., Erber, T., Soudan, O., and Stefanis, J., (1988), "Energy Method for Incremental Collapse Analysis of Framed Structures," Journal of Structural Engineering, Vol. 114, No. 1, Jan., 1988, pp. 31 - 49.

Guralnick, S. and Erber, T. (1990), The Hysteresis and Incremental Collapse of Complex Structures: A Paradigm for the Fatigue Failure of Materials, Annual Report submitted to Air Force Office of Scientific Research (grant no. 2302/B2) by the Civil Engineering Department of The Illinois Institute of Technology, Chicago, Ill., 60616.

Halford, G. and Morrow, J. (1962), "Low Cycle Fatigue in Torsion," Proceedings of the American Society for Testing and Materials, Vol. 62, 1962, pp. 695 - 707.

Halford, G. (1963), "The Strain Hardening Exponent - A New Interpretation and Definition," Transactions Quarterly, American Society for Metals, Vol. 56, No. 3, Sept., 1963, pp. 787 - 788.

Halford, G. (1966), "The Energy Required for Fatigue," Journal of Materials, Vol. 1, No. 1, March, 1966, pp. 3 - 18.

He, J. (1990), The Hysteresis and Incremental Collapse of Multi-Bay, Multi-Story Framed Structures, thesis, presented to The Illinois Institute of Technology, Chicago, Ill., in partial fulfillment of the requirements for the degree of Doctor of Philosophy, Aug., 1990.

Johnson, J. (1922), Materials of Construction, 5th ed., 1922.

Landgraf, R. (1970), "The Resistance of Metals to Cyclic Deformation," In Achievement of High Fatigue Resistance in Metals and Alloys, ASTM STP 467, American Society for Testing and Materials, 1970, pp. 3 - 35.

Launhardt (1873), "Formula for Range of Stress," Zeit. Arch. Ing. Vereins, Hanover, 1873.

Martin, D. (1961), "An Energy Criterion for Low Cycle Fatigue," Journal of Basic Engineering, Series D, Transactions of the American Society of Mechanical Engineers, Dec., 1961, pp. 565 - 571.

Miner, M. (1945), "Cumulative Damage in Fatigue," Transactions of the American Society of Mechanical Engineers, Vol. 67, Sept., 1945, pp. A159 - A164.

Mitchell, M. (1978), "Fundamentals of Modern Fatigue Analysis for Design," In Fatigue and Micro - Structures, papers presented at the 1978 ASM Materials Science Seminar, American Society for Metals, 1978, pp. 385 - 437.

Moore, H. and Kommers, J. (1927), The Fatigue of Metals, McGraw - Hill Book Co, Inc., NY, NY, 1927.

Morrow, J. (1964), "Cyclic Plastic Strain Energy and Fatigue of Metals," In Internal Friction, Damping, and Cyclic Plasticity, ASTM STP 378, American Society for Testing and Materials, 1964, pp. 45 - 87.

Nâdai, A. (1931), Plasticity, 5th impression, McGraw-Hill Book Co. Inc., NY, NY, 1931.

Neal, B. (1956), The Plastic Methods of Structural Analysis, Chapman and Hall, London, England, 1956.

Popov, E. and McCarthy, R. (1960), "Deflection Stability of Frames Under Repeated Loads," Journal of Engineering Mechanics Division, Proceedings of the American Society of Civil Engineers, Vol. 86, No. EM1, Jan., 1960, pp. 61 - 79.

Popov, E. and Bertero, V. (1973), "Cyclic Loading of Steel Beams and Connections," Journal of the Structural Division, Proceedings of the American Society of Civil Engineers, Vol. 99, No. ST6, June, 1973, pp. 1189 - 1204.

Popov, E. and Petersson, H. (1978), "Cyclic Metal Plasticity: Experiments and Theory," Journal of the Engineering Mechanics Division, Proceedings of the American Society of Civil Engineers, Vol. 104, No. EM6, Dec., 1978, pp. 1370 - 1387.

Sih, G. (1985), "Mechanics and Physics of Energy Density Theory," Theoretical and Applied Fracture Mechanics, No. 4, 1985, pp. 157 - 173.

Symonds, P. (1952), Discussion of "Welded Continuous Frames: Plastic Design and the Deformation of Structures," Welding Journal, 1952, pp. 33-s - 36-s.

Weyrauch, J. (1880-81), "On the Calculations of Dimensions as Depending on the Ultimate Working Strength of Materials," Proceedings of the Brittish Institute of Civil Engineering, Vol. 63, 1880-81, p. 275.

Wöhler, A. (1860-71), Zeit. für Bauwesen, Vols. 10, 13, 16, 20, 1860-71.

FATIGUE, HYSTERESIS AND
ACOUSTIC EMISSION

FINAL REPORT - PART II

Submitted to

THE AIR FORCE OFFICE OF SCIENTIFIC RESEARCH

by

The Department of Civil Engineering

of

Illinois Institute of Technology

Chicago
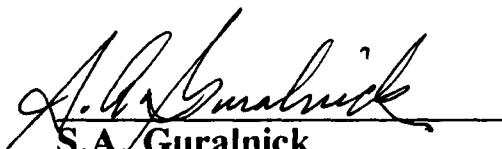
S.A. Guralnick
Principal Investigator

TECHNICAL ABSTRACT

Part I of this Report describes results from strain-controlled, cyclic load experiments performed upon nearly 100 specimens made of cold-drawn, rimmed, nominally AISI 1018 steel with 0.1640 carbon, Rockwell Hardness 46.5A and a tensile strength of 77,717 psi. This material was selected because extensive data on its performance exists in the engineering literature and because its stress-strain curve is of the gradual yielding type thus mirroring at least the monotonic stress-strain behavior of the aluminum and titanium alloys typically used in the aircraft industry. One half of the cyclic load experiments were performed with a strain ratio, R = -1, and the other half with a strain ratio, R = 0. The areas of the stress-strain hysteresis loops were measured cycle-by-cycle in the experiments performed on each of the nearly 100 samples. Empirical relationships were developed to connect the magnitude of the hysteresis energy loss in each cycle with the strain amplitude and number of cycles as well as the cumulative hysteresis energy loss up to the point of failure with the strain amplitude and the number of cycles to failure.

This Part II Report summarizes the principal findings of the Part I Report and interprets them in the light of well-established prior theory as well as in the light of more recent theories concerning the origin and inception of fatigue damage in metals. In particular, the argument is made herein that the total hysteresis energy dissipated by a metal which fails in fatigue has two principal components; one is a small damaging component, and the other, a very much larger component which represents that portion of the hysteresis energy which is converted into heat causing no damage. Moreover, the results of the experiments indicate that the total hysteresis energy loss per cycle as well as the damaging portion of the hysteresis energy loss per cycle are independent of the number of cycles and are functions of the strain amplitude only. As a consequence of these findings, it has been found possible to reinterpret the well-known Manson-Coffin and Palmgren-Miner relationships in an entirely new light.

It is also shown herein that simultaneous measurements of both mechanical hysteresis and acoustic emission are needed to follow the fatigue process from onset of plasticity-induced microcracking to ultimate rupture.

TABLE OF CONTENTS

LIST OF TABLES

LIST OF FIGURES

LIST OF NOTATIONS AND SYMBOLS

Notation	Description
σ	Unit Stress (ksi)
ε	Unit Strain (ksi)
$\Delta\sigma$	Stress Range (ksi)
$\Delta\sigma/2$	Stress Amplitude (ksi)
N_f	Number of Cycles to Failure
σ_{el}	Stress Amplitude Representing the Endurance Limit of the Material (ksi)
$\bar{\sigma}$	Mean Stress (ksi)
σ_{max}	Maximum Applied Tensile Stress During Cyclic Experiment (ksi)
σ_{min}	Maximum Applied Compressive Stress During Cyclic Experiment (ksi)
σ_o	Endurance Limit for Non-Alternating Stress Between σ_{max} and O (ksi)
r	Range Ratio, $\sigma_{min}/\sigma_{min}$
S_u	Ultimate Strength in Tension (ksi)
σ_{-1}	Endurance Limit for Alternating Stress between $\pm\sigma$ (ksi)
$\Delta\varepsilon_p$	Plastic Strain Range (in/in)
$\Delta\varepsilon_e$	Elastic Strain Range (in/in)
$\Delta\varepsilon_t$	Summation of Plastic and Elastic Strain Ranges (in/in)
ε_t	Unit Total Strain (in/in)
ε_p	Unit Plastic Strain (in/in)

ε_e	Unit Elastic Strain (in/in)
n	Strain Hardening Exponent
K	Strength Coefficient, Stress Intercept at $\varepsilon_p = 1$
σ_f	True Fracture Strength, True Stress at Failure (ksi)
ε_f	True Fracture Ductility, True Strain at Failure (in/in)
n'	Cyclic Strain Hardening Exponent
K'	Cyclic Strength Coefficient (ksi)
σ_f'	Fatigue Strength Coefficient (ksi)
ε_f'	Fatigue Ductility Coefficient (in/in)
ΔW	Plastic Strain Energy Associated with One Load Cycle (kip-in)/(in³)
W_p	Cumulative Plastic Strain Energy (kip-in)/(in³)
n_i	Number of Cycles at the ith Stress level
N_i	The Number of Cycles to Cause Failure at the ith Stress level
N_c	Number of Plastic Hinges Required to Create a Mechanism
S	Stress or Strain
$U_T(W_{max}, n)$	Total Amount of Energy Absorbed by a Structure When Cycled to Failure (kip-in)
$U_i(W_{max})$	Amount of Energy Absorbed by a Structure in One Load Cycle (kip-in)
$\Delta U_{ijk}(W_{max})$	Amount of Energy Absorbed by the kth Plastic Hinge of the jth Program Step of the ith Load Cycle Applied to a Structure
$\Delta U_i(\varepsilon)$	Hysteresis Loss of Cycle i (kip-in)/(in³)
$U_f(N_f, \varepsilon)$	Cumulative Hysteresis Loss at Failure (kip-in)/(in³)

N_o	Cycle Number in which Energy and Organization Rates are Coincident
U_m	Amount of Energy Associated with a Monotonic Tension Test to Failure (kip-in)/(in^3)
U_d	Amount of Damaging Energy Associated with a One Stroke Failure (kip-in)/(in^3)
$U_d(\varepsilon)$	Function Describing Damage Accumulation
$<\Delta U_i(\varepsilon)>$	Average Hysteresis Loss per Cycle (kip-in)/(in^3)
$<\Delta U_d(\varepsilon)>$	Average Damaging Energy per Cycle (kip-in)/(in^3)
$\varepsilon_{th}^{(1)}$	Strain Amplitude at which One-Sided Hysteresis Becomes Zero (in/in)
$\varepsilon_{th}^{(1)}$	Strain Amplitude at which Two-Sided Hysteresis Becomes Zero (in/in)

CHAPTER 1.

INTRODUCTION

1.1 General

It is well-known that the process of fatigue in metals subjected to cyclic loading is one of random, progressive and cumulative damage occurring at the sub-micron, sub-grain size level. Many of the features of fatigue damage (e.g. dislocation motion, generation and organization during slip) occur in the range of dozens to hundreds of atoms in size. The random nature and small size of the damage makes observation of the critical sites extremely difficult if not impossible to observe with either scanning electron microscope (SEM) or traditional transmission electron microscope (TEM) techniques. Thus, indirect techniques rather than direct measurements must be used to follow the damage that occurs in the fatigue process. A common indirect indicator of the origin and progress of the fatigue process is the evolution of energy from mechanical hysteresis. Acoustic emission may also be used to provide another kind of indirect indicator of the onset and progression of the fatigue process.

One purpose of this work was to examine mechanical hysteresis energy in cyclically stressed and cyclically strained steel specimens in order to follow damage processes that result in complete failure in fatigue. A second purpose of this research project was to undertake a series of preliminary experiments to determine whether acoustic emission (AE) measurements, obtained in conjunction with mechanical hysteresis measurements, could provide additional insights into the sub-micron fatigue damage process.

The energy losses associated with mechanical hysteresis during cyclic loading do not always result in fatigue failure. Nevertheless, the total irrecoverable mechanical work, converted to the thermal energy equivalent, done on a metal specimen during 500,000 cycles of loading is more than nine times the energy required to melt the metal. Surprisingly, however, many metals exhibit substantial mechanical hysteresis without failure after millions of cycles of loading. Hence, since the early 1960's, it has been assumed that total hysteresis energy cannot be directly equated with fatigue damage.

For steels at cyclic stress or strain levels in the neighborhood of the endurance (or fatigue) limit, hysteresis manifests itself from the first cycle onward — long before the first microcracks occur. This means that the hysteresis energy must somehow be associated with damage processes (e.g. dislocation motion during microplasticity) occurring within the material which lead to the onset of microcracking and the development of crack networks, the growth of the cracks within these networks and the ultimate separation of the material.

From their prior research on the incremental collapse behavior of structural frameworks, the writers became convinced that the question of the connection between mechanical hysteresis and the origin and inception of fatigue damage in metals should be reopened. In particular, the writers arrived at the notion, recently confirmed by others, that the cumulative energy loss in cyclical mechanical hysteresis could be split into two parts. A large segment is converted into thermal energy and is harmlessly dissipated during cycling. The other part, a small fraction of the total hysteresis, appears to be related to the accumulation of fatigue damage responsible for ultimate fatigue failure.

To test this hypothesis, experiments were conducted upon nearly 100 specimens made of rimmed, cold-drawn, nominally AISI 1018 steel with 0.1640 carbon, Rockwell hardness 4.65A and a tensile strength of 77,717 psi.

The tests were conducted with a closed-loop, servo-hydraulic machine operated at minimum hydraulic pressure levels to decrease both the acoustic and electrical background noise to the point where AE signals corresponding to the 10^{-20} J/cm^2 -sec threshold level could be detected.

1.2   Overview

Chapter 2 presents a summary of the observations contained in Part I of this report, an interpretation of observations of stress - strain behavior in the vicinity of the fatigue or endurance limit, an interpretation of the high-cycle fatigue process and an interpretation of the intermediate and low-cycle fatigue process. Chapter 3 contains conclusions about the connection between fatigue and hysteresis and recommended directions for future research.

CHAPTER 2.

INTERPRETATION OF OBSERVATIONS

2.1   Summary of Observations

Part I of this Report is devoted to a compilation of results from experiments conducted upon nearly 100 specimens made of rimmed, nominally AISI 1018 steel. This material was selected because extensive data on its performance exists in the engineering literature and because its stress - strain curve is of the gradual yielding type thus mirroring at least the monotonic stress - strain behavior of many of the kinds of aluminum and titanium alloys used in the aircraft industry. It should be noted, however, that steels typically show fatigue limits whereas aircraft alloys typically do not.

For the purpose of interpretation, the most significant results reported in Part I of this Report are reproduced herein as Figures 11A, 11B, 15, 16 and 17. Perhaps the most striking result is the observation that, with the exception of the first few cycles and the last one hundred or so cycles, the hysteresis loss per cycle, $\Delta U_i(\varepsilon)$, is very nearly a constant during most of the loading history of the metal. This is clearly shown in Figure 16. Moreover, even if the specimen is subjected to a number of "overloads", as shown in Figure 17, the hysteresis loss per cycle reverts to its previous, nearly constant, value as soon as the "overloads" are removed. This is a remarkably robust result that we have observed many times. And, one may certainly infer from the results of our experiments that the steady - state hysteresis loss per cycle, $\Delta U_i(\varepsilon)$, is very nearly equal to the average hysteresis loss per cycle, $<\Delta U(\varepsilon)>$, over the entire loading history of the specimen.

As expected, the average hysteresis loss per cycle, $<\Delta U(\varepsilon)>$, decreases as the strain amplitude decreases and the number of cycles to failure N_f increases. This is clearly shown in Figure 11A. This means that if graphs of hysteresis loss per cycle versus number of cycles for three different strain amplitude levels are plotted on the same chart, then such a chart would resemble Figure 18. Moreover, each of the graphs shown in Figure 18 is of the form shown in Figure 19 in which three distinct zones in the evolution of hysteresis loss per cycle are evident. These three zones are believed to correspond to the three stages in the progression that begins with microplasticity, random dislocation motion and dislocation interactions and continues to final rupture in fatigue through the stages shown in Figures 1 and 3.

The nearly 100 specimens investigated in this phase of the research program were divided into two nearly equal groups; one group was subjected to cyclic strains that varied between two strain limits which were equal in magnitude but opposite in sign (two-sided hysteresis, strain ratio $R = -1$, c.f. Figure 10) and the other group was subjected to cyclic strains that varied between zero and a constant maximum tensile strain, or strain ratio $R = 0$, (one-sided hysteresis). When the data from the $R = 0$ experiments was combined with the data from the $R = -1$ experiments, it was found that the measurements of the average hysteresis loss per cycle, $<\Delta U(\varepsilon)>$, versus the number of cycles to failure, N_f, and the measurements of the cumulative hysteresis loss, $U_T(\varepsilon, N_f)$, versus the number of cycles to failure, N_f, could both be fitted very well by simple power law relationships of the form,

$$<\Delta U(\varepsilon)> \approx 32 \ (N_f)^{-.53} \approx \frac{32}{\sqrt{N_f}} \qquad (2.1)$$

and

$$U_T(\varepsilon, N_f) = 32 \, (N_f)^{.47} = 32 \, \sqrt{N_f}, \qquad (2.2)$$

which is the equation of a parabola whose axis of symmetry coincides with the N_f - axis, or abscissa of the U_T versus N_f chart. These two relationships are also shown in Figures 11A and 11B respectively.

2.2 Stress-Strain Behavior in the Vicinity of the Fatigue or Endurance Limit: $10^{-3} < \varepsilon < 2 \times 10^{-3}$

One of the most important tasks of fatigue research is the identification of the endurance or fatigue limit. As indicated by the curves given in Figure 4, the critical loading thresholds for fatigue are usually determined by S-N_f or fatigue-life tests that may extend to well over 10^6 cycles. One objective of this research program was to provide additional criteria — based on microstructural processes — that will lead to a rapid identification of the endurance limit without the need to perform hundreds of tests.

Since scanning tunneling microscope measurements (c.f. T. Erber, et al 1990) indicate that microscopic imperfections are nucleated in materials at strain levels that are significantly smaller than the endurance limit, it is conjectured that this limit actually corresponds to a threshold where repeated load cycles progressively organize the dislocations and dislocation arrays (that can be viewed as micro-imperfections) that already exist. One model for the endurance limit, therefore, is to characterize it as the point where the dislocation distribution changes from a statistically random one to a more ordered pattern of clusters and tangles that leads to the inception of microcracking. It is surmised in this model that slip lines and bands such as those shown in Figures 5 and 6 occur

concurrently. This scenario is also consistent with the shakedown model of the fatigue process (c.f. Guralnick, 1975). In this model the endurance limit corresponds precisely to the demarcation between shakedown, i.e. stabilization, and incremental collapse. The connection between maximum stress, minimum stress, stress range and mean stress in fatigue is summarized by the Goodman-Gerber diagram or envelope shown in Figure 7. The organization of imperfections at stress levels which correspond to points which lie on the envelope is then represented by the coalescence of isolated microplastic zones into organized collapse mechanisms. Furthermore, the striations in Figure 6 can be associated with the analogous ratchetting behavior of an engineering structure's collapse mechanisms thus leading to the inference that the dislocation organization resulting from microplasticity in the material is analogous to the organization of plastic hinges occurring in an engineering structure into "mechanism patterns."

One of the basic consequences of the general hysteresis theory is that the degree of organization of dynamical systems is reflected by their hysteresis response. This implies that acoustic emission, which is one of the most sensitive probes of microstructure, should change in a characteristic way at the fatigue limit. In particular, the acoustic signature of fading hysteresis is the Kaiser effect (c.f. Pasztor and Schmidt, 1978); by contrast, the organization of imperfections or zones of microplasticity and the consequent constant hysteresis is related to the felicity effect (i.e. the persistence of acoustic emission).

Figure 8 shows both the monotonic stress-strain relation for the rimmed, nominally AISI 1018 steel and the average hysteresis energy losses per cycle. In this case, the proportional or elastic limit is $\sigma_{p\ell}$ = 48 ksi, and the endurance or fatigue limit is σ_e = 33 ksi.

It is evident that the endurance limit also corresponds to a stress value where that part of the hysteresis energy that drives local microstructural damage tends to fade and ultimately vanish.

2.3 The High-Cycle Fatigue Process: $2 \times 10^{-3} < \varepsilon < 6 \times 10^{-3}$

Conventionally, high-cycle fatigue refers to situations where the service life of components falls into the range greater than 10^5 cycles before failure finally occurs due to fatigue. A widely used empirical guide for estimating, N_f, the number of cycles to failure, is the Manson-Coffin power law (c.f. Bannantine, et al., 1990), which may be written as,

$$\Delta\varepsilon_p = B(N_f)^b, \tag{2.3}$$

where $\Delta\varepsilon_p$ is twice the plastic strain amplitude defined in Figure 9; B is a material constant sometimes called the fatigue ductility coefficient and b is the fatigue ductility exponent whose value typically lies between -0.5 and -0.7. By inverting (2.3), and inserting the estimate $(1/b) \cong -2$, one obtains,

$$N_f \approx \left(\frac{B}{\Delta\varepsilon_p}\right)^2. \tag{2.4}$$

It becomes clear that this relation is of limited practical use because of the extraordinarily sensitive dependence upon the strain range. In fact, for values of $\Delta\varepsilon_p$ close to the endurance limit, $\Delta\varepsilon_{end}$, equation (2.4) cannot even be qualitatively correct because the experimental correspondence of $\Delta\varepsilon_p \to \Delta\varepsilon_{end}$ with the limit $N_f \to \infty$ is incompatible with (2.4)

Empirical estimates of the form (2.3) are also deficient on a deeper level. It is well known from many experiments that the areas of stress-strain hysteresis loops tend to shrink

as N grows large in the vicinity of the endurance limit. In this high-cycle fatigue range it is evident from Figure 10 that there is no direct relation between the area of the hysteresis loop and the strain range, $\Delta \varepsilon$.

This problem can be resolved with the help of the general hysteresis theory. In this approach, Equations (2.3) and (2.4) are replaced by the relation,

$$N_f = \frac{c}{(<\Delta U(\varepsilon)>)^2} ,\tag{2.5}$$

where $<\Delta U(\varepsilon)>$ is the average hysteresis energy loss per cycle, i.e. the average total area of the shaded loop in Figure 10, corresponding to the maximum strain ε, and c is a material constant. A series of measurements with rimmed, nominally AISI 1018 steel specimens — summarized in Figure 11A — shows good agreement with (2.5).

Since the existence of hysteresis is a necessary but not sufficient condition for irreversible processes, the replacement of the plastic strain range, $\Delta \varepsilon_p$, in (2.4), by the average energy dissipation or average loop area, $<\Delta U(\varepsilon)>$, as given in (2.5), removes the contradictions latent in the older empirical estimates of fatigue life. It is in fact possible to establish a more direct connection between fatigue life, hysteresis energy dissipation, and the cumulation of damage. Figure 11B shows that the total hysteresis energy dissipated in high cycle fatigue tends to diverge near the endurance limit. If we denote this total energy dissipation by $U_T(\varepsilon)$, then

$$U_T(\varepsilon) = \sum_{i=1}^{N_f} \Delta U_i(\varepsilon) \approx N_f(<\Delta U(\varepsilon)>)\tag{2.6}$$

where $\Delta U_i(\varepsilon)$ is the energy dissipated during the ith cycle. Combining (2.6) with (2.5) we obtain the simple relationship,

$$U_T(\varepsilon) = \frac{c}{(<\Delta U(\varepsilon)>)}, \qquad (2.7)$$

which implies that $U_T \to \infty$ as $<\Delta U(\varepsilon)> \to 0$. Of course, most of this energy is dissipated as heat to the environment. If this were not so, then after about 10^5 cycles enough energy would have been pumped into the steel to completely vaporize the specimen. This simple argument shows that is essential to relate $\Delta U_i(\varepsilon)$ — the hysteresis energy loss per cycle — to $\Delta U_d(\varepsilon)$, the hysteresis energy per cycle that is directly associated with damage.

A quantitative connection can be derived by assuming that failure occurs when a characteristic limiting energy, $U_d(\varepsilon)$, is exceeded. In a first approximation, it is also convenient to assume that U_d is independent of ε, and that the accumulation of damaging energy is proportional to the number of cycles, i.e.

$$(\Delta U_d(\varepsilon)) \, N_f(\varepsilon) = U_d. \qquad (2.8)$$

It is shown in the Appendix to this Report that these approximations are equivalent to the Palmgren-Miner law of damage. In practice, the magnitude of U_d can be estimated from the area under the monotonic stress-strain curve in Figure 8.

Recently, LeMaitre and Chaboche, 1990, have reported results which also lend support to our hypothesis that the total hysteresis energy accumulated by a metal which fails in fatigue, U_T, possesses two principal components; one is a damaging component which is a constant, U_d, and the other represents the hysteresis energy which is converted into heat and harmlessly dissipated into the environment. Moreover, these researchers make the

same argument that is made herein with respect to the relationship between U_T, U_d and N_f. Namely, they propose the following equation (c.f. Figure 12),

$$U_T = U_d + N_f(\Delta \Phi) = A(N_f)^a \tag{2.9}$$

in which, $\Delta\Phi$ is a constant which represents the energy harmlessly dissipated as heat in each cycle; U_d, the damaging component of the hysteresis energy, is a constant and A and a are experimentally determined constants. Equation (2.9) is exactly similar in form to (2.2) which has been found in connection with the experiments described in Part I of this Report.

The ratio of the damaging energy per cycle $\Delta U_d(\varepsilon)$ to the average hysteresis energy per cycle can be obtained from (2.5) and (2.8), that is,

$$\frac{\Delta U_d(\varepsilon)}{<\Delta U(\varepsilon)>} = \frac{U_d}{c} (<\Delta U(\varepsilon)>) . \tag{2.10}$$

Measurements have shown that for AISI 1018 steel the ratio U_d/c is of the order of 0.02. This value is consistent with calorimetric estimates obtained from studies of the stored energy of cold work (Bever et al., 1973).

Equation (2.10) explains in a simple way how the total energy dissipated in high cycle hysteresis — U_T in (2.6) — can become very large, and at the same time, the total energy dissipated in damage — U_d in (2.8) — can remain fixed. The essential point is that not only is the damaging energy a small component of the total hysteresis energy dissipation (< 0.02), but the ratio itself is proportional to the energy dissipation. This is evident if (2.10) is rewritten to show explicitly the magnitude of the average damaging energy accumulated per cycle,

$$\Delta U_d(\varepsilon) = \frac{U_d}{c} (<\Delta U(\varepsilon)>)^2 \qquad (2.11)$$

For AISI 1018 steel, in high cycle fatigue, representative values are $<\Delta U(\varepsilon)> \sim 0.2 \, J/cm^3$, and $<\Delta U_d(\varepsilon)> \sim 8 \times 10^{-4} \, J/cm^3$.

The practical implication of Equations (2.6) and (2.11) for fatigue tests are illustrated in Figures 13 and 14. That is, if U_d is a constant, c is a constant and $<\Delta U_d(\varepsilon)>$ is independent of N_f, then ΔU_d, the damaging energy per cycle, must likewise be independent of N_f. Referring to the lower of the two charts shown in Figure 13, for a pre-selected value of the strain amplitude, ε_1, it is clear from graphs ℓ_1, and ℓ_2 in this figure that the accumulation of total hysteresis energy, U_T, and the accumulation of damaging energy, U_d, are both linear functions of N. That is, the derivative of the function whose graph is given by ℓ_1 is the constant, $<\Delta U(\varepsilon)>$, and the derivative of the function whose graph is given by ℓ_2 is the constant, $<\Delta U_d(\varepsilon)>$. However, ℓ_1 terminates at the parabola, $U_T = A(N_f)^x$, whereas ℓ_2 terminates at the horizontal line, U_d = constant. The total hysteresis energy at failure, U_T, is clearly dependent upon ε, the strain amplitude, and N_f, the number of cycles to failure; whereas the total damaging energy at failure, U_d, is a constant which is completely independent of ε and N_f.

The development of damage in both low-cycle and high-cycle fatigue proceeds through a variety of microstructural mechanisms. The principal components of this scenario include the following processes (c.f. Figure 1):

(1) Activation of dislocation sources resulting in fine transition slip lines (e.g. microslip).

(2)   Initiation phase of microcracks (stage 1)

- Dislocation climb accompanied by void formation.

- Formation of permanent slip bands and decohesion.

- Intrusion - extrusion mechanisms: nucleation of microcracks at points of intrusion.

(3)   Growth phase of microcracks (stage 2)

- Orientation of microcracks perpendicular to plane of maximum principal stress.

- Progression of microcracks through successive grains or along grain boundaries. Initiation of macroscopic cracks through coalescence of microcracks.

(4)   Growth phase of macrocracks (stage 3)

- The cyclic opening and closing of cracks results in alternating plastic slips at the crack tip. These, in turn, form a ridge of cleavage at each growth of the crack.

- The cracks grow until a critical size is reached where instability promotes an increase in crack propagation velocity.

(5)   Fractures organize into networks. When the connectivity is sufficiently high to achieve separation of components, complete rupture ensues.

Figures 15 and 16 indicate how this complex sequence of processes is reflected in the characteristics of stress-strain hysteresis. In particular, Figure 15 shows 50 successive hysteresis loops that exhibit the effects of strain softening. However, it is remarkable that

even though the shapes of the individual loops change, the areas of successive loops tend to remain constant. This is one of the reasons that the average hysteresis energy dissipation, $<\Delta U(\varepsilon)>$ in equation (2.5), can be determined with precision from the experiments.

As a specific example, AISI 1018 steel subjected to alternating stress-strain cycles with $|\varepsilon_{max}| = 0.0023$, reached a steady hysteresis energy dissipation of $<\Delta U> \simeq 0.063$ kip - in/in³ for N $\sim$ 5000 cycles. This gradually increased to $<\Delta U> \simeq 0.065$ at N $\sim$ 76,000 cycles — a 3% change. This specimen failed at $N_f = 83,277$ cycles; and only during the last 5000 cycles preceding rupture was there any conspicuous change in the rate of energy dissipation. Figure 19 is a schematic representation of the variation of $<\Delta U>$ with N: the portion marked 'range 2' corresponds to the nearly constant rate of total energy dissipation during most of the test cycles; whereas 'range 3' indicates the decrease in $<\Delta U>$ that usually signalizes impending failure. Presumably, the hysteresis changes in range 3 reflect the microstructural processes discussed in the preceding subsections. One of the objectives of future AE studies will be to correlate the cycle-by-cycle changes of hysteresis in range 3 with the patterns of acoustic pulses.

2.4 The Intermediate and Low-Cycle Fatigue Process: $\varepsilon > 6 \times 10^{-3}$; $N_f < 10^6$

The number of cycles to failure in this strain range can be estimated with the help of an empirical relation resembling the Manson-Coffin power law (2.3), i.e.

$$\Delta\varepsilon_p = B(N_f)^b \tag{2.12}$$

where $\Delta\varepsilon_p$ is the plastic strain range defined by the construction in Figure 10, B is the fatigue-ductility coefficient, and b is the fatigue-ductility exponent. Measurements show that

for many metals b falls into the range -0.5 < b < -0.7; (c.f. Morrow, 1965; Hempel, 1965). Since $\Delta\varepsilon_p$ is associated with the width of hysteresis loops, equation (2.12) represents a connection between fatigue life and hysteresis energy dissipation. In practice (2.12) is only useful if the hysteresis loops stabilize sufficiently so that an average value of the width $<\Delta\varepsilon_p>$ can be defined. Figure 15 illustrates an ambiguous case where strain softening spreads the values of $\Delta\varepsilon_p$.

This problem can be avoided by replacing $\Delta\varepsilon_p$ by the area of the hysteresis loop. As indicated schematically in Figure 16, and illustrated with specific measurements in Figure 17, the areas of individual hysteresis loops tend to remain invariant even in low-cycle fatigue. Furthermore, the loop areas are directly proportional to the hysteresis energy dissipation; and by virtue of (2.9), are also related to the cumulation of damage.

These arguments suggest replacing the Manson-Coffin relation (2.12) by a similar power law utilizing the average hysteresis energy dissipation, or,

$$<\Delta U(\varepsilon)> = D(N_f)^d. \tag{2.13}$$

Where D and d are material constants. Figure 11A summarizes the results of a series of fatigue tests with AISI 1018 steel. Clearly, the data are consistent with the power law (2.13) over a range of several decades. It is striking that both the low-cycle and intermediate fatigue range are described by a single value of the exponent, d $\approx$ - 0.53. In addition, equation (2.13) covers both R = -1 and R = 0 hysteresis without any separate adjustment of the parameters.

The particular value d = - ½ can be deduced from the general hysteresis theory (Erber and Gavelek, 1991). This result suggests two experimental tests with broad practical

implications: (i) Reanalyzing fatigue life tests for a variety of steels and other metals using (2.13) instead of (2.12) — the results should indicate a high clustering of values of d around -0.5 instead of the spread $-0.5 < c < -0.7$. (ii) The empirical Manson-Coffin relation,

$$\Delta\varepsilon = B(N_f)^b + C(N_f)^c, \tag{2.14}$$

incorporates two different sets of coefficients and exponents to cover both low and high-cycle fatigue tests. By replacing the indirect hysteresis measure $\Delta\varepsilon$ with the direct measure $<\Delta U(\varepsilon)>$, a single relation of the form,

$$<\Delta U(\varepsilon)> \cong D[N_f(\varepsilon)]^{-\frac{1}{2}}, \tag{2.15}$$

should describe the entire spectrum of fatigue behavior from the low-cycle range to the high-cycle range.

Figures 16 and 19 emphasize one of the basic difficulties of fatigue measurements. Even the most precise hysteresis energy measurements feasible with present instrumentation are not sufficiently sensitive to detect the cycle-by-cycle cumulation of damage. This is an immediate consequence of (2.10) which shows that precision of the order of one part in 10^5 would be necessary to distinguish the damaging component of the hysteresis energy dissipation. Nevertheless, intermittent overloads seem to be a practical means for enhancing the sensitivity of detecting the progression of damage. This approach is illustrated in Figure 17. In this case the MTS machine was programmed to apply repetitive strain-controlled loading cycles to a specimen with $|\varepsilon| \leq 0.0055$ applied every 500 cycles. The change in $<\Delta U(\varepsilon)>$ before and after the overload cycles is a sensitive index of the intrinsic 'ageing' of the specimen. We denote this change by $\delta<\Delta U(\varepsilon)>$. The variation of this quantity is indicated in the following table.

Table 1

Change in Hysteresis Loss Per Cycle as a Result of Overloads

Overload Group	1	2	3	4	5	6	7	8
$\delta<\Delta U(\varepsilon)>$	0.90	0.89	1.11	1.13	1.41	1.61	1.92	2.76

The specimen failed 60 cycles after the 9th overload group was imposed.

These effects are much more conspicuous in AE Tests — the pattern of acoustic pulse evolve in a definite way as the damage increases and affects the recovery from overload cycles late in the 'life' of a fatiguing specimen.

2.5   Acoustic Emission and Fatigue

The acoustic emission research carried out to date had two principal objectives:

(1)   To locate the endurance, or fatigue, limit of a structural steel with a minimum of measurements — thereby circumventing lengthy life tests.

(2)   For loading conditions above the endurance or fatigue limit and for metal alloys that do not show such a limit, to use acoustic emission patterns to estimate the remaining service life before fatigue failure.

Experimental results obtained to date indicate that it is feasible to reach both of these goals. The measurements have been carried out with a newly installed closed-loop, servo-hydraulic testing machine (i.e. MTS-810) which is operated at minimum hydraulic pressure levels so that the acoustic emission background noise or interference is negligible. This relatively

quiet environment permits an unambiguous interpretation of the acoustic signals emanating from the test sample.

Since fatigue is the result of cumulative damage, energy losses associated with sustained hysteresis always accompany fatigue failure. Acoustic emission is a manifestation of the irreversible microscopic processes that are responsible for cumulative damage. By contrast, if a material is subjected to cyclic conditions at stress or strain levels below the endurance limit, it can be cycled indefinitely without fatigue failure even though substantial hysteresis may occur.

It is well known that when metals are cycled at sufficiently low load levels, the corresponding acoustic emission is large on the first cycle, and decreases on subsequent cycles. This 'training away' of acoustic pulses is the Kaiser effect. Measurements show that the associated stress-strain hysteresis loops either have negligible areas, or tend to decrease with increasing numbers of cycles. In this sense, the Kaiser effect is a microscopic counterpart to strain hardening, or the approach to elastic response.

At stress or strain levels in excess of the endurance limit, the hysteresis loops stabilize with well defined areas, and all of the acoustic emission cannot be trained away. This correlation shows that the endurance limit is indeed associated with the cessation of the Kaiser effect, and the threshold of the felicity effect (i.e. the persistence of acoustic emission). This behavior has been verified in a number of samples of AISI 1018 steel. The transition from the Kaiser effect to the felicity effect occurs at peak strain values $\varepsilon = 0.0022$ for R = 0. Independent life tests confirm that this strain value also corresponds to the strain endurance limit for this material.

Detailed measurements of the cycle-by-cycle evolution of the stress-strain hysteresis of AISI 1018 steel samples — from the initial cold-worked state to ultimate fatigue failure — show a characteristic profile. In particular, all tests show a sudden decrease in the hysteresis loop areas before failure. Typically, this 'lead time' is of the order of 3000 cycles before a sample ruptures at 100,000 cycles. (c.f. Figure 16). The patterns of acoustic emission exhibit a corresponding evolution throughout the development of fatigue (c.f. Figure 20). For instance, it is well known that just before final rupture there is an enormous increase in the amplitude and frequency of acoustic pulses. The low noise background of our closed-loop, servo-hydraulic testing machine permits measurements that show that this trend actually begins at a much earlier stage; for example, in cases where the hysteresis area variations signal impending failure in another 3000 cycles (e.g. point c′ in Figure 20), the changes in the acoustic patterns have a significantly longer 'lead time' of the order of 6000 cycles (e.g. point b in Figure 20). It is expected that the changes in hysteresis energy arise as a result of localized absorption of the strain energy by a microcrack network having a lower compliance than the surrounding material.

Acoustic emission patterns contain additional information concerning the transition from dislocation-produced localized crack precursors and the organization of damage that is not apparent from variations in stress-strain hysteresis. A conspicuous example is the decay of acoustic emission under static conditions where, of course, there is no hysteresis. Specifically, after a few cycles of loading of an "as-received" specimen, if either the stress or strain is reduced to zero, the acoustic emission immediately ceases. However, if the specimen is aged with thousands of loading cycles, and then again permitted to 'rest', the

acoustic pluses do not vanish promptly, but slowly decrease. This response is typical of relaxation phenomena after anelastic strains. The characteristics of this decaying emission yield information concerning the number and nature of accumulated defects — hence the intrinsic fatigue age. Similarly, the acoustic response to overload cycles can be used as a measure of the exhaustion of life.

The conventional explanation of the process which leads from the inception of damage to ultimate rupture in fatigue is illustrated in Figure 2. It is assumed in the conventional explanation that fatigue failure is the culmination of a process which begins with the initiation of cracking and progresses to failure by means of the propagation of cracking. The overwhelming weight of evidence (c.f. Figure 5, 6 and 8) however, indicates that a far more complex set of processes are set in motion when a material is cyclically stressed (or strained) to levels in excess of the endurance or fatigue limit. This set of complex processes, which originates virtually at the atomic level, is summarized in Article 2.3 of this Report and in Figures 1 and 3.

Referring to Figure 3, if a material is cyclically stressed to a level S_1, which exceeds the endurance limit, then Region 1 pertains to the inception of microplasticity; Region 2, which is bounded by curves P and F, pertains to the 'cooperative organization' of zones of microplasticity and the slow accumulation of damage through micro-cracking; and Region 3, which is bounded by curve F and the conventional S vs. N_f curve, pertains to the initiation of macro-cracking and the rapid accumulation of damage through the organization and propagation of relatively large cracks (i.e. macro-cracking). Just prior to final rupture, at a value of N defined by S_1 (or ε_1) and curve M, (c.f. Figures 3 and 20) crack propagation

proceeds far more rapidly than was previously the case and the rate of damage accumulation increases sharply (c.f. points c, c' and c'' in Figure 20). By combining and correlating information obtained from simultaneous hysteresis and acoustic emission measurements performed on a series of individual samples subjected to cyclic loading, it is possible to locate points (e.g. points a'', b'', c'' and d'') on the curves designated P, F, M, and S-N (c.f. Figure 20) which bound the three zones or stages in the progression leading to ultimate rupture as illustrated in Figure 20. The lowermost curve in this figure is constructed by fitting a series of lines of regression to the respective AE measurements.

Referring again to Figure 20, in the low-cycle fatigue region ($N < 10^5$) the curve marked M diverges appreciably from the S-N curve whereas in the high-cycle fatigue region ($N > 10^5$) curve M merges into the S-N curve and these two curves cannot be distinguished from one another. Hence, the region bounded by the curves M and S-N in Figure 20 includes phenomena which cause the well-known differences in behavior between low-cycle fatigue and high-cycle fatigue. For example, it is in this region that the original Manson-Coffin relationship (2.3) and the original Palmgren-Miner relationship (A.6) break down. Figure 20 makes it clear just how and why these breakdowns occur. When N exceeds $N_{c'}$, the middle graph of Figure 20 indicates that the hysteresis energy per cycle, $\Delta U_i(\varepsilon)$, rapidly falls off from its previous nearly constant value. Also, $N_{c'}$ of the middle graph of Figure 20 corresponds to N_c in the lowermost graph in this same figure. This latter graph shows that when N exceeds N_c acoustic emission increases dramatically. Both of these facts — the fall-off in hysteresis energy per cycle and the dramatic rise in acoustic emission — indicate that new processes are occurring in the material in the region bounded by curves M and S-N

which differ considerably from those which occur when $N < N_c$ or N_c. These new processes must include the organization and propagation of macrocracks and a concomitant increase in the rate of damage accumulation. This means that neither $\Delta U_i(\varepsilon)$ nor $\Delta U_d(\varepsilon)$ are constant when N is in the range $N_c < N < N_f$. Under these circumstances it is perfectly understandable that neither the Manson-Coffin relationship (i.e. (2.3) or (2.19)) nor the Palmgren-Miner relationship (A.6) are applicable.

It is, therefore, clear, for the reasons cited above and the graphs and geometric constructions shown in Figure 20, that both hysteresis and acoustic emission measurements are needed to follow the fatigue process from onset of plasticity-induced microcracking to ultimate rupture.

CHAPTER 3.

CONCLUSIONS

3.1 The Connection Between Fatigue and Hysteresis

Although it is recognized that microplasticity, as evidenced by hysteresis, is merely a necessary condition and not a sufficient condition for the development of a substructure that leads to fatigue failure, it has been demonstrated herein that measurements of hysteresis can yield significant insights into the various stages of the development of a fatigue critical microstructure which culminates in complete rupture of the material. Specifically, the following observations have been made in connection with the research reported in. Part I of this Report:

(1) The total hysteresis energy dissipated by a metal which fails in fatigue possesses two principal components; one is a damaging component, which is small compared to the total hysteresis energy; and the other represents that portion of the hysteresis energy which is converted into heat causing no damage. This latter component is a large fraction of the total hysteresis energy. Moreover, the relationship among the various components of hysteresis energy and the total hysteresis energy is given by equation (2.9), or,

$$U_T = U_d + N_f(\Delta\Phi) = A(N_f)^a \qquad (2.16)$$

(2) Failure in fatigue occurs when a characteristic limiting energy, $U_d(\varepsilon)$, is reached. It is reasonable to presume that this quantity is independent of the strain amplitude, ε, based on the evidence presented by LeMaitre and

Chaboche, 1990, and by the fact that the usual form of the *Palmgren-Miner law of damage can be precisely derived if* U_d *is taken to be a constant (c.f. Figure 14 and the Appendix).*

(3)   By replacing $\Delta\varepsilon_p$ in the well-known Manson-Coffin power law (2.3),

$$\Delta\varepsilon_p = B(N_f)^b ,\qquad\qquad (2.17)$$

with the area of the hysteresis loop, $\Delta U_i(\varepsilon)$, an analogous formulation is obtained which is,

$$\Delta U_i(\varepsilon) = D(N_f)^d. \qquad\qquad (2.18)$$

It has been found that the area of the hysteresis loop in each cycle, $\Delta U_i(\varepsilon)$, is remarkably constant over nearly the whole fatigue life history of the material (c.f. Figure 16). Hence, $\Delta U_i(\varepsilon)$ in equation (2.18) may be replaced by the average area of all of the hysteresis loops, $<\Delta U(\varepsilon)>$, to yield,

$$<\Delta U(\varepsilon)> \simeq D\ (N_f)^d \qquad\qquad (2.19)$$

Moreover, it has been found that (2.19) adequately represents data accumulated in Part I of this Report for the entire spectrum of hysteresis behavior from low-cycle to high-cycle fatigue when $D \cong 32$ and $d \cong -\frac{1}{2}$ (c.f. Figure 11A) without the need for the sort of modification (2.14) originally proposed by Manson and Coffin, namely,

$$\Delta(\varepsilon) = B(N_f)^b + C(N_f)^c \qquad\qquad (2.20)$$

(4)   If equation (2.19) adequately represents the relationship between hysteresis loop area (or hysteresis energy per cycle) and the number of cycles, N, then the total hysteresis energy accumulated in N cycles, U_T, is given by,

$$U_T = N_f(<\Delta U(\varepsilon)>), \qquad (2.21)$$

or, in view of (2.19),

$$U_T = D(N_f)^{d+1}. \qquad (2.22)$$

If $D \cong 32$ and $d \cong -1/2$, then (2.22) becomes,

$$U_T \cong 32 \sqrt{N_f}, \qquad (2.23)$$

which is the equation of parabola whose axis of symmetry coincides with the abscissa of the graph of U_T vs. N_f. Moreover, it may be observed from Figure 11B that (2.23) adequately represents the entire collection of experimental observations shown therein.

(5)   The average _damaging_ energy accumulated in each cycle is given by (2.11) as,

$$\Delta U_d(\varepsilon) = \frac{U_d}{c} (<\Delta U(\varepsilon)>)^2 . \qquad (2.24)$$

If U_d is a constant, c is a constant and $<\Delta U_d(\varepsilon)>$ is independent of N_f, then $\Delta U_d(\varepsilon)$ must likewise be independent of N_f. This conclusion is illustrated by line ℓ_2 shown in the lowermost of the two graphs of Figure 13.

(6)   In view of the simplicity of equations (2.21), (2.23) and (2.24) and the fact that U_d may be estimated from the results of a simple monotonic, uniaxial tension test performed on the material, it is clear that relatively few tests are

required to obtain the information needed to construct a complete S vs. N_f curve for a given material. For this reason, it appears quite likely that one may also be able to make use of a relatively small number of experiments to obtain the data needed to make a useful estimate of the endurance or fatigue limit.

3.2   Recommended Directions for Future Research

Results from this research program suggests the existence of three distinct types of stress-strain hysteresis:

(i)   A fading hysteresis, or strain hardening, corresponding to a gradual attainment of microstructural stability and the concomitant cessation of microplastic flow and micro-cracking. This is the analogue of structural shakedown in engineering structures.

(ii)   A steady hysteresis due to alternating microplastic flow at isolated defect sites.

(iii)   An apparently steady hysteresis accompanying the gradual 'organization' of microplastic zones and the propagation of micro-cracking. In engineering structures this type of hysteresis is associated with the formation of incremental collapse mechanisms.

Since less than one part in 10^5 of the mechanical energy dissipated in hysteresis is associated with the cumulation of damage and the rest is heat which is harmlessly dissipated, it is extremely difficult to discriminate between type (ii) and type (iii) hysteresis by purely macroscopic measurements. However, our preliminary results have shown that it is feasible

to develop acoustic emission diagnostics that can distinguish between localized defects and patterns of organized plastic deformation and the inception and propagation of micro-cracks (c.f. Figure 20). The Kaiser effect measurements discussed earlier will provide an opportunity to search for acoustic signatures of microplastic organization.

The foregoing discussion implies that future directions for research ought to have four principal objectives:

1) Improving the 'lead time' of fatigue failure predictions for individual specimens by means of variable-step, simultaneous hysteresis and AE measurements.

2) Development of a more accurate and rapid determination of the endurance limit based on a combination of hysteresis analysis and AE diagnostics.

3) Extension of the measurements to several other types of steel to build confidence in the general applicability of the methods outlined herein. This is a prerequisite for eventual practical applications.

4) Refining the AE diagnostics, in conjunction with generalized hysteresis theory and SEM and TEM 'post-mortem' measurements, to yield direct information concerning the inception, organization and accumulation of microstructural damage.

APPENDIX

Miner's Law

Let us consider the results from a number of fatigue life experiments carried out upon samples made of the same material. It has been shown earlier that if U_d is a constant, then $\Delta U_d(\varepsilon)$ is likewise a constant for any preselected value of the strain amplitude, ε. Referring to Figure 14, the lines ℓ_1, ℓ_2..., ℓ_5 are graphs of the accumulation of damaging energy versus the number of cycles of load application. Failure occurs when the total accumulation of damaging energy reaches the limiting value, U_d. Or, in other words, when one of the inclined lines ℓ_1, ℓ_2, ..., ℓ_5 intersects the horizontal line, $U = U_d$.

Let $u_d(\varepsilon)$ be the damaging energy accumulated in n cycles,

n be the number of cycles of load applied to the specimen such that $n < N_f$,

N_f be the number of cycles of load applied to the specimen up to failure in fatigue, and

$\Delta U_d(\varepsilon)$ be the damaging energy accumulated in one cycle at a pre-selected strain amplitude, ε.

Suppose a _single_ sample, made of the material which exhibits the fatigue behavior shown in Figure 14, is subjected to five different patterns of cyclic load applications in which the strain amplitudes are ε_1, ε_2, ..., ε_5 and the number of applications of load at these five strain amplitudes are n_1, n_2, ..., n_5 respectively. Then we may write that the damaging energy accumulated at each of these strain levels is given by,

$$u_d(\varepsilon_1) = n_1 \, \Delta U_d(\varepsilon_1) \left.\vphantom{\begin{array}{c}1\\1\\1\\1\\1\end{array}}\right\}$$
$$u_d(\varepsilon_2) = n_2 \, \Delta U_d(\varepsilon_2)$$
$$u_d(\varepsilon_3) = n_3 \, \Delta U_d(\varepsilon_3) \qquad (A.1)$$
$$u_d(\varepsilon_4) = n_4 \, \Delta U_d(\varepsilon_4)$$
$$u_d(\varepsilon_5) = n_5 \, \Delta U_d(\varepsilon_5)$$

Failure will occur when,

$$u_d(\varepsilon_i) = U_d, \text{ a constant.} \qquad (A.2)$$

From Equations (A.1) and (A.2) and the definitions given above,

$$N_{f1} \, \Delta U_d(\varepsilon_1) = N_{f2} \, \Delta U_d(\varepsilon_2) = N_{f3} \, \Delta U_d(\varepsilon_3) \, ... \, = U_d \qquad (A.3)$$

When a sample of material is subjected to cyclic loading at several different strain levels, $\varepsilon_1, \varepsilon_2, ..., \varepsilon_5$ say, then failure due to cumulative damage will occur when,

$$n_1 \, \Delta U_d(\varepsilon_1) + n_2 \, \Delta U_d(\varepsilon_2) + n_3 \, \Delta U_d(\varepsilon_3) + \, ... \, \le U_d \qquad (A.4)$$

in which, $n_1 < N_{f1}$, $n_2 < N_{f2}$, $n_3 < N_{f3}$, ...

Dividing both sides of Equation (A.4) by U_d, we obtain,

$$n_1 \, \frac{\Delta U_d(\varepsilon_1)}{U_d} + n_2 \, \frac{\Delta U_d(\varepsilon_2)}{U_d} + n_3 \, \frac{\Delta U_d(\varepsilon_3)}{U_d} + ... \, \le 1 \qquad (A.5)$$

Substituting for U_d in Equation (A.5) the appropriate value given by Equation (A.3) we obtain,

$$\frac{n_1}{N_{f1}} + \frac{n_2}{N_{f2}} + \frac{n_3}{N_{f3}} + \, ... \, \le 1 \qquad (A.6)$$

which is the usual form of the Palmgren-Miner equation (c.f. Palmgren, 1924).

REFERENCES

Anon, 1978, "Fatigue and Microstructure", Papers presented at the 1978 ASM Materials Science Seminar, American Society for Metals, Metals Park, Ohio.

Bannantine, J.A., Comer, J.J., and Handrock, J.L., 1990, "Fundamentals of Metal Fatigue Analysis", Prentice-Hall, Inc., Englewood Cliffs, New Jersey.

Bernstein, B., Erber, T., Guralnick, S.A., 1991, "The Thermodynamics of Plastic Hinges with Damage", Journal of Continuum Mechanics and Thermodynamics, No. 3.

Bever, M.B., Holt, D.L., and Titchener, A.L., 1973, Progr. in Materials Science, 17, 5.

Erber, T. et al., 1990, Jr. Appl. Phys. 68, 1370.

Erber, T. and Gavelek, D., 1991, Physica A177, 394.

Erber, T. and Guralnick, S.A., 1988, "Hysteresis and Incremental Collapse: The Iterative Evolution of a Complex System", Annals of Phys. 181, 25-53.

Erber, T. and Guralnick, S.A., and Latal, H.G., 1972, "A General Phenomenology of Hysteresis", Annals of Phys. 69, No. 1, 161-192

Foppl, O., Jr., 1936, Iron and Steel Inst. 134, 393-423.

Guralnick, S.A., 1973, "Incremental Collapse Under Conditions of Partial Unloading," Publications, International Association for Bridge and Structural Engineering, Zurich, Switzerland, 33, 64-84.

Guralnick, S.A., 1975, "Incremental Collapse Model for Metal Fatigue", Publications, International Association for Bridge and Structural Engineering, Zurich, Switzerland, 35, 83-99.

Guralnick, S.A., Singh, S., and Erber, T., 1984, "Plastic Collapse, Shakedown and Hysteresis", J. Struct. Engrg., ASCE, 110, 2103-2119.

Guralnick, S.A., et al., 1986, "Plastic Collapse Shakedown and Hysteresis of Multi-Story Steel Structures", J. Struct. Engrg., ASCE, 112, 2610-2627.

Guralnick, S.A., et al., 1988, "Energy Method for Incremental Collapse Analysis of Framed Structures", J. Struct. Engrg., ASCE, 114, 31-49.

REFERENCES (Continued)

Halford, G.R., 1966, "Stored Energy of Cold Work Changes Induced by Cyclic Deformation", Ph.D. Dissertation (University of Illinois, unpublished).

Halford, G.R., 1966, "The Energy Required for Fatigue, Journal of Materials", 1, No. 1, 3-18.

Hempel, M., 1965, "Some Problems of Fatigue Testing", Materials Testing 7, 401-412.

Hertzberg, Richard W., 1989, "Deformation and Fracture Mechanics of Engineering Materials", Third Edition, John Wiley and Sons, New York, N.Y.

Lazan, B.J., 1968, "Damping of Materials and Members in Structural Mechanics", Pergamon Press.

Lemaitre, J. and Chaboche, J., 1990, "Mechanics of Solid Materials", Cambridge University Press, New York, N.Y.

Miner, M.A. 1945, "Cumulative Damage in Fatigue", Journal of Applied Mechanics, 12, No. 3 159, September.

Morrow, J., 1965, ASTM Special Technical Publication No. 378.

Morrow, J., "Cyclic Plastic Strain Energy and Fatigue of Metals", INSTRON Application Series MN-20.

Palmgren, A., 1924, "The Endurance of Ball Bearings (in German)", Z. Wer. Deut., Ing. 68, 339, April.

Parker, A.P., 1981, "The Mechanics of Fracture and Fatigue", E. and F.N. Spon, in association with Methuen, Inc., New York, N.Y.

Pasztor, G. and Schmidt, C., 1978, Journal of Applied Physics, 49, 886.

Puskar, A., and Golovin, S.A., 1985, "Fatigue in Materials: Cumulative Damage Processes", Elsevier Science Publishing Co., Inc., New York, N.Y.

Sandor, B.I., 1972, "Fundamentals of Cyclic Stress and Strain", The University of Wisconsin Press, Madison, Wisconsin.

Suresh, S., 1991, "Fatigue of Materials", Cambridge University Press, New York, N.Y.

Teague, E.C., Jr., 1989, Vac. Sci. Technol. B7, 1898.

FIG.1 STAGES IN THE PROGRESSION LEADING TO RUPTURE
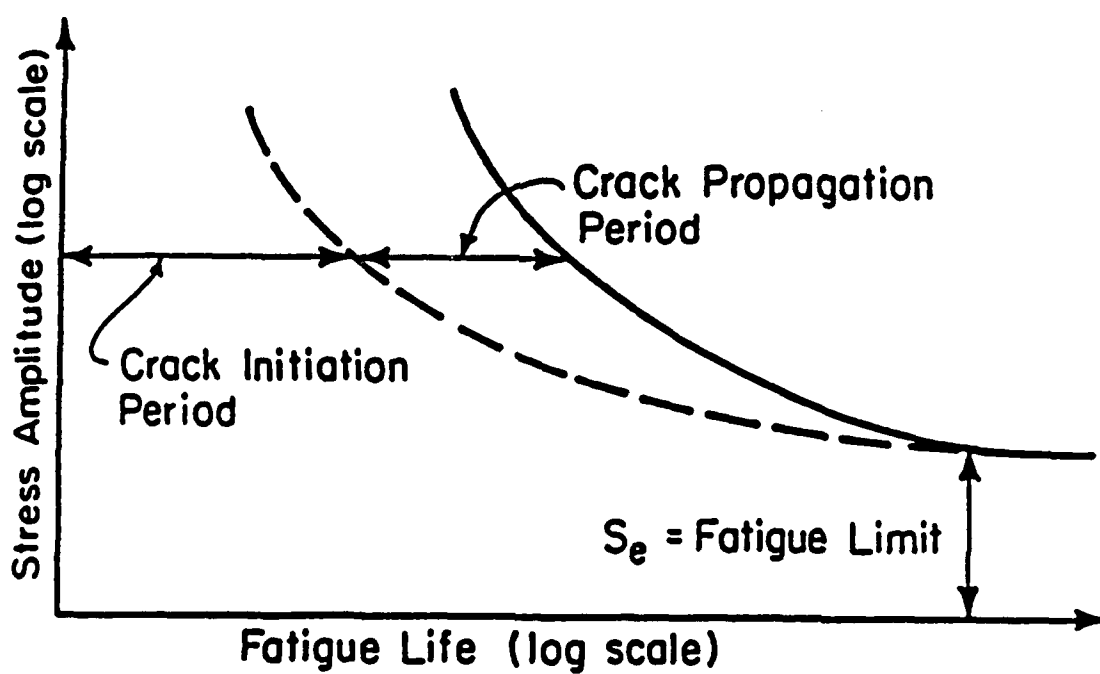
FIG.2 CONVENTIONAL REPRESENTATION OF THE FATIGUE FAILURE PROCESS
(AFTER BANNANTINE, COMER AND HANDROCK, 1990)
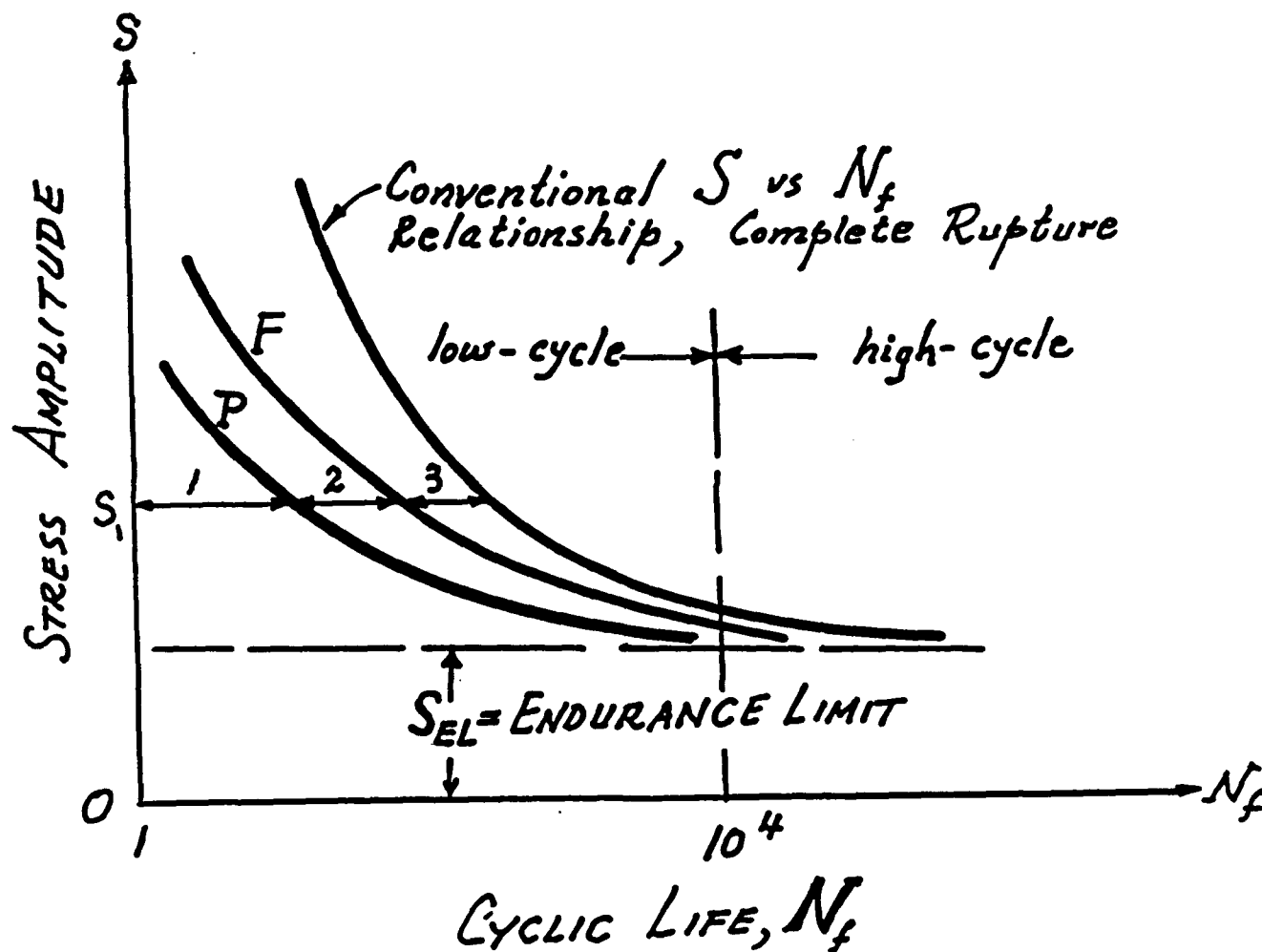
FIG.3 INCEPTION OF MICROPLASTICITY, P, INCEPTION OF MACROCRACKING, F, AND THE S VS. N_f DIAGRAM
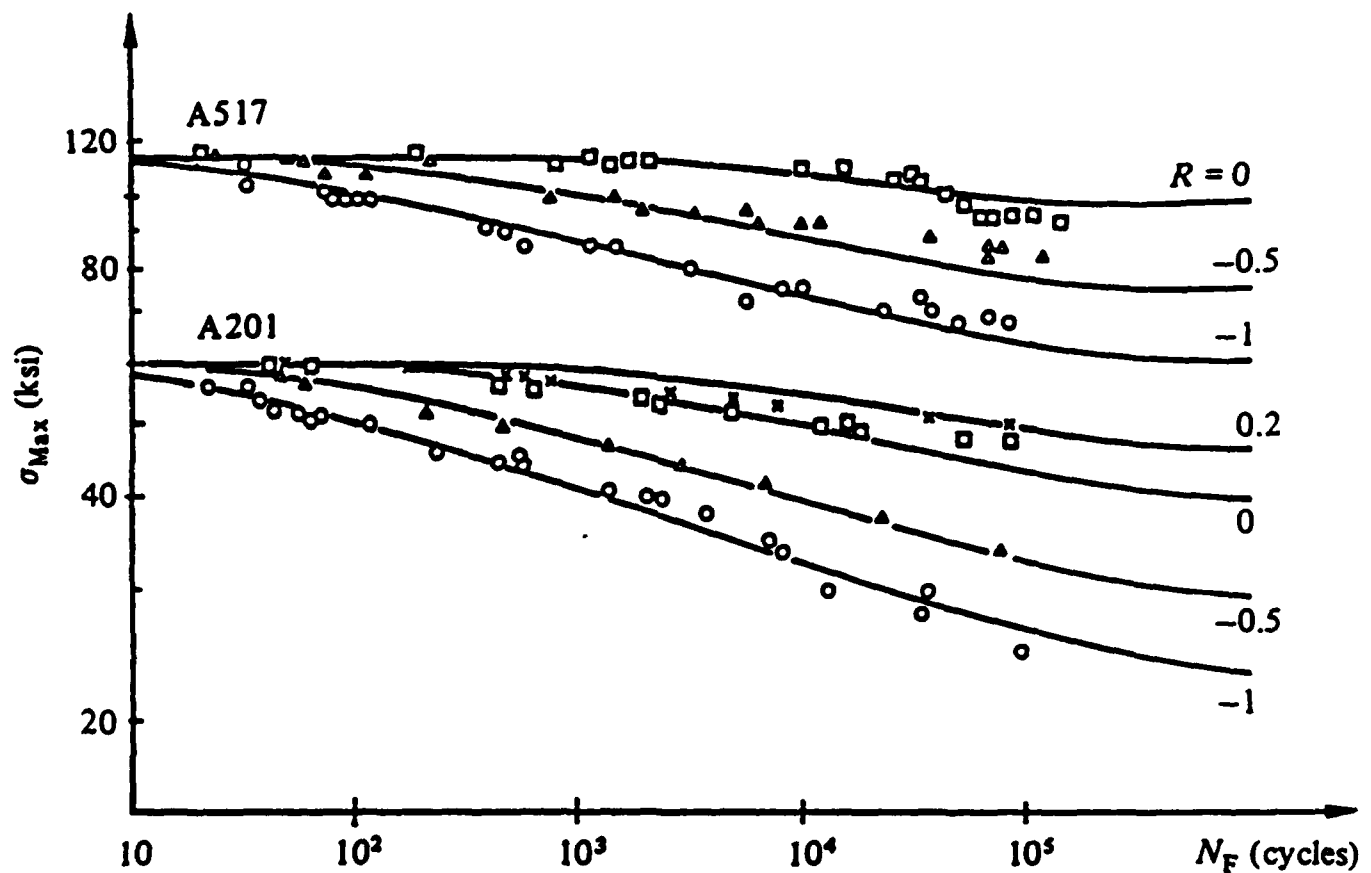
FIG.4   MAXIMUM STRESS VS. CYCLIC LIFE CURVES
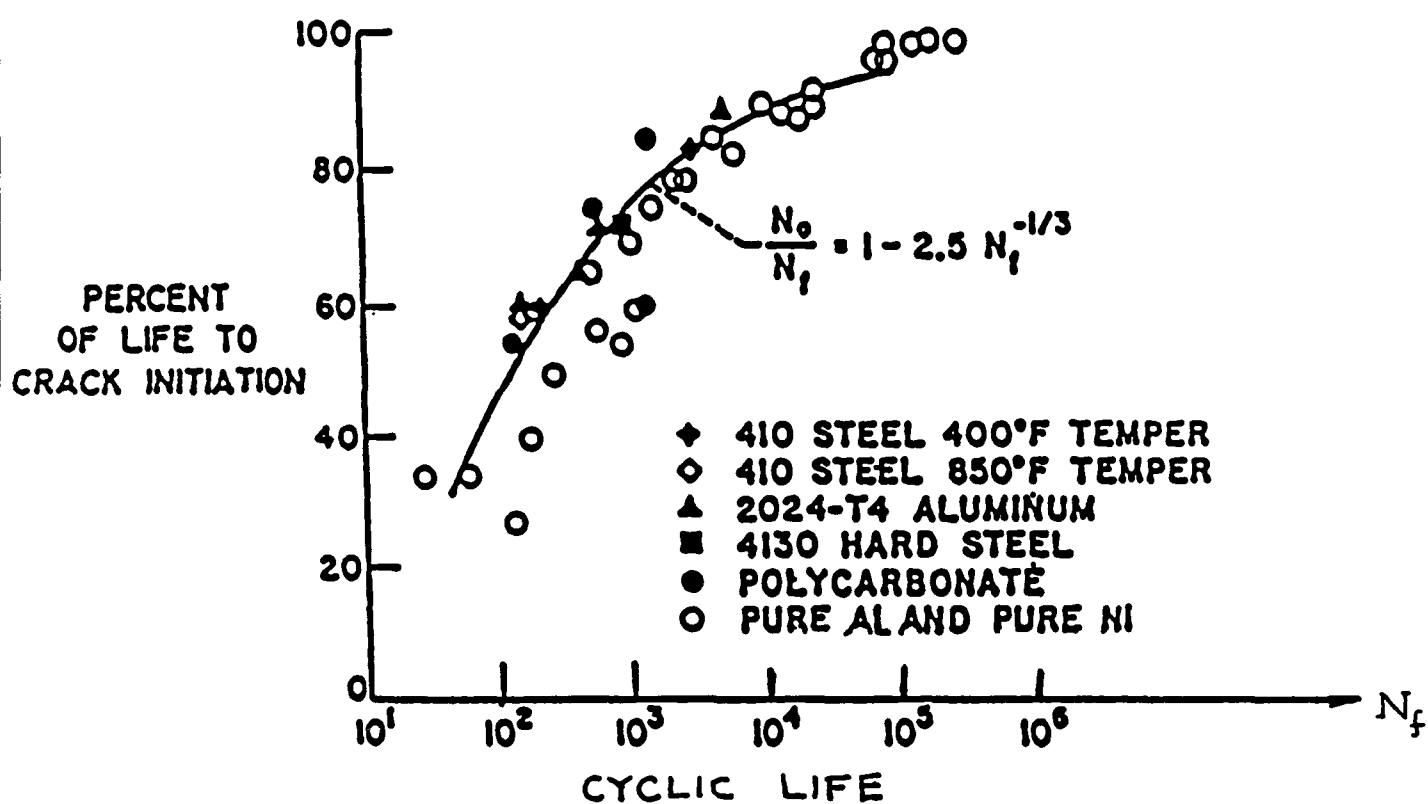(AFTER LEMAITRE AND CHABOCHE, 1990)

(a)

(b)

(c)

2µ
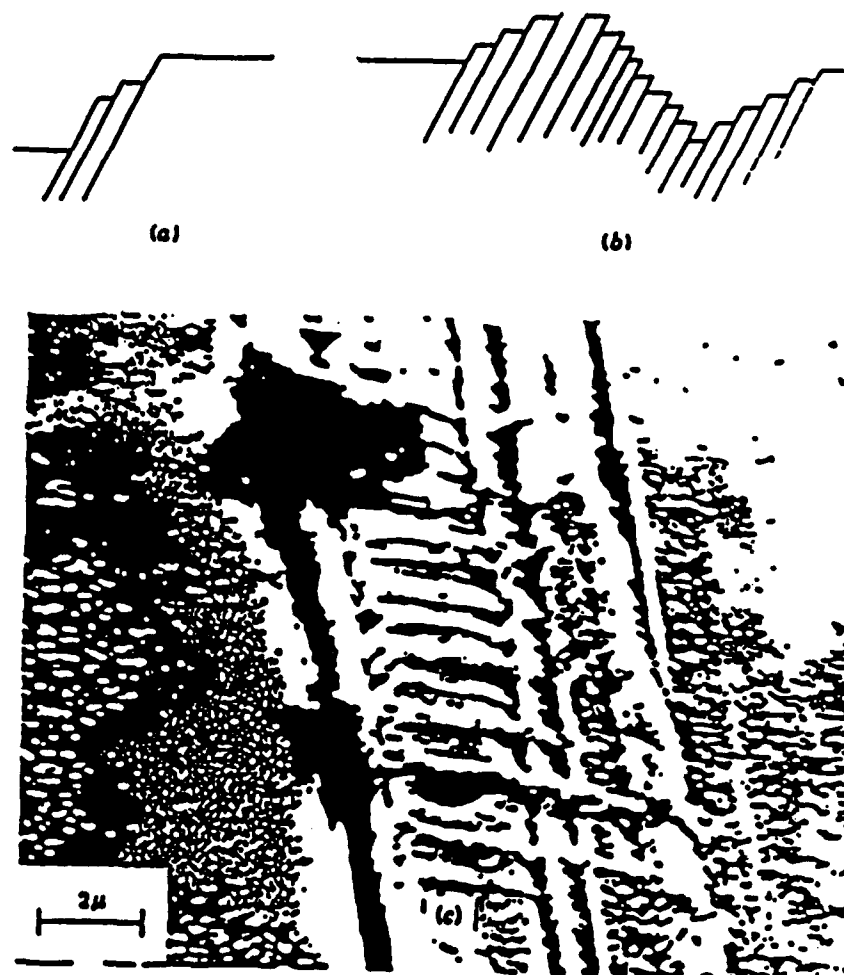
FIGURE 5   Plastic Strain-Induced Surface Offsets (A) Monotonic Loading, (B) Cyclic Loading Leading to Extrusions and Instrusions and (C) Photomicrograph of Instrusions and Extrusion on Prepolished Surface
(After Herzberg, 1984)

$\sigma_a = \pm 2.5$ ksi

$\sigma_a = \pm 11.25$ ksi

$\sigma_a = \pm 7.5$ ksi

1μ
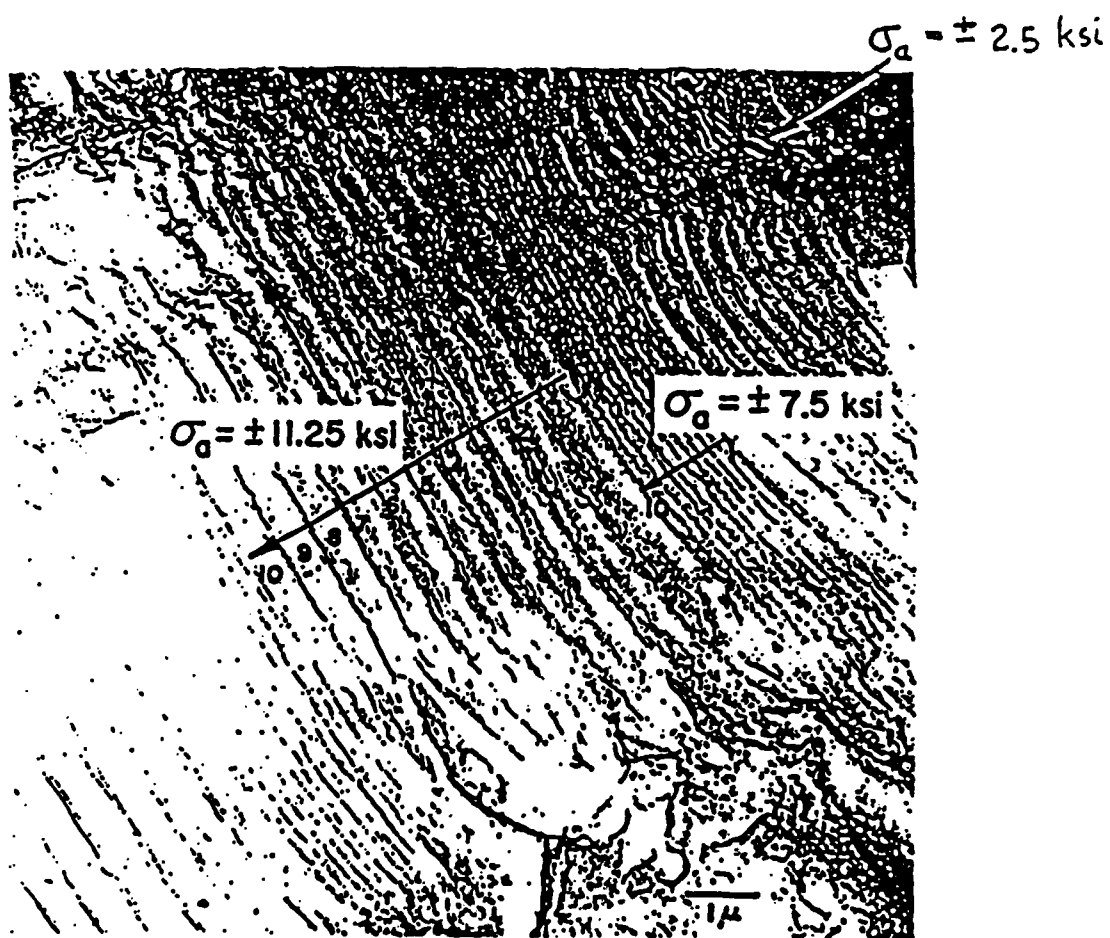
FIGURE 6   Striations Produced at Various Alternating Stress Levels
(After Sandor, 1972)
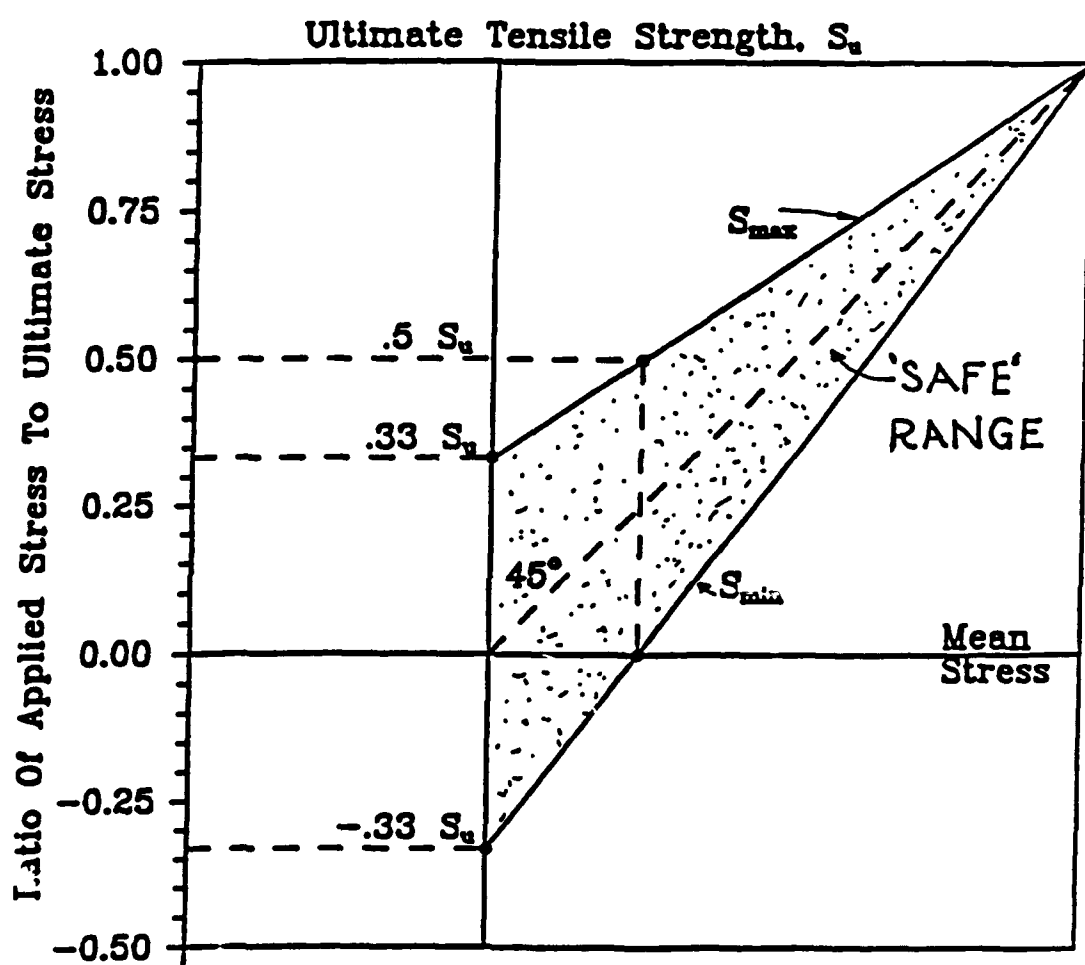
**FIG.7   GOODMAN - GERBER DIAGRAM FOR
SAFE RANGE OF STRESS**

$$\frac{N_o}{N_f} = 1 - 2.5 \, N_f^{-1/3}$$

PERCENT
OF LIFE TO
CRACK INITIATION

♦ 410 STEEL 400°F TEMPER
◊ 410 STEEL 850°F TEMPER
▲ 2024-T4 ALUMINUM
■ 4130 HARD STEEL
● POLYCARBONATE
○ PURE AL AND PURE NI

N_f

CYCLIC LIFE

**FIG.8   PERCENT OF LIFE TO CRACK INITIATION
VS. CYCLIC LIFE**
(AFTER LAIRD AND SMITH, 1963)

$$R = \frac{\sigma_{min}}{\sigma_{max}}$$
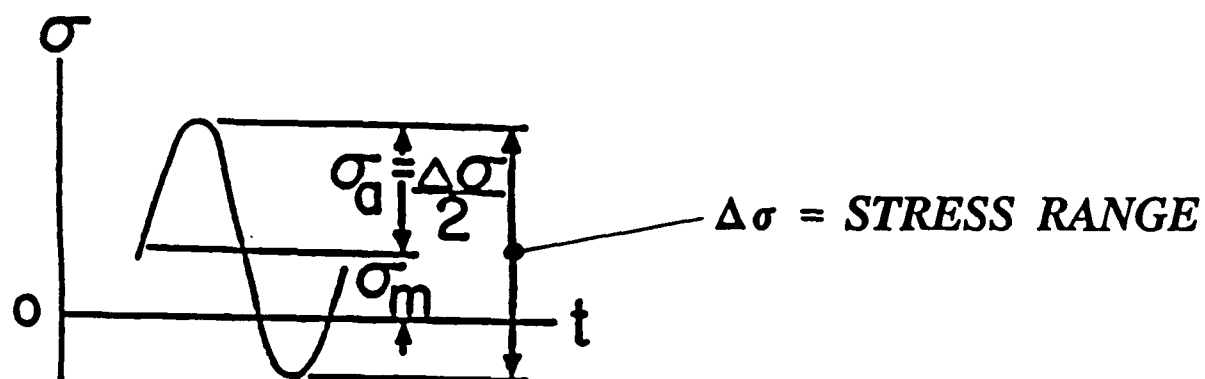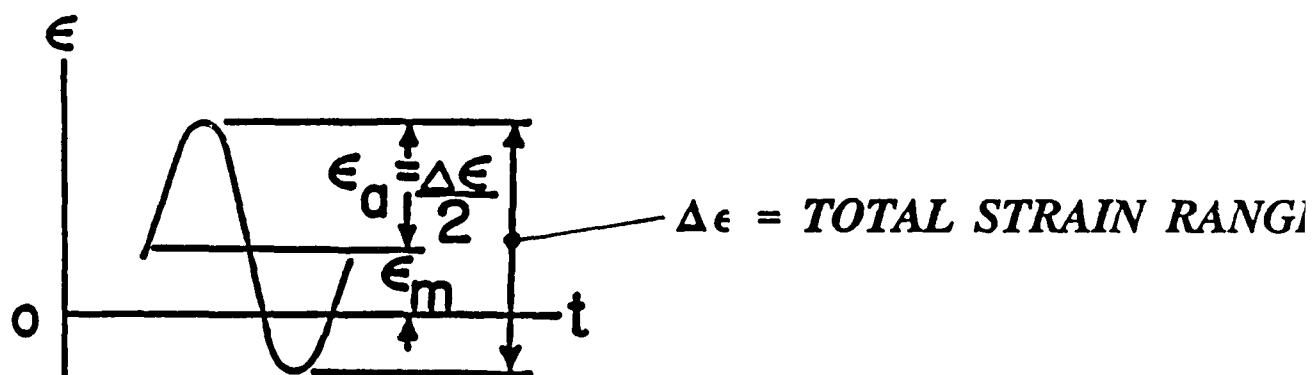
FIG.9   DEFINITIONS   OF
CYCLIC STRESS AND CYCLIC STRAIN PARAMETERS
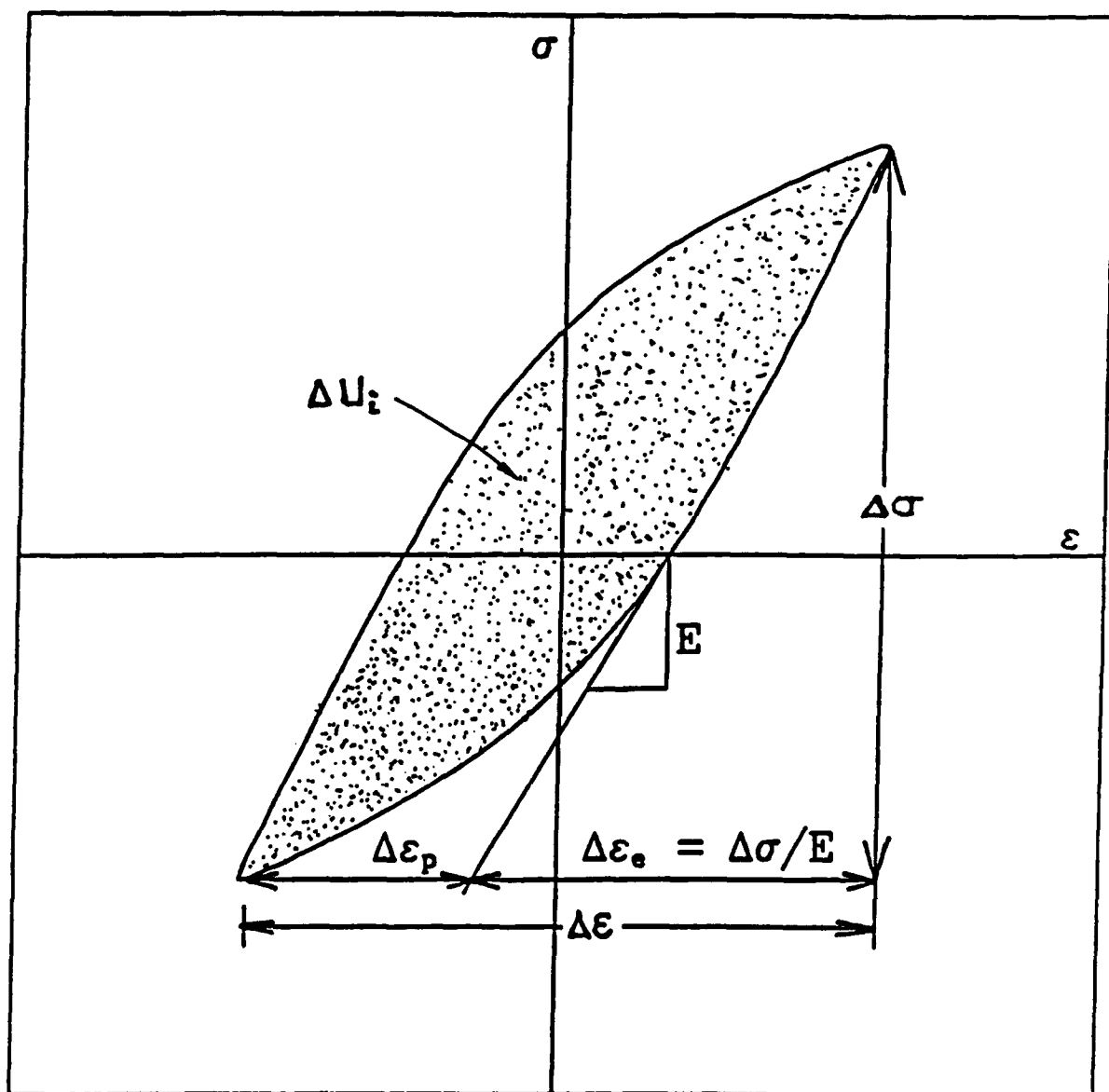
**FIG.10   TYPICAL HYSTERESIS LOOP SHOWING
ELASTIC - PLASTIC STRAIN DIVISION**
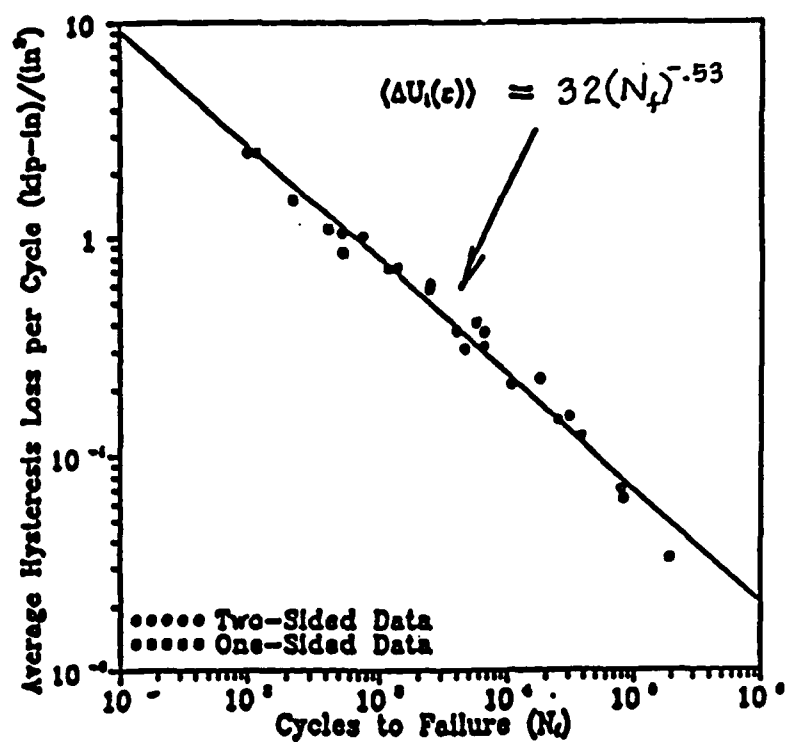
FIGURE 11A   **Average Hysteresis Loss per Cycles vs. Cycles to Failure: Combined Data**
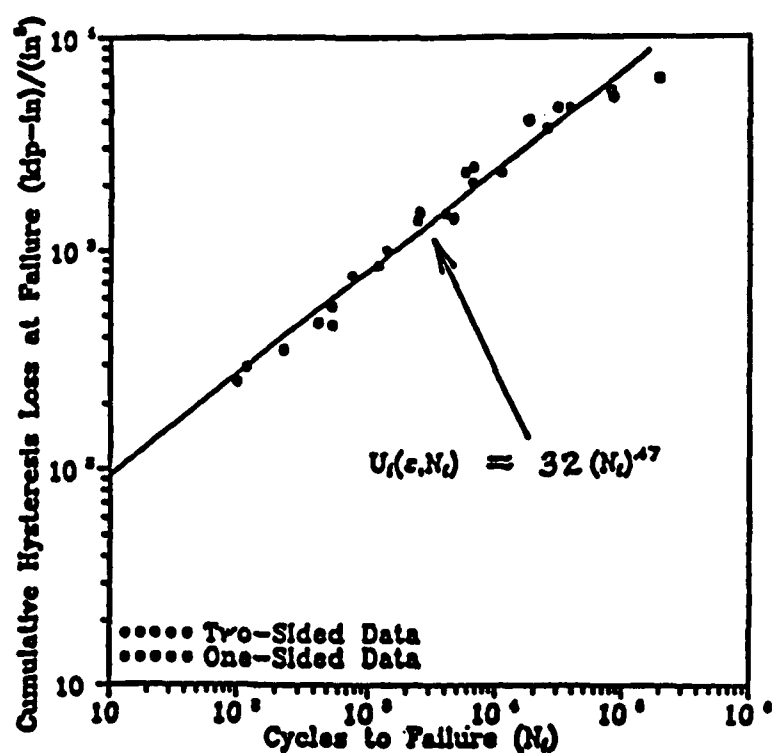
FIGURE 11B   **Cumulative Hysteresis Loss at Failure vs. Cycles to Failure: Combined Data**
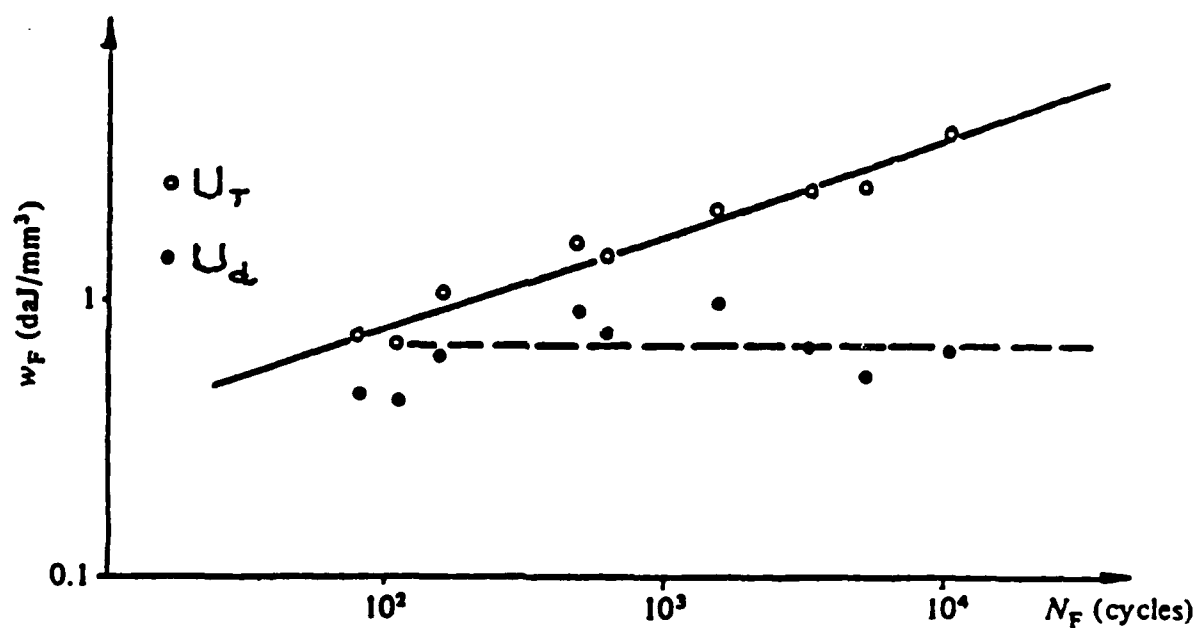
**FIG.12   DISSIPATED ENERGY OF PLASTIC DEFORMATION
UNTIL FAILURE AND ITS ACTIVE PART,
TYPE 316 STAINLESS STEEL AT ROOM TEMPERATURE**
(AFTER LEMAITRE AND CHABOCHE, 1990)
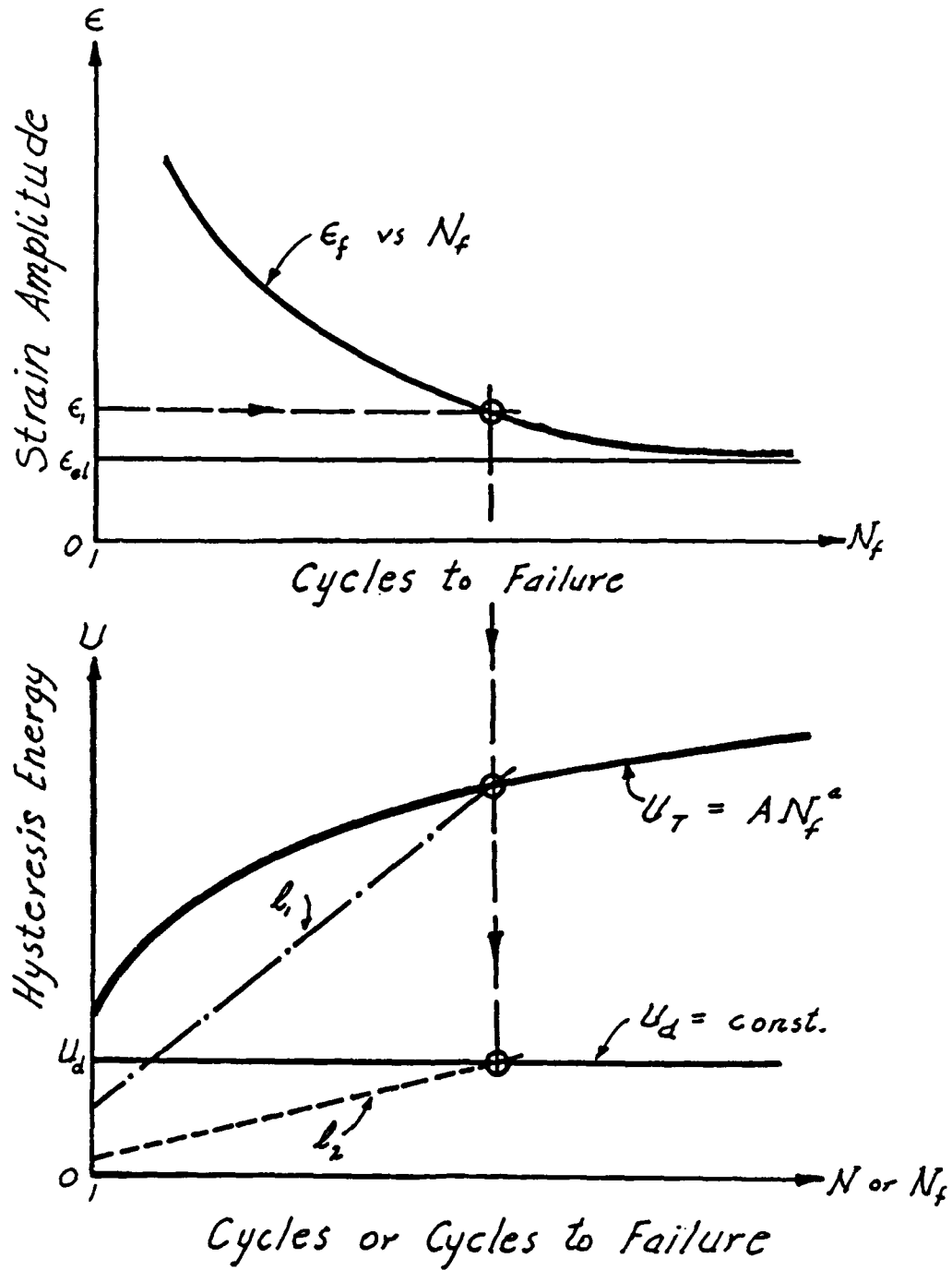
FIG. 13   THE CONNECTION BETWEEN CUMULATIVE HYSTERESIS LOSS, U_F, ENERGY OF DAMAGE, U_D, STRAIN AMPLITUDE AND NUMBER OF CYCLES TO FAILURE
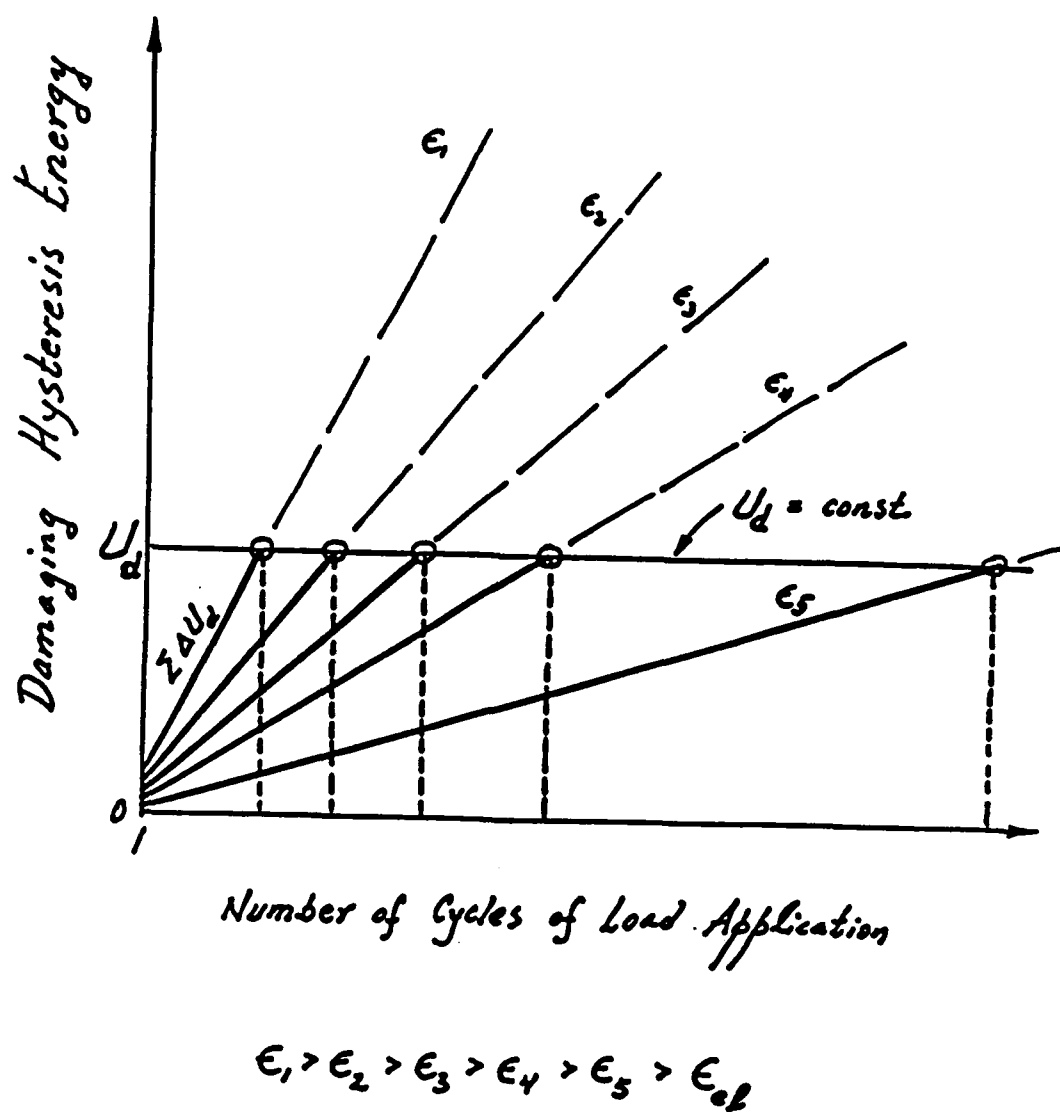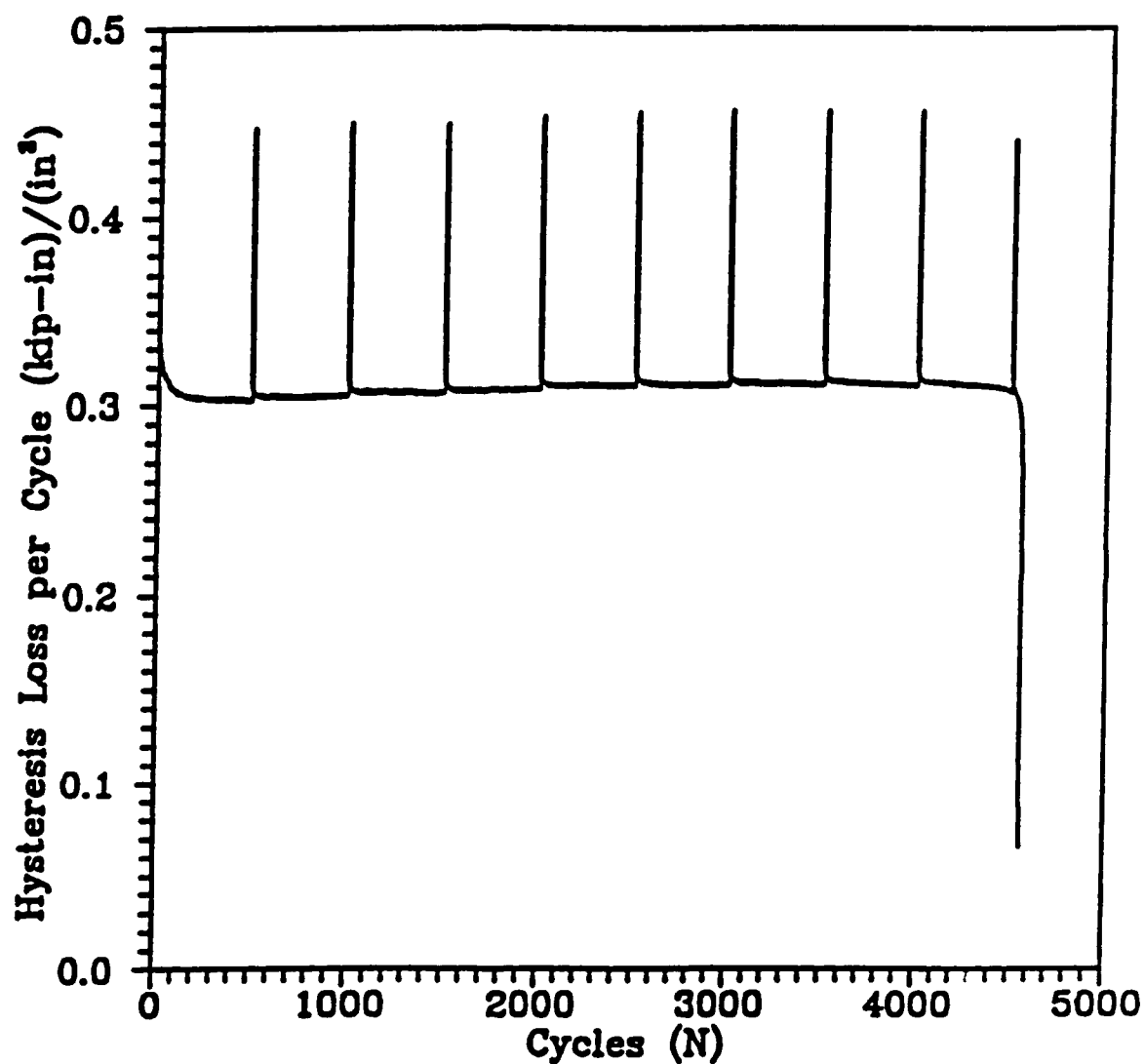
FIGURE 14 Cumulative Damage and Strain Level
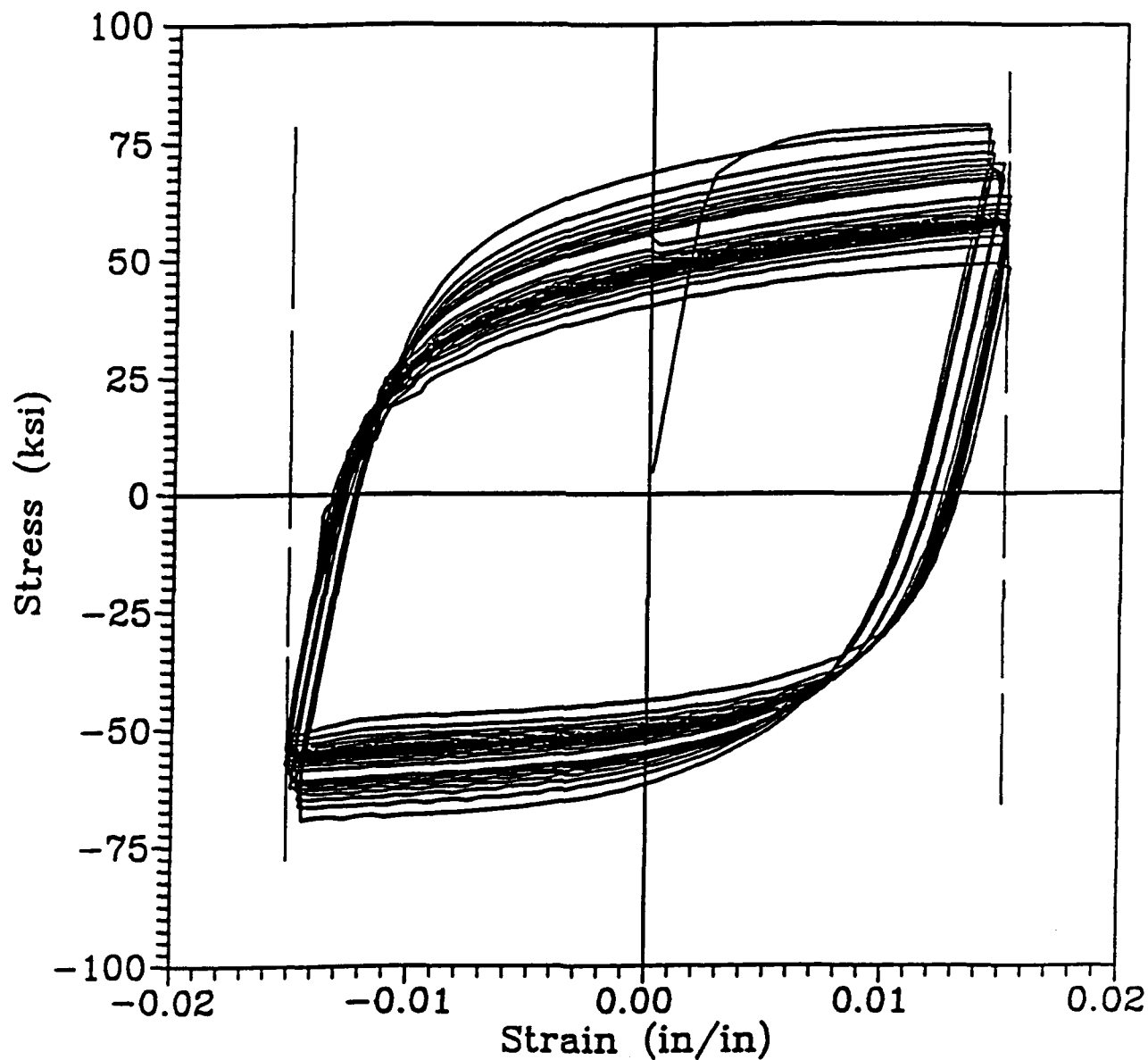
**FIG.15 RESPONSE OF A STRAIN - SOFTENING MATERIAL
TO CYCLIC APPLICATIONS OF LOAD
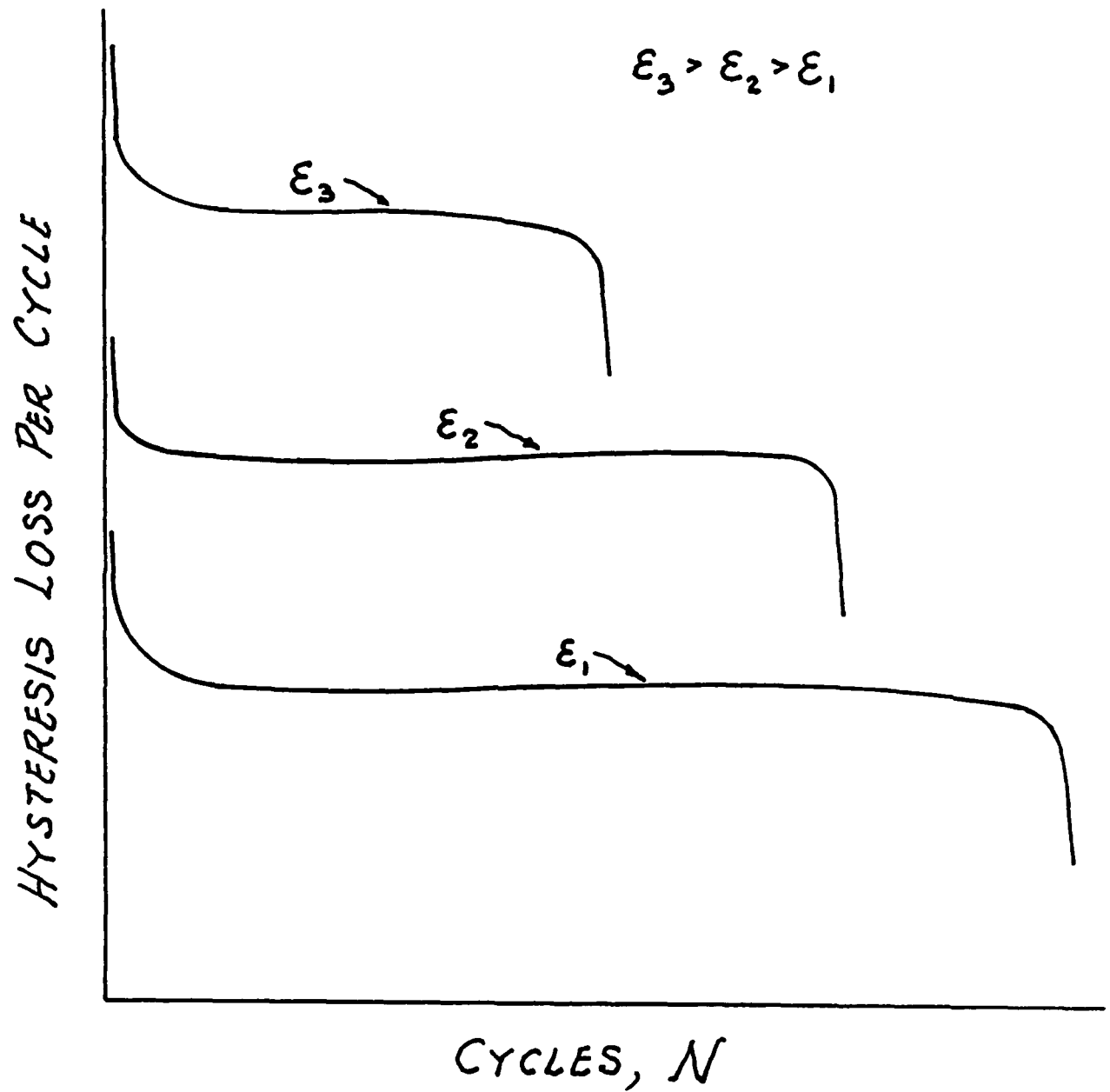UNDER STRAIN CONTROL**
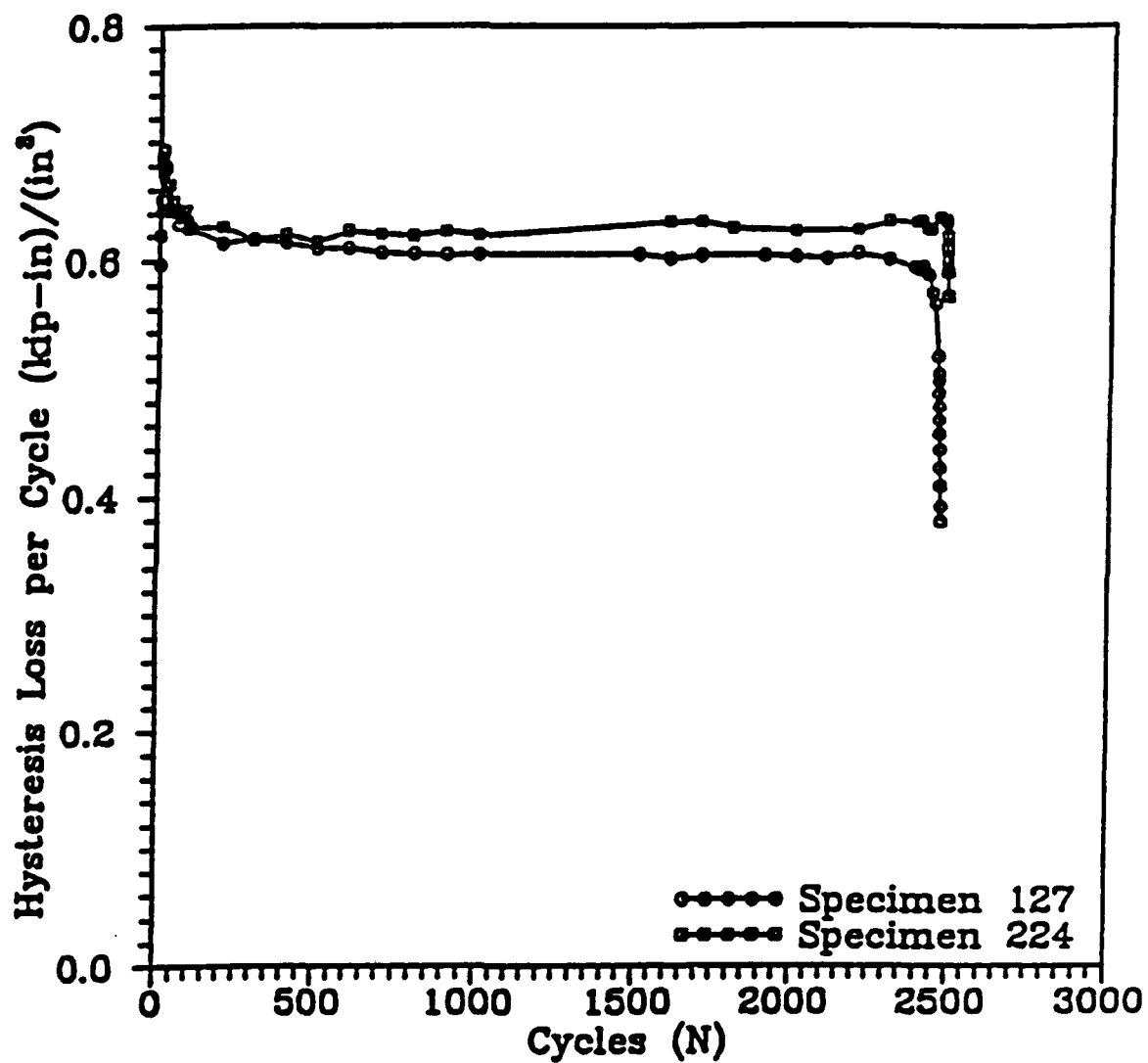
FIG.16   HYSTERESIS LOSS PER CYCLE VS. NUMBER OF CYCLES

$(\Delta e/2 = .006 \text{ in/in})$

FIG.17   HYSTERESIS LOSS PER CYCLE VS. NUMBER OF CYCLES FOR A SPECIMEN SUBJECTED TO OVERLOADS

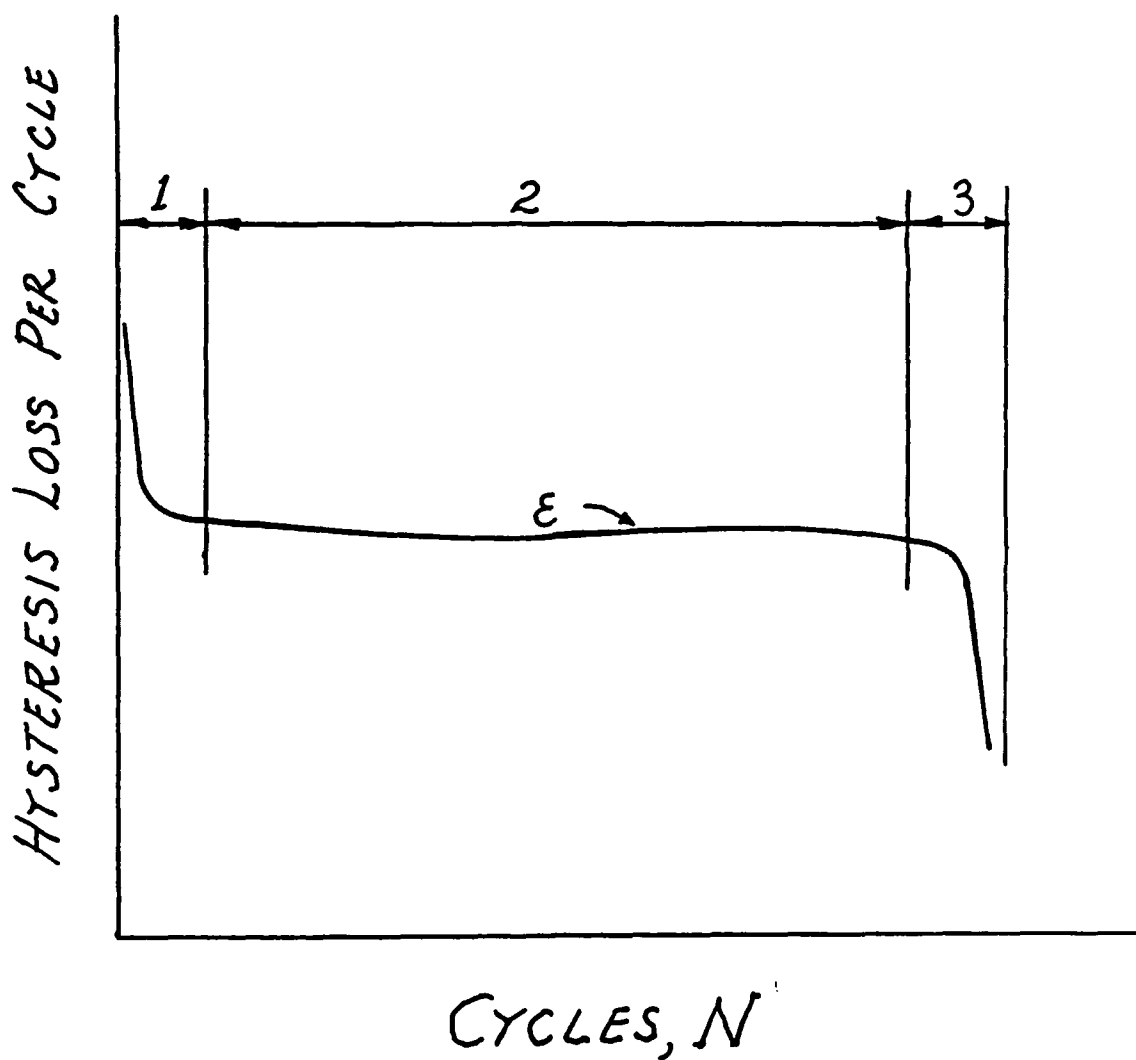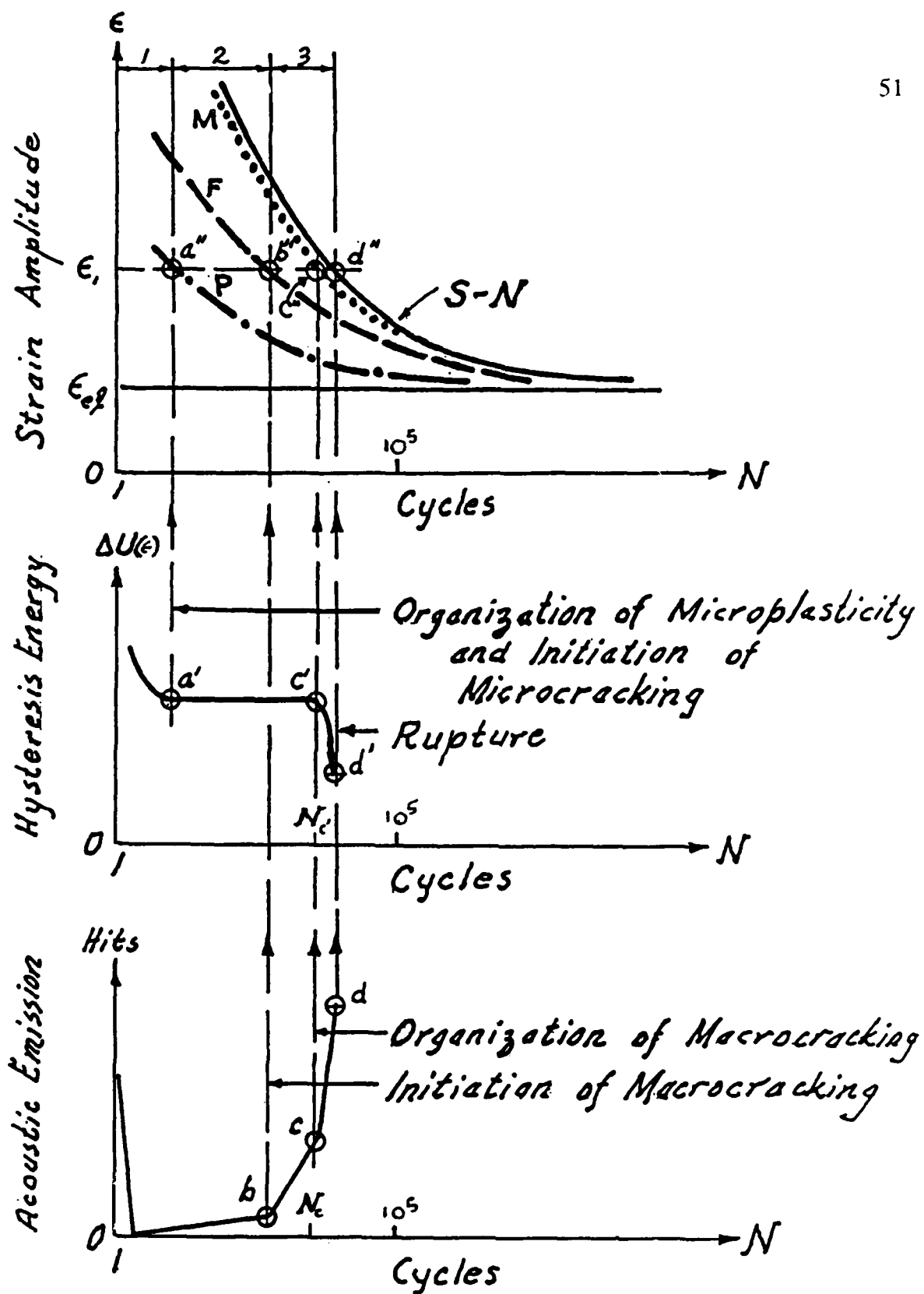**FIG.18   HYSTERESIS LOSS PER CYCLE VS. NUMBER OF CYCLES**

**FIG.19 ZONES IN THE EVOLUTION OF HYSTERESIS LOSS PE
CYCLE**

FIG. 20   FATIGUE FAILURE, HYSTERESIS AND ACOUSTIC EMISSION